University of Alabama in Huntsville

LOUIS

Dissertations | UAH Electronic Theses and Dissertations

2008

Theoretical and computational considerations for an approximation to the medium thrust two-body problem

Robert B. Adams

Follow this and additional works at: https://louis.uah.edu/uah-dissertations

Recommended Citation

Adams, Robert B., "Theoretical and computational considerations for an approximation to the medium thrust two-body problem" (2008). *Dissertations*. 265.
https://louis.uah.edu/uah-dissertations/265

This Dissertation is brought to you for free and open access by the UAH Electronic Theses and Dissertations at LOUIS. It has been accepted for inclusion in Dissertations by an authorized administrator of LOUIS.

THEORETICAL AND COMPUTATIONAL CONSIDERATIONS FOR AN APPROXIMATION TO THE MEDIUM THRUST TWO-BODY PROBLEM

by

ROBERT B. ADAMS

A DISSERTATION

Submitted in partial fulfillment of the requirement
for the degree of Doctor of Philosophy
in
The Department of Mechanical and Aerospace Engineering
to
The School of Graduate Studies
of
The University of Alabama in Huntsville

HUNTSVILLE, ALABAMA

2008

In presenting this thesis in partial fulfillment of the requirements for a master's degree from The University of Alabama in Huntsville, I agree that the Library of this University shall make it freely available for inspection. I further agree that permission for extensive copying for scholarly purposes maybe granted by my advisor or, in his/her absence, by the Chair of the Department or the Dean of the School of Graduate Studies. It is also understood that due recognition shall be given to me and to The University of Alabama in Huntsville in any scholarly use which may be made of any material in this thesis.

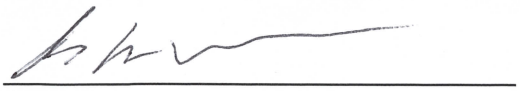

6-30-08

DISSERTATION APPROVAL FORM

Submitted by Robert B. Adams in partial fulfillment of the requirements for the degree of Doctor of Philosophy with a major in Mechanical Engineering and accepted on behalf of the Faculty of the School of Graduate Studies by the dissertation committee.

We, the undersigned members of the Graduate Faculty of The University of Alabama in Huntsville, certify that we have advised and/or supervised the candidate on the work described in this dissertation. We further certify that we have reviewed the dissertation manuscript and approve it in partial fulfillment of the requirements for the degree of Doctor of Philosophy with a major in Mechanical Engineering.

Committee Chair — (Date) 6/26/08

Technical Advisor — 6/27/08

6/27/08

6/27/08

Department Chair

College Dean

Graduate Dean — 7/29/08

ABSTRACT

The School of Graduate Studies

The University of Alabama in Huntsville

Degree: Doctor of Philosophy

College/Department: Engineering/Mechanical and Aerospace Engineering

Name of Candidate: Robert B. Adams

Title: Theoretical and Computational Considerations for an Approximation to Medium Thrust Spacecraft Trajectories

Trajectory analysis and mission design for launch vehicles and spacecraft is complex under the simplest of situations. The mission designer must trade a number of variables inherent in the vehicle design to create a mission profile that maximizes payload, minimizes mission time, and meets all requirements for launch/arrival dates and capabilities of the proposed vehicle. Closed-form or easily integrable solutions are available for what the literature refers to as high or low thrust solutions. However, medium thrust missions, characterized by all launch vehicles and many advanced propulsion systems intended for deep space operation, require full integration of the equations of motion, or use of highly simplistic closed-form solutions that introduce considerable error. Additionally there are not clear boundaries between when high, medium or low thrust solutions are pertinent.

This treatise focuses on the goal of contributing to the medium thrust literature by developing a simpler algorithm for analyzing trajectories. This algorithm is shown to apply to all high thrust and medium thrust trajectories as well as most low thrust

trajectories with an estimate of payload fraction within 10%. In the course of research for this new algorithm a new maneuver was discovered that can dramatically increase the efficiency of escape trajectories under certain conditions. Finally a new model for describing two-body orbits is discussed. This new model simplifies visualization of the orbit and how maneuvers affect the spacecraft's orbit. It is hoped that this new model will help to simplify trajectory analysis in the future.

Abstract Approval: Committee Chair 6/26/08

(Date)

Department Chair 6/26/08

Graduate Dean 7/29/08

ACKNOWLEDGMENTS

The author would like to acknowledge his wife, Laura Lee, for the support she has shown during the completion of this dissertation. Without her encouragement, this dissertation would not have been completed. Also the author thanks his son, Kyle, who brings a little more joy into his life every day.

The author notes with deep regret the passing of Dr. Clark Hawk, the original committee chair for this dissertation. Dr. Hawk was a mentor and a friend and he will be sorely missed. And the author thanks Dr. Georgia Richardson, whose willingness to volunteer as chair made it possible for the author to complete this treatise.

TABLE OF CONTENTS

LIST OF FIGURES xi

LIST OF TABLES xiii

LIST OF SYMBOLS xiv

Chapter

1 INTRODUCTION 1

2 PROBLEM STATEMENT 4

3 RELEVANT BACKGROUND 6

3.1 Introduction 6

3.2 Vehicle Systems 6

3.3 Ideal Rocket Equation 12

3.4 Astrodynamics 15

3.5 General Trajectory Analysis 22

3.6 High Thrust Approximation 26

3.7 Low Thrust Approximation 34

3.8 Medium Thrust Approximation 48

3.9 Uses of Analytic Approximations 57

4 METHODOLOGY 61

5 DERIVATION OF TWO-BODY APPROXIMATION 63

5.1 Introduction 63

5.2 Issues Regarding Optimal Thrust and Acceleration 64

5.3 Analytic Comparison of Medium Thrust Model to Existing Models 78

5.4 Geometric Representation of a Thrust Trajectory 80

6 COMPUTATIONAL RESULTS 90

6.1 Introduction 90

6.2 Comparison to High Thrust Solutions 90

6.3 Comparison to Low Thrust Solutions 91

6.4 Statistical Analysis of Goodness of Fit 92

6.5 Uncertainty Analysis to Results using Proposed Solution 95

7 CONCLUSIONS AND RECOMMENDATIONS 102

APPENDICES 105

Appendix A: CELESTIAL CONSTANTS USED IN THIS TREATISE 106

Appendix B: CONSERVATION OF ENERGY FOR THE NEW MANEUVER 108

Appendix C: UNSUCCESSFUL ATTEMPTS TO DETERMINE AN OPTIMAL GUIDANCE SCHEDULE 111

Appendix D: EXTENSION OF THE ISOPERIMETRIC PROBLEM TO SECOND ORDER DIFFERENTIAL EQUATIONS AND FUNCTIONS OF TWO VARIABLES 121

Appendix E: NON-DIMENSIONAL ANALYSIS 123

E.1 Non-dimensional Analysis 123

E.2 Relationships between Non-dimensional Variables 132

E.3 Relationship between r and V 136

E.4 Application of Non-dimensional Variables to High Thrust Equations 139

E.5 Application of Non-dimensional Variables to Low Thrust Equations 141

E.6 Application of Non-Dimensional Variables to Medium Thrust Equations 142

Appendix F: ACCIDENTAL DERIVATION OF A NEW MANEUVER 146

F.1 Derivation.....146

F.2 New Maneuver Applied to a Semi-tangential Transfer Scenario 166

Appendix G: PAPER SUBMITTAL TO *SCIENCE MAGAZINE* 172

REFERENCES 196

LIST OF FIGURES

Figure page

3.1 Mass breakout for a typical in-space vehicle 8

3.2 Power flow diagram for typical in-space vehicle 9

3.3 Free body diagram for a typical in-space vehicle 13

3.4 Earth Centered Inertial (ECI) coordinate system [6] 17

3.5 Heliocentric coordinate system [6] 18

3.6 Keplerian six parameter system for orbit definition [6] 19

3.7 Definition of trajectory variables for in-space mission 24

3.8 Hohmann and bi-elliptic transfer options 29

3.9 Semi-tangential transfers for high thrust trajectories 32

3.10 Encke's formulation for propagation of low thrust trajectories 43

3.11 Straight line approximation for medium thrust trajectories 51

3.12 Linearized computational model diagram 55

5.1 Plots of acceleration and acceleration^2 vs. time 65

5.2 Payload fraction as a function of J (extending downward) and the ratio of propulsion system mass to initial mass (extending left to right) 71

5.3 Exploded view of Figure 5.2 near origin. X-axis is J, y-axis is b, Contour values are for payload fraction 72

5.4 Intersection of cone and plane to create conic sections. From Vallado [6]. 81

5.5 Intersection of a plane and a paraboloid of revolution. 85

5.6 Intersection after ΔV maneuver changing pitch of the plane 86

6.1 Comparison of the analytical approximation to the high thrust solution.....91

6.2 Comparison of analytical approximation to low thrust solutions. 92

6.3 Uncertainty contributions to payload mass fraction for independent variables under the considered scenarios 99

C.1 Lambert's problem 112

C.2 Relationship between *r, V* and *a* 115

C.3 Differential change in trajectory from initial to final position 116

F.1 New maneuver 148

F.2 New maneuver specific mechanical energy ξ_3 vs. ΔV_1 for varying ΔV_{total} . Vertical asymptote at initial orbital velocity, 29.784 km/s. Values represent solar orbit starting at 1 AU (Earth-like orbit) 157

F.3 Ratio of V_{inf} for the new maneuver to the V_{inf} attained through a direct burn. Vertical asymptote is at initial orbital velocity, 29.784 km/s. Values represent solar orbit starting at 1 AU (Earth-like orbit) 164

F.4 Break even point in trip time between the inverse bi-elliptic and Hohmann orbit transfers 167

F.5 Comparison of semi-tangential transfer vs. transfer using the new option from Earth to Mars at various periapse radii.....168

F.6 Total ΔV vs. trip time for orbit raising maneuvers from Earth orbit to 100 AU.....169

F.7 Ratio of V_{inf} achieved with the first burn at the designated thrust angle vs. the direct and new maneuvers. Black lines indicate a 35 km/sec budget with 25 km/sec used on first burn. Red lines are 29 km/sec budget with 20 km/sec first burn. 171

LIST OF TABLES

Table page

3.1 Typical High Thrust propulsion concepts and performances....27

3.2 Typical low thrust propulsion concepts and performances....34

3.3 Typical Medium Thrust propulsion concepts and performances....48

6.1 Results of χ^2 test for analytical approximation....93

6.2 Independent variables and typical values for high, low, and medium thrust missions to escape low Earth orbit. 98

A.1 Celestial constants....106

E.1 List of pertinent variables for trajectory analysis 124

E.2 List of non-dimensional variables 126

E.3 List of non-dimensional numbers and their physical meanings 131

LIST OF SYMBOLS

a	semi-major axis
c	speed of light
e	eccentricity
f	force components
g	gravity
h	angular momentum
i	inclination
m	mass
p	pressure
r	radius from central body
t	time
v	jet velocity
x	variable
A	Area
C	Constant
D	Drag
E	Eccentric Anomaly
	Energy
F	Thrust
H	Hamiltonian

I	Impulse
J	Integral of acceleration^2 with time
L	Lift
M	Mean anomaly
MW	Molecular Weight
P	power
	Period
R_u	universal gas constant
S	distance
T	time at epoch
TOF	time of flight
TW	Thrust to weight
U	Uncertainty
V	velocity
V_c	non-dimensional velocity

Greek Letters

α	specific power
	argument of perigee plus mean anomaly
	angle of attack
β	out of plane thrust angle
δ	thrust angle
δr	change in radius

γ	flight path angle
	ratio of specific heats
ε	structural mass fraction
η	efficiency
λ	Lagrangian multiplier
	Payload fraction
μ	central body gravitational constant
π	non-dimensional variable
υ	true anomaly
ξ	specific orbital energy
ΔV	delta velocity
Ω	longitude of ascending node

Subscripts

a	apogee
amb	ambient
b	burn
c	chamber
	coast
conv	conversion
cyc	cycle
exit	exit

exp	expansion
i	initial
int	internal
f	final
h	out of plane
jet	jet
lat	latent
m	mission
n	normal
opt	optimal
p	propulsion
	perigee
prop	propellant
reac	reactor
s	structural
sp	specific
t	tank
	tangential
tot	total
vac	vacuum
L	payload

CHAPTER 1

INTRODUCTION

Trajectory analysis is critical in determining the performance of an in-space vehicle. The trajectory analyst defines the momentum (or ΔV) requirements that the propulsion system must provide, as well as the propellant mass stored in the system. The analyst is also responsible for determining the optimal mission trip time for the required payload (or vice versa). To generate this data, the analyst manages several variables, such as departure and arrival time, thrust and thrust angle vs. time, use of coasting phases, etc.

To acquire a high fidelity solution, the analyst will integrate the equations of motion for the vehicle. This integration requires an ephemeris of the positions and gravitational attributes of the major and minor bodies of the solar system. Additionally, the analyst must employ an optimization routine to give the best answer for the desired inputs. Considering the number of desired outputs and the fact that they are usually mutually exclusive, in optimization the analyst is frequently forced to employ a weighting scheme. Thus, the analyst optimizes over tens to hundreds of variables to produce the highest weighted average of trip time, payload and required initial vehicle mass.

A high fidelity solution frequently provides too much information for the early stages of vehicle design and development. Considerable time and effort is required for such an analysis. A simpler approximation can be found for many vehicles of interest.

Vehicles with short burn times and high thrust levels are indicated as high thrust systems. Similarly vehicles with very low accelerations and nearly continuous operation are referred to as low thrust systems.

High thrust systems typically have very low specific impulses, which then require massive amounts of fuel to provide the vehicle momentum change requirements. High thrust systems tend to expand a very hot gaseous propellant through a converging-diverging nozzle to produce thrust. Thus high thrust systems tend to use power production methods that can produce a high amount of thermal power in a short period of time. Chemical, nuclear thermal and solar thermals systems are examples of high thrust systems.

Low thrust propulsion requires power production systems that comprise most of the overall vehicle size. Low thrust systems produce high power levels too, but here the power is concentrated in a lower propellant mass flow rate, which results in both lower propellant consumption and lower thrust. Examples include electrothermal, electrostatic and electromagnetic thrusters such as resistojets, ion/Hall thrusters, and magneto-plasma dynamic thruster (MPD's) respectively. Other low thrust options such as solar sails and plasma sails fit into the low thrust category.

A new class of propulsion systems, referred to as medium thrust systems, seeks to overcome the limitations of high and low thrust systems by striking a better balance between thrust and specific impulse. Medium thrust systems have the ability to run at both moderately high thrusts and moderately high specific impulses. Achieving high thrust and high specific impulse simultaneously requires power levels well above that for conventional high and low thrust propulsion systems. Therefore medium thrust systems

typically are powered by high energy reactions such as nuclear explosions or fusion reactions.

Unfortunately, medium thrust systems are difficult to model. Medium thrust systems are usually capable of providing more than enough thrust to accelerate past the target orbit. Thus, these trajectories frequently employ an acceleration phase, followed by a coast phase and then a deceleration phase. Current efforts to develop an approximation for medium thrust systems are outlined in this treatise. These efforts fall short of yielding a realistic approximation of the vehicle trajectory. These approximations must ignore critical elements of trajectory analysis, such as coasting times and gravitational losses, to yield a closed-form solution.

This treatise describes the author's efforts to develop a new medium thrust approximation to the two-body problem. The specific problem statement is contained in Chapter 2. Chapter 3 reviews the results of relevant efforts as described in the literature. Chapter 4 describes the methodology used in creating the results contained in this effort. This treatise includes an analytical derivation of a closed-form solution (Chapter 5) plus computational analyses generated for comparison (Chapter 6). Finally, this treatise describes in Appendix F some interesting results from an accidental derivation of a particular maneuver. The author hopes that this approximation will speed development of medium thrust propulsion systems, which hold great promise of enabling humanity's further exploration of outer space.

CHAPTER 2

PROBLEM STATEMENT

In general, the task of this treatise is to enable trajectory analysis of medium thrust systems without having to resort to full numerical integration of the equations of motion. The author anticipates that a closed-form solution to medium thrust trajectories can be developed. This solution would build on the extensive database of high and low thrust trajectory approximations. The medium thrust approximation should also produce high and low thrust approximations in the appropriate limits. Once the medium thrust approximation is complete, it should be simple to define the crossover points between high and medium and medium and low thrust.

The approximation must be validated before it can enter into general use. Thus parametrics will be created using computational routines in general use in the industry. The analytical approximation will be compared to these routines and conclusions drawn on its effectiveness. Statistical and uncertainty methods will yield insight into the accuracy and applicability of the approximation.

Finally, this treatise will illustrate some applications of the medium thrust approximation. The approximation will enhance current propulsion and power system development. Trajectory analysis can be simplified by use of dimensionless analysis techniques incorporating the approximation. Finally sensitivities and uncertainty in the

trajectory can be controlled, enabling higher confidence in the conceptual vehicle's ability to meet performance goals.

CHAPTER 3

RELEVANT BACKGROUND

3.1 Introduction

All of the components of an in-space vehicle must work in concert if the vehicle is to meet the mission's objectives. Thus, it should come as no surprise that several vehicle components contribute significantly to vehicle performance. The next section discusses vehicle mass properties, power management and the ideal rocket equation. The section after outlines the basics for astrodynamics and the nomenclature used in this treatise. This information exists in many different references; however, each of those references uses subtly different definitions and nomenclature. Thus, the information is repeated here for clarity.

The final section reviews previous attempts at analytical approximations found in the literature. These approximations are broken into high, medium and low thrust categories. These categories have no firm definition but are terms generally used to delineate between propulsion systems and trajectory configurations. In each category, relevant propulsion systems and their general performance parameters are listed.

3.2 Vehicle Systems

Defining vehicle performance requires an understanding of the mass breakout for the vehicle. The terminology for mass breakout used in this treatise follows the AIAA/ANSI standard closely [1]. Figure 3.1 illustrates how vehicle mass properties are

broken down. Starting from the top the payload mass, m_L, is the mass that the mission planners desire to have delivered to the mission objective. The propellant mass, m_{prop}, is the total amount of propellant that will be expended during the mission. Note that this does not include residual and ullage propellant that cannot be extracted from the vehicle during the mission. Tanks, feed lines, and other components used to contain and manage the propellant mass contribute to the tankage mass, m_t. This mass is usually modeled as a ratio to the propellant mass. The propulsion mass, m_{prop}, includes all of the mass required for the propulsion and power system. This mass typically scales with either the power of the jet produced by the propulsion system or the onboard generated power. The inert mass, m_s, is the entire vehicle mass not included above. As such, it includes propellant residuals and ullage, structural components, and any ancillary components. In some places, the tankage mass is not identified, but is rolled into the structural mass. The total initial mass of the vehicle, M_i, is the summation of all of the above masses.

Power management is a critical part of vehicle performance. A power schematic can be found in Figure 3.2. This schematic uses nomenclature found in the literature [2]. Power can be generated in several ways. Typical production methods include capturing and converting solar energy, use of nuclear reactions, or chemical exothermic reactions. Assuming the latter, Figure 3.2 illustrates the latent energy of the reactants feeding into the power generation loop. There is a combustion efficiency involved which when included yields a reactor power P_{reac}. For the solar and nuclear options, the analysis starts with the reactor power. This power is frequently not in a suitable form for use in producing thrust. Therefore, the power must be converted into another form. The conversion cycle efficiency, η_{conv}, yields a new power level, P_{cyc}. The new form of

power may be a hot exhaust that should flow through a converging-diverging nozzle. Or the power may be electrical and used to accelerate plasma. In whatever case, the propellant must be expanded and there is an efficiency η_{exp} that must be considered. This efficiency yields a jet power P_{jet}, which is typically used in performance and scaling relations.

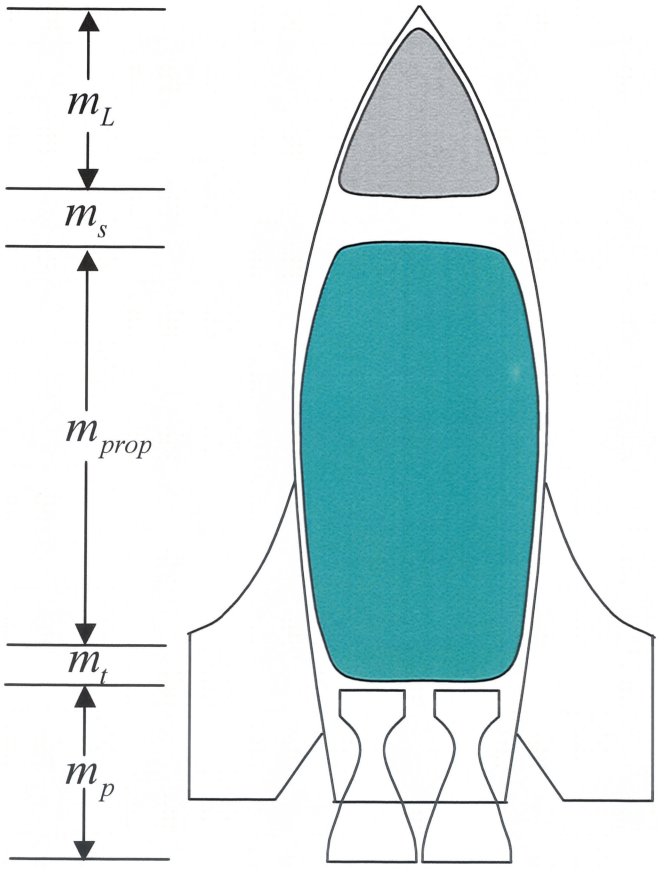

Figure 3.1 Mass breakout for a typical in-space vehicle

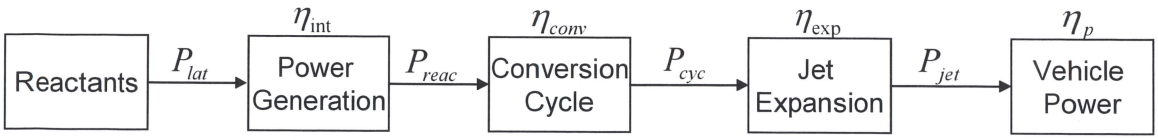

Figure 3.2 Power flow diagram for typical in-space vehicle

One might be tempted to equate the power of the jet with the power increase of the vehicle. Unfortunately that is not the case. If the jet velocity exceeds the instantaneous velocity of the vehicle from an inertial reference, then some of the jet power is lost. The lost power is proportional to the residual velocity the jet has relative to the inertial reference. Additionally, if the vehicle is moving faster than the exhaust velocity of the jet, then the jet still has some residual velocity relative to the inertial reference and some jet power is lost. The conversion efficiency from jet power to vehicle power is given in the following equation

$$\eta_p = \frac{2\frac{V}{V_e}}{1+\left(\frac{V}{V_e}\right)^2}, \tag{3.1}$$

where V is the vehicle velocity and V_e is the jet velocity. It is obvious from the above that the conversion efficiency η_p is unity only when the vehicle is at the exact same speed as the exhaust velocity. Thus the exhaust will have zero velocity relative to inertial space.

Combining all of the above efficiencies can easily be done and is shown in the equation below.

$$\eta_{tot} = \eta_{\text{int}}\eta_{conv}\eta_{\text{exp}}\eta_p . \tag{3.2}$$

This total efficiency is a key parameter in vehicle performance. Another is the specific power, alpha, shown below.

$$\alpha = \frac{P_{lat}}{m_p} \quad . \tag{3.3}$$

In many texts, specific power is shown as the inverse of the above equation. It is defined as shown here to be consistent with the use of the word "specific'. Specific is frequently used to indicate division by the relevant mass, such as specific volume is the volume of a gas divided by its mass. Other examples include specific enthalpy, specific heat and specific entropy.

Specific power is also defined using the jet power instead of the latent power. The relationship between the two is as follows.

$$\alpha = \frac{P_{lat}}{m_p} = \frac{P_{jet}}{\eta_{tot} m_p} \quad . \tag{3.4}$$

Another factor of importance in evaluating vehicle design is specific impulse. Specific impulse can be interpreted in several ways. First, it is the total impulse delivered by the engine divided by the weight at earth sea level of the propellant.

$$I_{sp} = \frac{\int_0^t F dt}{g_o \int_0^t \dot{m} dt} = \frac{I_T}{g_o m_p} \quad . \tag{3.5}$$

Specific impulse is usually given in seconds. When constant thrust is assumed, it is the ratio of thrust to weight flow rate of fuel as shown below.

$$I_{sp} = \frac{F}{g_o \dot{m}} \quad . \tag{3.6}$$

Thus specific impulse can be interpreted as the amount of time an engine can burn one lbf/s of fuel and produce on lbf of thrust.

We now have all of the information necessary to relate power, thrust and specific impulse. First, the jet power coming out of the engine is defined as

$$P_{jet} = \frac{1}{2}\dot{m}V_e^{\,2}, \tag{3.7}$$

where V_e is the exhaust velocity of the jet relative to the vehicle. Noting that

$$F = \dot{m}V_e + (p_{exit} - p_{amb})A_{exit}. \tag{3.8}$$

Here A_{exit} is the cross-sectional area of the engine nozzle at the exit plane and p_{exit} and p_{amb} are the jet pressure at the exit plane and the ambient freestream pressure, respectively. The second term in equation (3.8) is very small compared to the first in a properly designed engine. We neglect it here for convenience and because for missions in a vacuum the propulsion system is well expanded. Combining equations (3.6) and (3.8) yields

$$V_e = g_o I_{sp}. \tag{3.9}$$

Replacing terms in (3.7) with those in (3.8) and (3.9) yields

$$P_{jet} = \frac{1}{2}g_o I_{sp} F. \tag{3.10}$$

This relationship is very important. It indicates for a given jet power, which is limited by the specific power of the propulsion and power system, there is a tradeoff between specific impulse and thrust.

3.3 Ideal Rocket Equation

Consider the force balance on a vehicle on a flight trajectory as shown in Figure 3.3. The Ideal Rocket Equation, first derived by Konstantin Tsiolkovsky, can be developed by use of this force balance. This derivation is contained in several references [3], [4], [5]; however, none include all of the loss mechanisms given here.

Figure 3.3 illustrates several forces and angles of interest in vehicle performance. L and D are the vehicle lift and drag respectively. While they are usually not of great importance for in-space vehicles, they do sometimes appear in analysis and are included here for purposes of completion. F is the thrust generated by the vehicle propulsion system. The gravitational force is defined by mg: the instantaneous mass of the vehicle multiplied by the local gravitational vector. The velocity vector, V, illustrates the instantaneous direction and magnitude of flight. The flight path angle, γ, is the angle between the vehicle's velocity vector and the local ground horizontal. The vehicle angle of attack, α, is the angle between the vehicle reference line and the velocity vector. The thrust angle, δ, is the angle between the reference line and the thrust. The angle α' is a convenient angle used to define the difference between the thrust vector and the velocity vector.

Equation (3.11) gives the force balance for the vehicle in the directions parallel and perpendicular to the direction of flight.

$$M\frac{dV}{dt} = \left(F_{vac} - p_{amb}A_{exit}\right)\cos\alpha' - D - Mg\sin\gamma \tag{3.11}$$

$$MV\frac{d\gamma}{dt} = \left(F_{vac} - p_{amb}A_{exit}\right)\sin\alpha' + L - Mg\cos\gamma + \frac{V\cos\gamma}{r}$$

Note here the instantaneous thrust F has been replaced by the design vacuum thrust minus the force needed to push against the local ambient pressure, $p_{amb}A_{exit}$. Drag always acts against the direction of flight and the gravitational force has a component here. The combination of these forces defines the rate of change of the vehicle velocity, as shown on the left hand side. The perpendicular component has similar thrust and gravitational components except here drag is replaced by lift. Additionally there is a Coriolis acceleration that must be accounted with the last term on the right hand side. This term is neglected here, as the coordinate systems we use are nearly inertial. The sum of these forces accounts for the rate of change in the flight path angle, as defined on the right hand side.

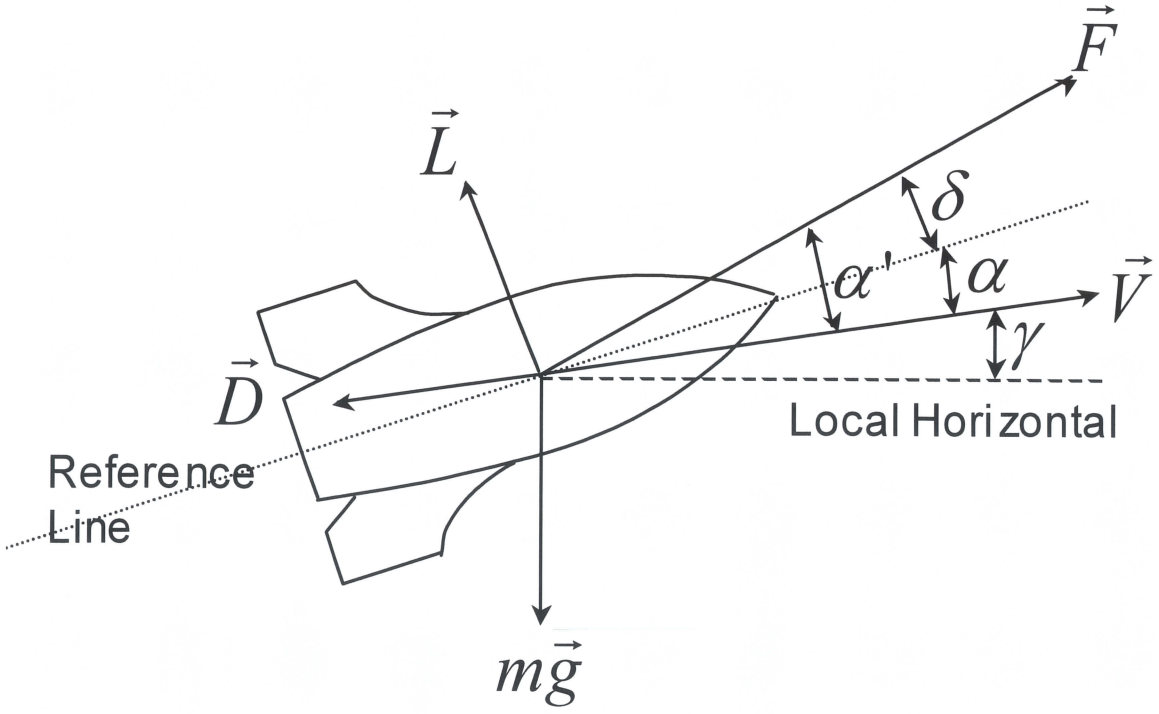

Figure 3.3 Free body diagram for a typical in-space vehicle

Concentrating on the parallel component for a moment, we can divide through by mass to obtain

$$\frac{dV}{dt} = \frac{F_{vac} - p_{amb}A_{exit}}{M} - \frac{F_{vac} - p_{amb}A_{exit}}{M}(1-\cos\alpha') - \frac{D}{M} - g\sin\gamma \tag{3.12}$$

Now by integrating over the total flight time from $t=0$ to $t=t_f$

$$\int_0^{t_f} dV = \int_0^{t_f}\frac{F_{vac}}{M}dt - \int_0^{t_f}\frac{F_{vac}}{M}(1-\cos\alpha')dt - \int_0^{t_f}\frac{D}{M}dt - \int_0^{t_f} g\sin\gamma dt - \int_0^{t_f}\frac{A_{exit}P_{amb}}{M}dt \tag{3.13}$$

We obtain a relationship for the change in velocity (ΔV) generated by the vehicle. The first part of the equation below is the ideal rocket equation, which is the maximum ΔV the vehicle can generate when there are no loss mechanisms.

$$\underbrace{\Delta V = g_o I_{sp}\ln\left(\frac{m_o}{m_f}\right)}_{\text{Ideal Rocket}} \underbrace{- \int_0^{t_f}\frac{F_{vac} - p_{amb}A_{exit}}{m}(1-\cos\alpha')dt}_{\text{steering}} - \tag{3.14}$$

$$\underbrace{\int_0^{t_f}\frac{D}{m}dt}_{\text{drag}} - \underbrace{\int_0^{t_f} g\sin\gamma dt}_{\text{gravitational}} - \underbrace{\int_0^{t_f}\frac{p_{amb}A_{exit}}{m}dt}_{\text{Atmospheric}}$$

Additionally, we have defined the losses that subtract from the total ΔV the vehicle generates for a particular mission. The drag loss is significant for launch vehicles but typically does not apply for in-space vehicles. Similarly there is little atmosphere that the propulsion system is expanding against, so the atmospheric pressure loss can also be neglected. The long mission times for most in-space trajectories require relatively small turning angles, thus steering losses are also neglected. Only the gravitational losses are

significant for the vast majority of in-space missions. However, as will be shown in later sections, the gravitational losses can dominate in many missions of interest.

3.4 Astrodynamics

As with vehicle mass properties, there are many different takes on the definitions pertaining to astrodynamics. Each reference uses a slightly different nomenclature; therefore, this treatise includes a general description of the astrodynamic terms and variables of interest to the research.

A vehicle that only undergoes acceleration due to a much more massive single body is defined as two-body motion [6]. This motion is of primary interest in most in-space applications as the vehicle is strongly affected by the planet (or sun) it is orbiting. Other astronomical bodies tend to only produce small perturbing forces on the vehicle. Neglecting the perturbing forces, the summation of forces on the vehicle is simply

$$\ddot{\vec{r}} = -\frac{\mu}{r^2}\left(\frac{\vec{r}}{r}\right), \tag{3.15}$$

where $\ddot{\vec{r}}$ is the vehicle acceleration and $\vec{r}$ is the vector from the center of mass of the massive body to the vehicle. This equation is frequently referred to as the trajectory equation. It is obvious from the above equation that the gravitational force is a function of the square of this radius vector. In the above equation μ defines the gravitational constant for the massive body. This value is the product of the mass of the body and the universal gravitational constant.

From equation (3.15) several other equations of primary interest can be derived. Taking the cross product of the above equation with respect to $\dot{\vec{r}}$ and integrating with respect to time yields

$$\vec{h} = \vec{r} \times \vec{V} = rV\cos\gamma = const., \tag{3.16}$$

where $\vec{h}$ is the vehicle angular momentum. This value is constant assuming no other forces act on the vehicle.

Similarly taking a dot product of equation (3.15) with respect to $\vec{r}$ yields

$$\xi = \frac{V^2}{2} - \frac{\mu}{r} = -\frac{\mu}{2a}, \tag{3.17}$$

where ξ is referred to as the specific orbital energy of the vehicle. It is the sum of the specific kinetic energy, shown as the first term in the above equation and the specific potential energy, shown as the second term. In deriving this equation, it is convenient to assume that the reference line for potential energy is at infinity. Thus all potential energies are negative. The right hand side of the equation expresses specific orbital energy as a function of the semi-major axis. It is found through a combination of equations (3.16) and (3.17).

Taking equation (3.17) and solving for velocity yields

$$V^2 = \mu\left(\frac{2}{r} - \frac{1}{a}\right). \tag{3.18}$$

This is a convenient form of the equation known as the vis-viva equation.

It is convenient to define a coordinate system to act as a reference for the position and velocity vectors mentioned above. The Earth Centered Inertial system shown in Figure 3.4 is commonly used for this sort of analysis. The x-axis starts at the center of

mass for the Earth and points through the first point of Aries. Aries is a fictitious star that would be located by going through the 0 longitude (Greenwich) line at noon on the first day of spring (vernal equinox). The z-axis starts at the center of mass for the Earth and points through the geometric North Pole. The y-axis is defined such as to complete a right hand system.

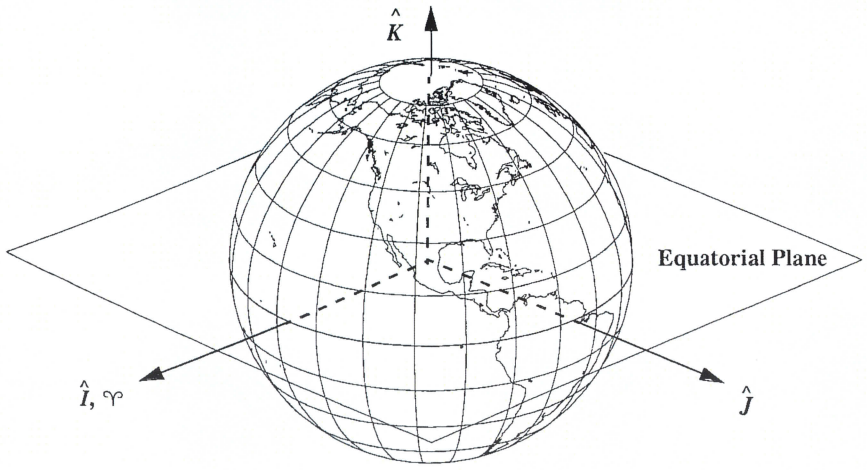

Figure 3.4 Earth Centered Inertial (ECI) coordinate system [6]

The Heliocentric coordinate system is found in Figure 3.5. Here, the X-axis is defined as the vector from the center of the sun through the center of the earth at the first point of Aries. The Y-axis is in the plane of the Earth's orbit around the sun rotated 90 degrees to the right. The Z-axis completes a right-handed system. This coordinate system is of primary relevance for the two-body studies in this treatise.

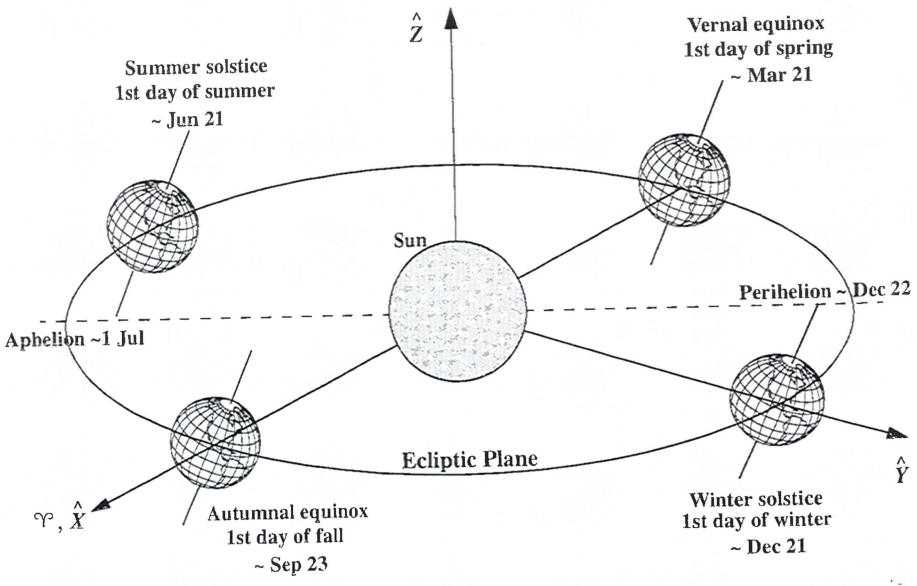

Figure 3.5 Heliocentric coordinate system [6]

A vehicle's position and velocity vectors define its orbit. Each of these vectors contains three elements that each change with respect to time. It is convenient to define a set of orbital elements that reduce the number of elements that change with respect to time. The Keplerian orbital elements [7], [8] are such a set and are popularly used in astrodynamics texts. These elements are depicted in Figure 3.6. Each orbital element is defined without proof below.

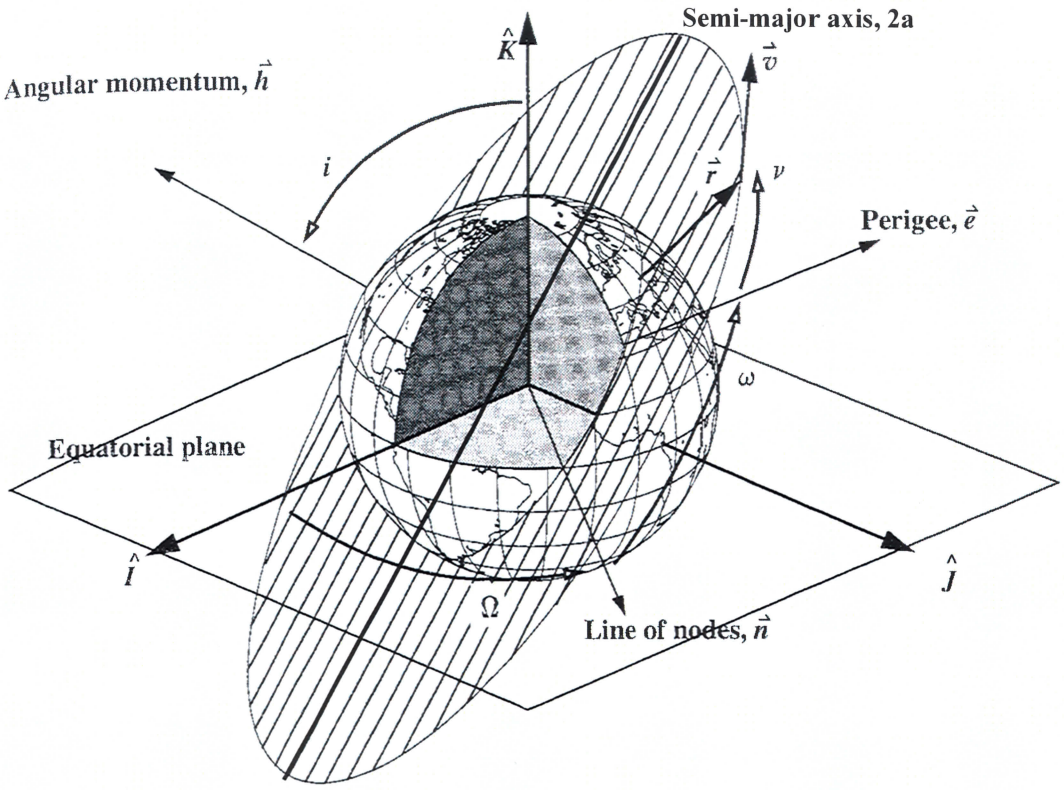

Figure 3.6 Keplerian six parameter system for orbit definition [6]

The semi-major axis, a, is the sum average of the orbital radius at periapsis and apoapsis. Here periapsis is the point of the orbit closest to the major body and apoapsis is the point furthest from the body. When the major body is Earth, these points are referred to as perigee and apogee. For the sun the points are perihelion and aphelion.

$$a = \frac{r_a + r_p}{2} \quad . \tag{3.19}$$

The eccentricity, e, is a measure of the 'oblateness' of the orbit. It is defined as

$$e = \frac{r_a - r_p}{r_a + r_p} \quad . \tag{3.20}$$

A circular orbit has an eccentricity of zero. Thus a circular orbit would have a periapsis and apoapsis equal in magnitude. Elliptical orbits have eccentricities between 0 and 1. An eccentricity equal to unity indicates a parabolic orbit. An eccentricity greater than unity indicates a hyperbolic orbit.

The orbital inclination, i, is defined as the angle between the orbital plane and the ecliptic plane. It is also determined by the angle between the orbital angular momentum and the Z-axis.

The argument of perigee, ω, is the angle between the line of nodes and the perigee point.

The longitude of the ascending node, Ω, is the angle between the x-axis and the point of the trajectory that intersects the x-y plane. In all but co-planar orbits (zero inclination), there will be two points of intersection between the orbit and x-y plane. Therefore the point where a vehicle on this orbit will ascend from below to above the x-y plane is used here.

The true anomaly, υ, is the angle determining the current position of the vehicle relative to the radius vector pointing to periapsis.

The time of perigee passage, T, is a time when the vehicle passed the periapsis point. Knowing the difference between current time and time of perigee passage locates the vehicle on the orbit.

Using the definitions for orbital elements, one can derive the rates of change of these elements when the vehicle is accelerated by additional forces. The details of finding the rates of change of the elements are fairly complicated. The results are the Lagrange variational equations [7]. These equations are defined below without proof.

$$\frac{\partial a}{\partial t} = \frac{2aF_t}{V} \tag{3.21}$$

$$\frac{\partial e_x}{\partial t} = \frac{2F_t \cos\alpha}{V} - \frac{F_n \cos\alpha}{V} \tag{3.22}$$

$$\frac{\partial e_y}{\partial t} = \frac{2F_t \sin\alpha}{V} + \frac{F_n \cos\alpha}{V} \tag{3.23}$$

$$\frac{\partial i}{\partial t} = \frac{F_h \cos\alpha}{V} \tag{3.24}$$

$$\frac{\partial \Omega}{\partial t} = \frac{F_h \sin\alpha}{V \sin i} \tag{3.25}$$

$$\frac{\partial \alpha}{\partial t} = n + \frac{2F_n}{V} - \frac{F_h \sin\alpha}{V \tan i} \tag{3.26}$$

The solution to equations (3.21)-(3.26) depend upon the magnitude and direction of the perturbing force. The force may be broken into components in the tangential, normal and out of plane directions using the mean position defined as

$$\alpha = \omega + M \tag{3.27}$$

and the out of plane yaw angle, β. The thrust components tangential, normal and out of plane to the current orbit are

$$F_t = F\cos\beta\cos\alpha \tag{3.28}$$

$$F_n = F\cos\beta\sin\alpha \tag{3.29}$$

$$F_h = F\sin\beta \tag{3.30}$$

The above Keplerian orbital elements are limited in their use. They tend to asymptotic values when the orbit is nearly circular or equatorial or both. Equinoctial

elements [6] were defined to overcome these limitations. They are defined without proof below.

$$k_e = e\cos(\omega + f_r\Omega) \tag{3.31}$$

$$h_e = e\sin(\omega + f_r\Omega) \tag{3.32}$$

$$p_e = \frac{\sin i \sin\Omega}{1+\cos i} \tag{3.33}$$

$$q_e = \frac{\sin i \cos\Omega}{1+\cos i} \tag{3.34}$$

$$\lambda_M = M + \omega + f_r\Omega \,. \tag{3.35}$$

These elements are combined with the longitude of periapsis ω to make a six element set. In the set only λ_M is a "fast" element, i.e., it is the only one that changes rapidly.

Note that the equinoctial elements are still limited by the possibility of retrograde orbits. Thus a factor has been included that handles necessary sign changes for retrograde orbits. It is defined as

$$f_r = \begin{cases} 1 & direct \\ -1 & retrograde \end{cases}. \tag{3.36}$$

3.5 General Trajectory Analysis

Computing a trajectory for an in-space vehicle requires an extensive amount of data. Most of this data is independent of the vehicle and the type of trajectory. Thus, it can be modified to optimize the trajectory. The data input can be broken down into three categories, mass properties, guidance and thrust schedule, and departure/arrival dates.

First are the vehicle mass properties. This was defined in an earlier section. Additionally, parts of a mission may require instantaneous changes in vehicle mass in the form of dropped stages or components or deployment and acquisition of payloads.

Second is the guidance and thrust schedule. The orientation of the vehicle and its thrust vector with respect to time, in conjunction with the times and magnitudes of vehicle thrust, will determine the vehicle's flight path. This guidance schedule should be optimized so that the vehicle reaches its target destination with minimum losses. Additionally, the vehicle's engines may be capable of throttling, changing the thrust magnitude. Coast phases are frequently built into the trajectory to save propellant (and thereby vehicle mass) at the expense of additional trip time. Throttle and coast schedule must also be optimized in conjunction with the guidance schedule to minimize trajectory losses.

Finally, a trajectory is defined by the departure and arrival dates for each mission design point the vehicle will visit. Figure 3.7 illustrates an example of this list of variables. As an example, for a round trip from Earth to Mars, the Earth departure date, Mars arrival date, Mars departure date, and Earth arrival date must be defined. Since these planets are constantly moving relative to one another, these dates are of critical importance. Usually, the mission planner does not require a given departure or arrival time ahead of time, so the trajectory analyst optimizes these variables to give the least energy result. Limitations may be placed on the time difference between Mars arrival and Mars departure to limit planet stay time. The trajectory analyst must account for the heliocentric trip time as well as possible spiral out and spiral in times at departure and arrival. These spiraling times are affected by the initial and final orbits and are also

optimized relative to constraints placed by the mission planner. Additional energy can be gained by fly-bys that generate gravity assists. The trajectory analyst must optimize arrival and departure points to take advantage of this opportunity.

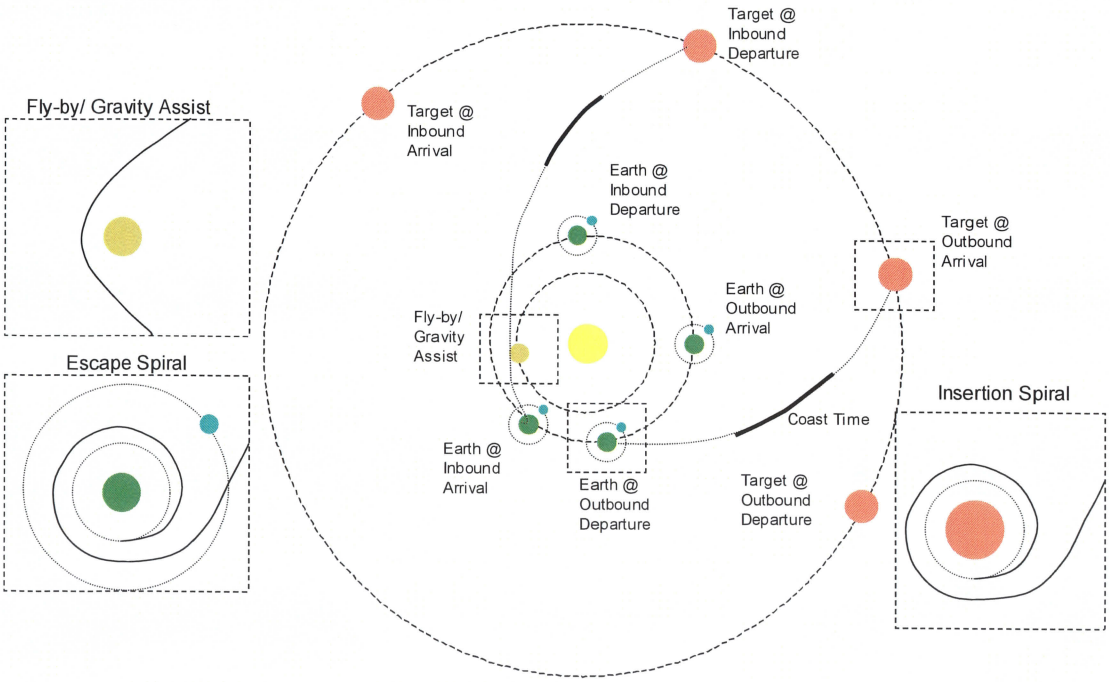

Figure 3.7 Definition of trajectory variables for in-space mission

As was mentioned in the introductory material on propulsion systems, the vehicles on which those systems are placed, and their corresponding trajectories are classified as high thrust, medium thrust or low thrust. The reason for this classification can be found by examining equation (3.10), repeated below for convenience.

$$P_{jet} = \frac{1}{2} g_o I_{sp} F \qquad (3.37)$$

For a given jet power, there is an inverse relationship between specific impulse and thrust. The attainable jet power is a function of the alpha of the power and propulsion system. The propulsion system has to carry, at minimum, itself along the trajectory. To be used, it must also carry of payload, structural mass, tanks, etc. The total energy related to the trajectory accounts for transfer orbit requirements and gravitational and other losses. The jet power integrated over the thrusting time must be sufficient to meet the trajectory energy requirement. Scaling up the propulsion system increases the available jet power but also increases the energy required to achieve the mission. Thus there is a minimum propulsion system size that meets the power requirements of the trajectory.

The trajectory is largely dictated by the selection and performance of the propulsion system. A high thrust system accelerates a vehicle in minimal time. High thrust trajectories have minimal losses, thus their trajectories tend to have the lowest energy requirements. A system that has low thrust levels must burn longer to generate the same accelerations and therefore experience higher gravitational losses. These gravitational losses can double or triple the total energy requirements. Why use a low thrust system then? Considering equation (3.10) again, we see that these low thrust systems can achieve much higher specific impulses than those of high thrust systems. Vehicles powered by low thrust systems are not dominated by propellant, like high thrust systems, but by their power and propulsion systems. In most cases, the linear relationship between propulsion and power system and vehicle size is more attractive than the exponential relationship between propellant mass and vehicle size. Thus the expense of a trajectory is small relative to that of a more efficient (albeit larger) propulsion system.

Low-thrust systems can still require significant time and mass to achieve high-energy trajectories. Accelerating out of a planetary gravitational well can add years to the required time of flight for a low thrust trajectory. For short interplanetary missions (to Mars or Venus), high thrust systems are still competitive.

Medium thrust systems attempt to have the high thrust with the high specific impulse. To do so, these systems must achieve higher specific powers and thus higher jet powers for a given mission. Thus medium thrust systems are usually associated with advanced propulsion and power systems. These systems are still in the early developmental stages. It is the intent of this treatise to analyze their complex trajectory requirements. A closed-form solution for their trajectories would be useful as a guide to developers in finding the most attractive specific impulse – specific power trades for these promising propulsion and power systems.

3.6 High-Thrust Approximation

As mentioned above, high-thrust systems typically have low specific impulses and high specific powers. Table 3.1 contains a chart of propulsion concepts commonly identified as high-thrust and their respective performance values. These propulsion systems invariably heat a propellant to high temperatures and then expand the heated gas for thrust. The heat source can be the propellant latent energy (chemical) or an external nuclear reactor or solar collector. The achievable specific impulse is limited by the expansion process which depends on the peak chamber pressure temperature and pressure [2]. This relation is shown without proof in equation (3.38).

Table 3.1 Typical High Thrust propulsion concepts and performance

Concept	**Isp**	**α**	**F/Weng**
	(sec)	**(kW/kg)**	**(kN/kN)**
Chemical [2]			
Storable (N2O4/UMDH)	320	1650	110
Lox/RP	340	1400	95
Lox/LH2	450	1200	55
Nuclear Thermal			
Solid Core [3]	900	100	2
Liquid Core [9]	1500	160	2
Gas Core [9]	5000	10	0.04
Solar Thermal [10]	800	1	0.01

$$V_e = \sqrt{\frac{2\gamma}{\gamma - 1}\frac{R_u}{MW}\left(1 - \frac{p_{exit}}{p_c}\right)^{\frac{\gamma-1}{\gamma}}}, \tag{3.38}$$

where γ is the ratio of specific heats, R_u is the universal gas constant, MW is the propellant molecular weight, p_e is the nozzle exit pressure and p_c is the engine chamber pressure. Note that specific impulse is also an inverse function of molecular weight. This is the reason why so many high thrust systems use hydrogen, the lowest molecular weight element, as fuel.

High-thrust trajectories are relatively simple to calculate and plot. In fact, high-thrust systems are most often calculated assuming the thrusting time is instantaneous. Thus, the trajectory is calculated using a Kepler or Universal propagator. These propagation methods are well covered in the literature [7], [11] and are only briefly considered here.

Two of the most common transfer orbits used on the two-body approximation are the Hohmann and bi-elliptic transfer orbits. The Hohmann transfer is an elliptical transfer orbit where the perigee of the transfer orbit touches the inner initial orbit and the apogee of the transfer just touches the final orbit. The velocities of the initial orbit and transfer orbit at perigee can be calculated using equation (3.18), repeated for convenience below.

$$V^2 = \mu\left(\frac{2}{r} - \frac{1}{a}\right). \tag{3.18}$$

Note the radius magnitude r is the same for both orbits, but the semi-major axis is not. The difference between the two velocities is the ΔV required to inject into the transfer orbit. Similarly equation (3.18) can be used to calculate the difference in velocities between the apogee of the transfer orbit and the final circular orbit. The difference is the ΔV necessary to inject into the final orbit. The Hohmann transfer orbit is illustrated in Figure 3.8.

For many years, the Hohmann orbit was believed to be the most efficient transfer method available. However, it was later found that in cases when the ratio of outer and inner orbit radii is sufficiently high, the bi-elliptic transfer has lower energy requirements. Figure 3.8 also illustrates the bi-elliptic transfer. Bi-elliptic transfers that do not require inclination changes are more efficient than Hohmann transfers when the ratio of final to

initial orbit radii is over 12. With inclination changes the breakeven point is lower as the majority of the inclination change can be made at the intermediate orbit where the vehicle velocity is lower and therefore easier to turn.

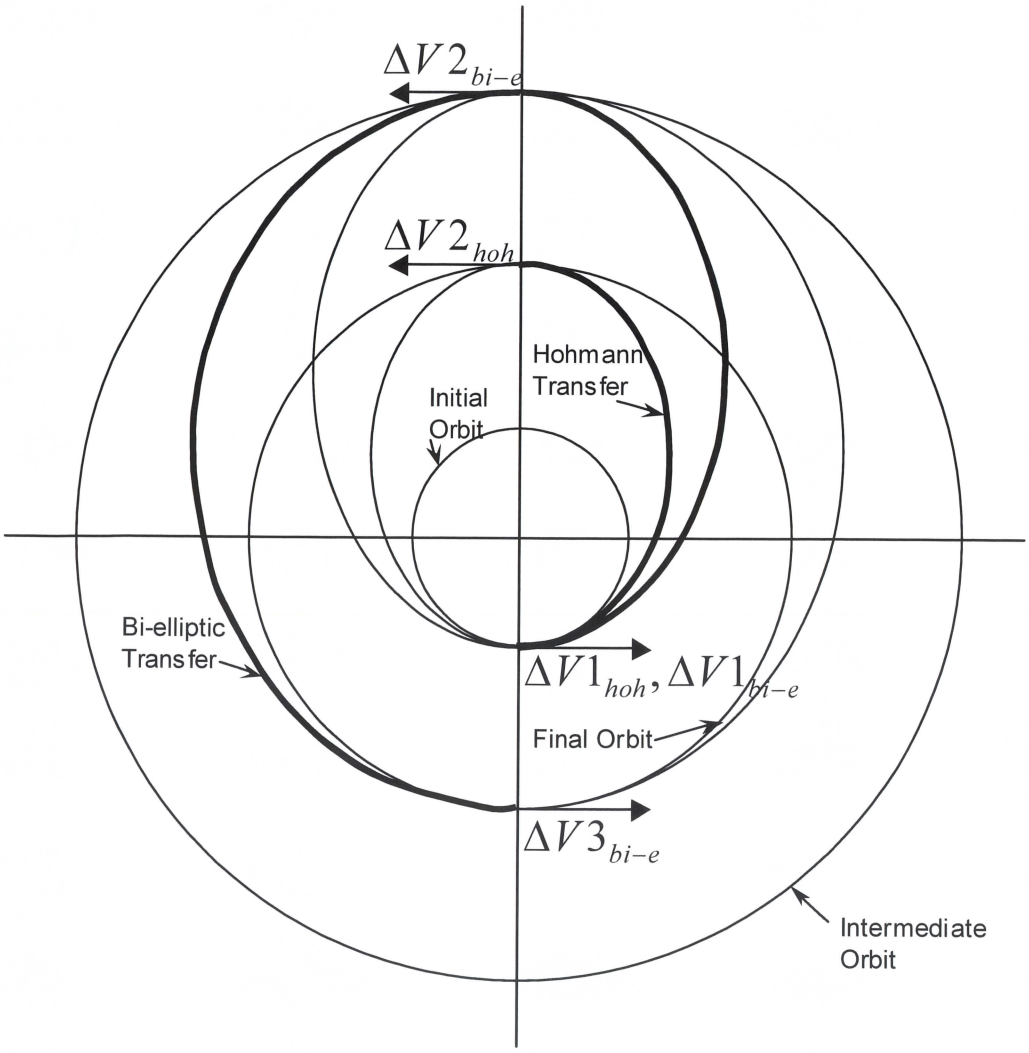

Figure 3.8 Hohmann and bi-elliptic transfer options

The actual flight path and time of flight for these transfer options are simply found. First, the orbit period is determined using the equation,

$$P = \frac{2\pi}{\sqrt{\mu}} a^{\frac{3}{2}} \tag{3.39}$$

The semi-major axis is found using equation (3.19). The periapsis radius and apoapsis radius are equal to the initial and final orbits. The periods of the two segments of the bi-elliptic transfer are also easily found. The semi-major axes for each segment are found using the initial and intermediate orbit radii and the intermediate and final orbit radii respectively. The time of flight, τ, is exactly half the orbital period for the Hohmann transfer or the segments of the bi-elliptic transfer as shown below.

$$\tau_{Hoh} = \frac{\pi}{\sqrt{\mu}} a^{\frac{3}{2}} \tag{3.40}$$

$$\tau_{bi-e} = \frac{\pi}{\sqrt{\mu}} a_1^{\frac{3}{2}} + \frac{\pi}{\sqrt{\mu}} a_2^{\frac{3}{2}} \tag{3.41}$$

Calculating the position with respect with time is a little more involved. The mean anomaly, *M*, defined below, can be calculated as a function of time. The eccentric anomaly, *E*, is also defined in the equation below. Determining the eccentric anomaly from the mean anomaly requires determination of the orbital eccentricity from equation (3.20).

$$M = \sqrt{\frac{\mu}{a^3}}(t - T) + M_0 = E - e\sin E \tag{3.42}$$

The true anomaly is determined by knowledge of the eccentric anomaly and the eccentricity.

$$\tan\frac{\upsilon}{2} = \sqrt{\frac{1+e}{1-e}} \tan\frac{E}{2} \tag{3.43}$$

The radius can then be calculated by using the true anomaly plus the semi-major axis and the eccentricity, determined previously. The true anomaly and radius are sufficient to determine the position of the vehicle with respect to time in the orbital plane.

$$r = \frac{a\left(1-e^2\right)}{1+e\cos\upsilon}. \tag{3.44}$$

Note that the above technique does not locate the orbital plane with respect to the ECI or heliocentric coordinate system.

A third option for high thrust transfer between two circular orbits is the semi-tangential transfer [7], [11]. This option is illustrated in Figure 3.9.

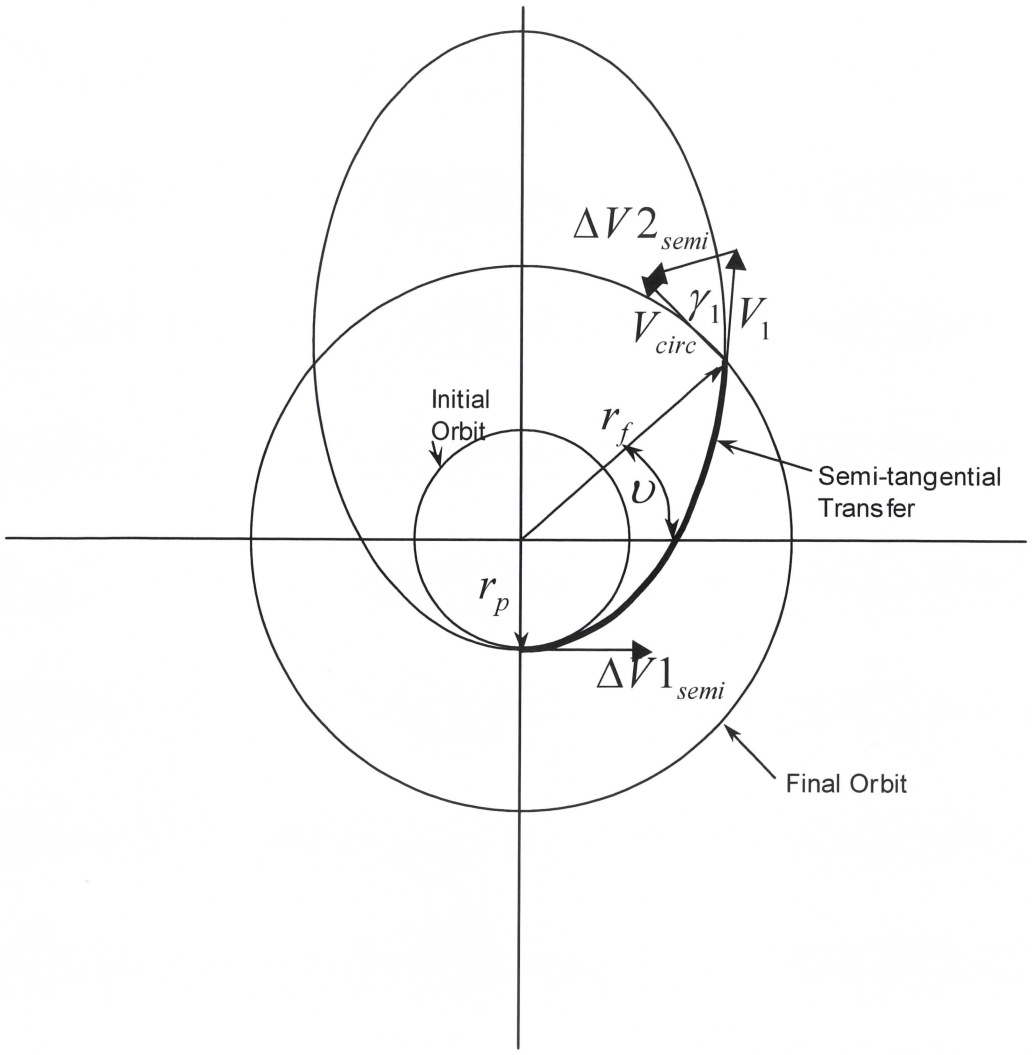

Figure 3.9 Semi-tangential transfers for high thrust trajectories

The semi-major axis of the transfer ellipse after the first burn is

$$a = \left(\frac{2}{r_p} - \frac{V_p^2}{\mu} \right)^{-1} . \tag{3.45}$$

This equation is simply equation (3.18) solved for semi-major axis. Note that this semi-major axis is larger than that for a Hohmann transfer. The eccentricity is simply calculated with

$$e = 1 - \frac{r_p}{a} \tag{3.46}$$

The true anomaly at the intersection point can be calculated using

$$\cos \upsilon_1 = \frac{1}{e}\left(\frac{a\left(1-e^2\right)}{r_f} - 1 \right) \tag{3.47}$$

And the flight path angle at the intersection point is shown as

$$\cos \gamma_1 = \frac{e \sin \upsilon_1}{1 + e \cos \upsilon_1} \tag{3.48}$$

The flight path angle is necessary to calculate the ΔV necessary to insert into the final orbit. The velocity of the vehicle along the transfer orbit is found using equation (3.18). The velocity of the final orbit is similarly found. Thus these velocities and the flight path angle can be inserted into the law of cosines below to calculate the ΔV for the second maneuver.

$$\Delta V^2 = V_1^2 + V_{circ}^2 - 2V_1 V_{circ} \cos \gamma_1 \tag{3.49}$$

As seen above, high thrust trajectory simulation has been well explored in the literature. However several issues still remain in how it pertains to mission analysis. Understanding the maximum ΔV that can be produced for a given I_{sp} and α. Similarly the sensitivity of the vehicle payload ratio m_L/m_0 and time of flight, τ, to I_{sp} and α is yet to be explored. The maximum burn time as a function of I_{sp} and α is also important for comparison with low and medium thrust trajectories.

3.7 Low Thrust Approximation

Low thrust propulsion systems typically have high specific impulses and low specific powers relative to the high thrust propulsion systems. Table 3.2 lists several propulsion technologies generally considered to be in the low thrust category. Electrothermal systems heat a propellant using electrical discharges and then are expanded for thrust. In this manner, they are similar to the thermal operation of high thrust systems. The electrostatic systems accelerate charged particles in the propellant with a difference in electrical potential. Electromagnetic systems similarly accelerate charged particles in the propellant, this time using electromagnetic forces. Other systems use interactions with solar photonic energy (solar sails) or the solar wind (plasma sails) to produce an accelerating force. These engines tend to produce thrusts much lower than the local gravitational acceleration. Thus, propulsive accelerations can be treated as perturbations to a coasting trajectory. This approach is completely different than that for high thrust systems.

Table 3.2 Typical low thrust propulsion concepts and performance

Concept		**Isp**	**α**	**F/Weng**
		(sec)	**(kW/kg)**	**(kN/kN)**
Nuclear Electric [9]				
	Electrothermal (Arcjets)	850	0.05	0.001
	Electromagnetic (MPD)	5,000	0.025	0.0001
	Electrostatic (Ion)	10,000	0.005	0.00001

Table 3.2 Cont.

Concept		Isp	α	F/Weng
		(sec)	(kW/kg)	(kN/kN)
Solar Electric (@ 1AU) [2]				
	Electrothermal	850	0.025	0.0005
	Electromagnetic	5,000	0.012	0.00005
	Electrostatic	10,000	0.0025	0.000005
Solar Sail (@ 1 AU) [12]			200	0.0001
Plasma Sails [13]		80,000	200	0.05
LAPPS [14]		8,000,000	0.01	2.5*10-11

The trajectory equation, equation (3.15), assumes that the only gravitational forces apply to the vehicle. Polar non-dimensional equations of motion [15] can be derived that include the perturbing force of a low thrust propulsion system. These equations are

$$\frac{d^2\rho}{d\tau'^2} = F_t + \rho\left(\frac{d\theta}{d\tau'}\right)^2 - \frac{1}{\rho^2} \tag{3.50}$$

$$\frac{d}{d\tau'}\left(\rho^2 \frac{d\theta}{d\tau'}\right) = F_r \tag{3.51}$$

,

where

$$\rho = \frac{r}{r_o} \quad \tau' = \sqrt{\frac{g}{r_o}}\tau \tag{3.52}$$

.

The solution of these equations is covered in the following pages. Historically interested parties applied themselves first to escape trajectories from Earth and then to

interplanetary solutions. Given the non-dimensional nature of these equations, they are generally applicable to both planet-centric and heliocentric scenarios as long as the two-body assumption applies.

Tsien found one of the first solutions to the low thrust problem in 1953 [16]. A solution to the above equation can be found by assuming a constant acceleration continually operating in a particular direction. Tsien first applied this assumption in a direction radially outward from the central body. The time of flight equation is

$$\tau = \sqrt{\frac{2}{\mu'}}\left[\frac{\sqrt{2(\mu'+1)}}{2\mu'+1} + F\left(\frac{1}{\sqrt{8\mu'}}, \cos^{-1}\frac{2\mu'-1}{2\mu'+1}\right) + E\left(\frac{1}{\sqrt{8\mu'}}, \cos^{-1}\frac{2\mu'-1}{2\mu'+1}\right)\right]. \tag{3.53}$$

Here the constant acceleration is represented by μ'. F and E are the first and second elliptic integrals. Using the time of flight above the ratio of initial to final mass can be determined by

$$\ln\left(\frac{m_o}{m_f}\right) = \frac{\sqrt{gr_o}}{g_o I_{sp}}\mu'\tau \tag{3.54}$$

Tsien also applied a constant acceleration ν', circumferential to the direction of the gravity gradient [17]. The time of flight equation under this assumption is

$$\upsilon'\tau_1 = 1-(2\upsilon')^{1/4} = \frac{g_o I_{sp}}{\sqrt{gr_o}}\ln\left(\frac{m_o}{m_f}\right). \tag{3.55}$$

The ratio of initial to final mass is also defined above.

It is worth exploring the constant acceleration and constant thrust angle assumptions used above. The constant thrust angle assumption is an interesting premise. Acceleration in the circumferential direction would avoid gravitational losses. This can be seen by an investigation of equation (3.14). A circumferential direction would yield a

flight path angle of zero and thus no contribution from the gravitational term. At first glance this would indicate that thrust in the circumferential direction would be optimal. It will be seen later that this is not true. A constant acceleration assumes that the jet power drops as propellant is expelled along the trajectory. For the high specific impulse systems considered in this system, the change in vehicle mass is less substantial than in comparable high thrust systems. For a first approximation, an average acceleration over the trajectory is frequently used.

Levin derived similar results to Tsien for directions tangential and normal to the flight path [17]. For constant acceleration α' in the tangential direction, the resulting time of flight and mass ratio are

$$\alpha'\tau \approx 1-\left(20\alpha'^{2}\right)^{1/8} = \frac{g_o I_{sp}}{\sqrt{g r_o}} \ln\left(\frac{m_o}{m_f}\right). \tag{3.56}$$

Levin also determined that constant acceleration α' in the direction normal to the flight path did not enable an escape trajectory [18]. Thrust in this direction did not add to the specific energy of the orbit but merely modified the orbit's eccentricity. The maximum eccentricity of this method is given as

$$e = 2\alpha'. \tag{3.57}$$

All of these methods presume a thrust angle. Determining the thrust angle that is optimal for escape trajectories can be found with the use of Lagrangian multipliers [18], [19]

$$\frac{\partial}{\partial\alpha}\frac{\partial}{\partial\beta}\left[\frac{da}{dt}\frac{1}{a_o} + \lambda_1\frac{de}{dt} + \lambda_2\frac{di}{dt}\right] = 0 \tag{3.58}$$

Here, the Lagrangian multipliers λ_1 and λ_2 are manipulated to target required changes in semi-major axis, eccentricity and inclination. The solution of the above equation yields relations for an optimal flight path angle.

$$\tan \alpha_{opt} = \frac{\lambda_1 \sin \upsilon}{2(1+\cos \upsilon)} \tag{3.59}$$

$$\tan \beta_{opt} = \frac{\lambda_2 \cos(\omega + \upsilon)}{\sqrt{4(1+\lambda_1 \cos \upsilon)^2 + \lambda_1 \sin^2 \upsilon}} . \tag{3.60}$$

From equation (3.58) it is obvious that if changes in semi-major axis only is desired, the Lagrangian multiplier λ_1 is zero and the optimal flight path angle is zero. This provides the tangential approximation. If only changes in eccentricity are required, then λ_1 is infinite and the thrust vector is perpendicular to the flight path and the normal approximation is obtained.

For escape

$$\tan \alpha_{opt} = 1/2 \tan \upsilon . \tag{3.61}$$

The justification for constant acceleration being optimal for low thrust trajectories is found in many references [20], [21] and generally is based on the following explanation. The thrust is defined by equation (3.8) and is balanced by the mass of and acceleration experienced by the vehicle. Jet power was defined by equation (3.10). Combining the two equations yields

$$V_e^2 = \frac{2m_{prop}}{\alpha \dot{m}} . \tag{3.62}$$

In the above, the specific power is defined as propulsion system mass divided by jet power. This is the only time the specific power used in this treatise differs from the definition in equation (3.4). Combining the above with equation (3.8) yields

$$\frac{\dot{m}}{M^2} = \frac{\alpha}{2m_{prop}} a^2 \quad . \tag{3.63}$$

Integrating both sides over the burn time and realizing that M equals the vehicle initial mass, M_i, at t=0 and the vehicle final mass, M_f, at t=t_b yields

$$\frac{1}{M_f} = \frac{1}{M_f} + \frac{\alpha}{2m_{prop}} \int_0^{t_b} a^2 dt \tag{3.64}$$

The integral is usually designated by J. The integral is minimized when acceleration is constant over the burn time. And from this equation, it is clear that minimizing the integral maximizes the final mass of the spacecraft for a given initial mass.

Another common assumption is that acceleration will be constrained to be in the tangential direction; or in other words, the acceleration vector is parallel to the velocity vector. A reasonable explanation is given by Battin [22]. Given

$$\vec{V}_g = \vec{V}_r - \vec{V} \quad , \tag{3.65}$$

where $\vec{V}_r$ is the velocity required to meet the mission objectives, $\vec{V}$ is the current vehicle velocity and $\vec{V}_g$ is the velocity to be gained, the vehicle is undergoing the following accelerations

$$\frac{d\vec{V}}{dt} = g(\vec{r}) + \vec{a}_T \quad , \tag{3.66}$$

where $g(\vec{r})$ is the acceleration due to the attraction of the central body and $\vec{a}_T$ is the acceleration vector due to thrust and any other perturbative forces.

Taking the derivative of equation (3.65) yields

$$\frac{d\vec{V}_g}{dt} = \frac{d\vec{V}_r}{dt} - \frac{d\vec{V}}{dt} \quad . \tag{3.67}$$

Combining the last two equations results in

$$\frac{d\vec{V}_g}{dt} = \frac{d\vec{V}_r}{dt} - \left(g(\vec{r}) + \vec{a}_T\right) \quad . \tag{3.68}$$

The chain rule on $\vec{V}_r$ is

$$\frac{d\vec{V}_r}{dt} = \frac{\partial \vec{V}_r}{\partial t} + \frac{\partial \vec{V}_r}{\partial \vec{r}}\frac{\partial \vec{r}}{\partial t} = \frac{\partial \vec{V}_r}{\partial t} + \frac{\partial \vec{V}_r}{\partial \vec{r}}\vec{V} \quad . \tag{3.69}$$

Substituting back into the previous equation yields

$$\frac{d\vec{V}_r}{dt} = \frac{\partial \vec{V}_r}{\partial t} + \frac{\partial \vec{V}_r}{\partial \vec{r}}\left(\vec{V}_r - \vec{V}_g\right) \quad . \tag{3.70}$$

Now define

$$\vec{p} = \frac{\partial \vec{V}_r}{\partial t} - g(\vec{r}) \quad . \tag{3.71}$$

And note that

$$\vec{a}_T \times \vec{V}_g = \vec{p} \times \vec{V}_g \quad . \tag{3.72}$$

Which can be seen by substituting

$$\left(\frac{\partial \vec{V}_r}{\partial t} - g(\vec{r}) - \frac{\partial \vec{V}_g}{\partial t}\right) \times \vec{V}_g = \left(\frac{\partial \vec{V}_r}{\partial t} - g(\vec{r})\right) \times \vec{V}_g \quad . \tag{3.73}$$

Equation (3.73) is only true if

$$\frac{\partial \vec{V}_g}{\partial t} \times \vec{V}_g = \vec{0} \quad . \tag{3.74}$$

Thus the acceleration is along the velocity vector. Commonly referred to as cross product steering, accelerating in line with the velocity vector is believed to be locally optimal. Another way to look at it is to consider the following equation.

$$\frac{dE}{dt} = \vec{V} \cdot \vec{a} \tag{3.75}$$

So parallel acceleration will maximize the rate of change of the energy of the accelerating vehicle. However this equation is worth more scrutiny. The rate of energy change is also proportional to the magnitude of the current velocity. It will be shown in Chapter 5 that in some cases it is worthwhile to fly a trajectory that will initially have a negative energy change so as to perform a burn at a higher velocity at a later point.

Interestingly, several authors have supplied guidance schedules that do not assume tangential acceleration. Using variation of parameters, Lawden [23] derived the following guidance schedule

$$\tan\varphi = \frac{V_f - g(T-t)}{V_i} \tag{3.76}$$

where V_i and V_f are the initial and final desired velocity of the vehicle, T is the total burn time and t is the instantaneous time. The derivation is extensive and is not included here.

Chobotov [7] uses calculus of variation in combination with the Lagrange variational equations to come up with

$$\tan\beta_0 = \frac{\sin\left(\frac{\pi}{2}\Delta i\right)}{\frac{V_0}{V} - \cos\left(\frac{\pi}{2}\Delta i\right)} \tag{3.77}$$

Here β is the yaw angle necessary to generate the required inclination change Δi. This guidance schedule addresses the need for an inclination change, but not the angle of acceleration necessary for raising or lowering an orbit. It also does not include gravity losses.

The above formulations were developed with the intent to escape from Earth's orbit. These equations have broader application to escape and capture from other planetary bodies and the sun.

Interplanetary trajectories do not endeavor to escape but to maneuver from one planet to another. In can be shown that for accelerations that drop off with the square of the distance from the central body the position and time of flight for these trajectories are

$$r(\upsilon) = r_o \exp(\upsilon \tan\alpha) \tag{3.78}$$

$$TOF = \frac{1}{3}\left(r^{3/2} - r_o^{3/2}\right)\sqrt{\frac{1-\beta'\cos^3\alpha}{\beta'^2\,\mu\cos^4\alpha\sin^2\alpha}} \tag{3.79}$$

These trajectories represent a logarithmic spiral [24] around the central body. They are most applicable to solar sails where the level of thrust produced by the sail is proportional to the inverse square of the distance from the sun.

Most interplanetary trajectory solutions incorporate numerical methods. Encke's formulation is one such method [6]. Instead of integrating all forces of a trajectory, this method only integrates the perturbing forces on the vehicle. Thus, the orbit is propagated assuming a non-changing orbit. This orbit is periodically rectified with the effects of the perturbing forces. The methodology of Encke's formulation is shown in Figure 3.10. The equation for calculating the effects of the perturbative forces is shown below.

$$\delta\ddot{\vec{r}} = \vec{a}_p + \frac{\mu}{r^3}\left[\left(1 - \frac{r^3}{r_p^3}\right)\vec{r}_p - \delta\vec{r}\right]. \tag{3.80}$$

Here $\vec{a}_p$ is the perturbative acceleration, caused by a low thrust propulsion system for our purposes.

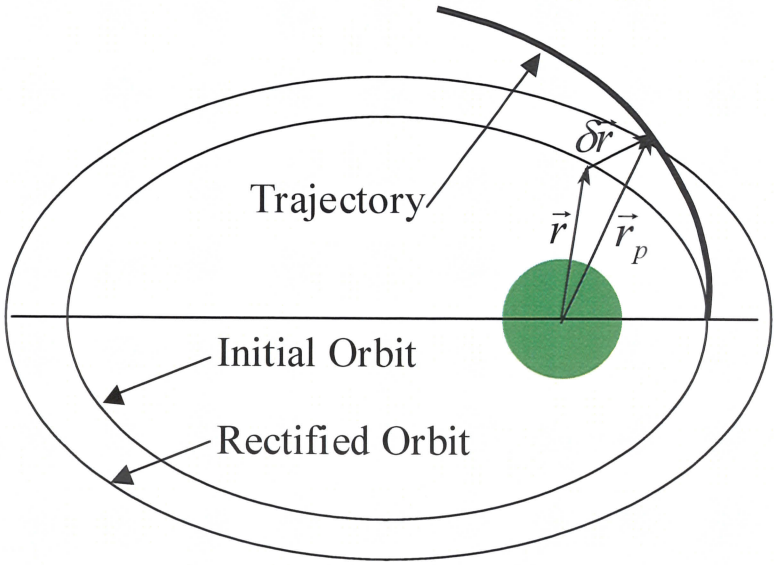

Figure 3.10 Encke's formulation for propagation of low thrust trajectories

A very common method for calculating an interplanetary trajectory involves solution of the Chebyshev partial differential equation [25], [26]. First, the equation of motion is identified as

$$\ddot{x}(t) + \frac{\mu x(t)}{\left|x^3(t)\right|} = a^2(t) \tag{3.81}$$

The right hand side is related to the J integral as defined in equation (3.64). So substituting into the integral yields

$$J = \int_0^{t_b} \left(\ddot{x}(t) + \frac{\mu x(t)}{\left| x^3(t) \right|} \right)^2 dt \tag{3.82}$$

Defining

$$s = \frac{t}{t_b} \tag{3.83}$$

Given that it is simple to derive

$$ds = \frac{dt}{t_b} \tag{3.84}$$

Define

$$J = 2t_b^{-3} P \tag{3.85}$$

So

$$J = 2t_b^{-3} P = t_b \int_0^1 \left(\frac{\ddot{x}(s)}{t_b^2} + \frac{\mu x(s)}{\left| x^3(s) \right|} \right)^2 ds \tag{3.86}$$

Solving for P yields

$$P = \frac{t_b^4}{2} \int_0^1 \left(\frac{\ddot{x}(s)}{t_b^2} + \frac{\mu x(s)}{\left| x^3(s) \right|} \right)^2 ds \tag{3.87}$$

Now, the assumption is made that the Chebyshev polynomials are an option for simplifing the integral above. These polynomials are defined as

$$\hat{f}(s) = \sum_{k=1}^{n} \Phi_k T_{k-1}(s) \tag{3.88}$$

where

$$T_k(s) = \cos\left(k \cos^{-1} s\right), \quad s = \frac{1}{2}(1 - \cos \pi\sigma) \tag{3.89}$$

The basic idea is that the coefficients for this polynomial will be selected to minimize the error between the actual equation and the Chebyshev polynomial. The theory states, without proof, that calculating coefficients at the Chebyshev points, defined below, so that the polynomial and the actual function have zero error, will minimize the error across the entire polynomial.

$$s_\upsilon = \frac{1}{2}\left(1 - \cos \pi\left(\frac{\upsilon - 1}{n - 1}\right)\right) \tag{3.90}$$

Using the Chebyshev points above, a column vector of the functional result at each Chebyshev point is created.

$$F^\nu = f(s_\nu) \tag{3.91}$$

And a constant matrix A is defined such that

$$\Phi = AF \tag{3.92}$$

So substituting equation (3.88) yields

$$\hat{f}(s) = T'(s)AF \tag{3.93}$$

The second derivative of a Chebyshev polynomial is a function of the original polynomial, i.e.,

$$\ddot{T}_k(s) = BT_k(s) \tag{3.94}$$

Substituting above yields,

$$\ddot{\hat{f}}(s) = T'(s)BAF \tag{3.95}$$

Also, note that a property of the Chebyshev polynomials is

$$C = \int_0^1 T(s)T'(s)ds \tag{3.96}$$

Now, these equations will be used to minimize *P*. Assign the mth coordinate of *x(s)* to be

$$x(m,s) = x(s_m) \tag{3.97}$$

So then the following hold true

$$r(s) = \sqrt{\sum_{m=1}^{nd} x(m,s)^2} \tag{3.98}$$

$$y(m,s) = \frac{\mu\tau^2 x(m,s)}{r(x,s)^3} \tag{3.99}$$

$$w(s) = \frac{\mu\tau^2}{r(s)^2} \tag{3.100}$$

These equations may be substituted into the equation for *P*

$$P = \frac{1}{2}\int_0^1 \left(\ddot{x}(s) + \frac{\mu\tau^2 x(s)}{r^3(s)} \right)^2 ds \tag{3.101}$$

Squaring terms and substituting for *w(s)* yields

$$P = \frac{1}{2}\int_0^1 \left(\ddot{x}(s)^2 + 2y(m,s)\ddot{x}(s) + w(s)^2 \right) ds \tag{3.102}$$

Assign

$$x^v(m) = x(m, s_v) \tag{3.103}$$

$$w^v = w(s_v) \tag{3.104}$$

These variables will be used to interpolate for *x(m,s)*, *y(m,s)* and *w(s)* at the Chebyshev points. So

$$\ddot{\hat{x}}(s) = T''(s)BAx(m) \tag{3.105}$$

$$\hat{y}(s) = T''(s)Ay(m) \tag{3.106}$$

$$\hat{w}(s) = T''(s)Aw(m) . \tag{3.107}$$

Substituting these definitions into *P* yields

$$P = \frac{1}{2}\sum_{m=1}^{nd}\int_0^1 \left(T''(s)BAx(m)\right)^2 ds + \frac{1}{2}\sum_{m=1}^{nd}\int_0^1 T''(s)BAx(m)y(m)ds + \frac{1}{2}\sum_{m=1}^{nd}\int_0^1 ds \tag{3.108}$$

Johnson goes on to take the derivatives of *P* and solve for the minima. The Chebyshev approximation has been developed into a code called ChebyTOP [27], [28]. It is widely used in low thrust trajectory optimizations where the need for quick analysis of the parameter space at moderate accuracy is needed. ChebyTOP performs very quickly, in due to the part of the simplicity of the final equations and the fact that several of the underlying matrices can be computed once for the trajectory. It is generally considered accurate for accelerations of 0.01 g's and less.

Other numerical approximations for low thrust trajectories are available [29], [30] generally using some combination of the variation of parameters which are then numerically integrated. It is unclear the advantage of numerically integrating these equations as opposed to simply integrating the equations of motion.

Like the high thrust approximation, low thrust trajectories have been explored in detail. However, they too lack several characteristics desired for trajectory modeling and vehicle performance estimation. First there exists no approximation for a transition

between escape/arrival and interplanetary trajectories. Also, the closed-form relations for mass ratio and time of flight would benefit by updating with a more optimal guidance schedule. Finally a more distinct rule defining a low to medium thrust approximation boundary would assist in selecting which method is more appropriate in a given situation.

3.8 Medium Thrust Approximation

Many of the propulsion system concepts under scrutiny today fall under the medium thrust approximation. These concepts invariably involve fission or fusion reactions that have very high energy densities. This energy density enables performance combining high specific impulses with high specific powers. Thus, these propulsion systems can generate thrusts near the level of high thrust systems for durations as long as or longer than low thrust systems. The combination enables missions not possible with the high and low thrust systems. A caveat, however, is that medium thrust systems are not near the level of technological maturity of high and low thrust systems. Nevertheless, medium thrust systems like the ones listed in Table 3.3 are required to enable many missions (especially crewed missions) of interest.

Table 3.3 Typical Medium Thrust propulsion concepts and performance

Concept	**Isp**	**α**	**F/Weng**
	(sec)	**(kW/kg)**	**(kN/kN)**
Nuclear Pulse [31]	5,000	1250	5

Table 3.3 Cont.

Concept	Isp	α	F/Weng
	(sec)	(kW/kg)	(kN/kN)
Fusion – Inertial Confinement			
IEC [32]	50,000	1200	0.5
ICF [15]	13,000	10	0.02
Mag. Ins. ICF [33]	77000	100	0.04
Fusion – Magnetic Confinement			
Spherical Torus [15]	35,000	10	0.006
Gas Dynamic Mirror [15]	110,000	4	0.0007
Pulsed FRC [15]	100,000	15	0.003
Magnetized Target Fusion [15]	77000	100	0.04

Medium thrust trajectories have thrust levels that are not easily considered perturbative compared to gravitational forces like with low thrust systems. These thrust levels act on the vehicle over a considerable portion of the trajectory. Thus they cannot be considered impulsive as with high thrust trajectories. Hence analysis of medium thrust trajectories can be quite complex. In most cases, the analyst is forced to resort to full integration of the equations of motion over the entire trajectory. This is an unfortunate situation, as the analysis codes are required to find the optimal guidance schedule for the trajectory. In practice, the optimization algorithm for these codes requires an existing solution to perturb. Thus, the analyst must "play" with the trajectory input parameters to

achieve the desired mission objectives before the code can optimize that solution. In other words, the analyst must have a solution to get a solution.

Several approximate techniques have been developed to determine the performance capabilities of medium thrust systems. These techniques were derived primarily by those developing the propulsion systems mentioned in the table above. Unfortunately, the number of approximations required to make the medium thrust trajectory approximation tractable also makes the results poorly representative of the real world. All of the approximations mentioned below assume that the vehicle flies a straight line between points and neglects any gravitational losses. This assumption alone is enough to considerably overestimate performance. Note that this assumption also eliminates any need to consider a guidance schedule. Finally, the points used in the straight-line approximation are usually taken from the sphere of influence of the departure planet to that of the arrival planet. Not accounting for the trajectories in the gravitational wells of the departure and arrival planets also causes an overestimation in performance. The straight-line approximation is illustrated in Figure 3.11. Other assumptions made are described with the approximation to which they are connected.

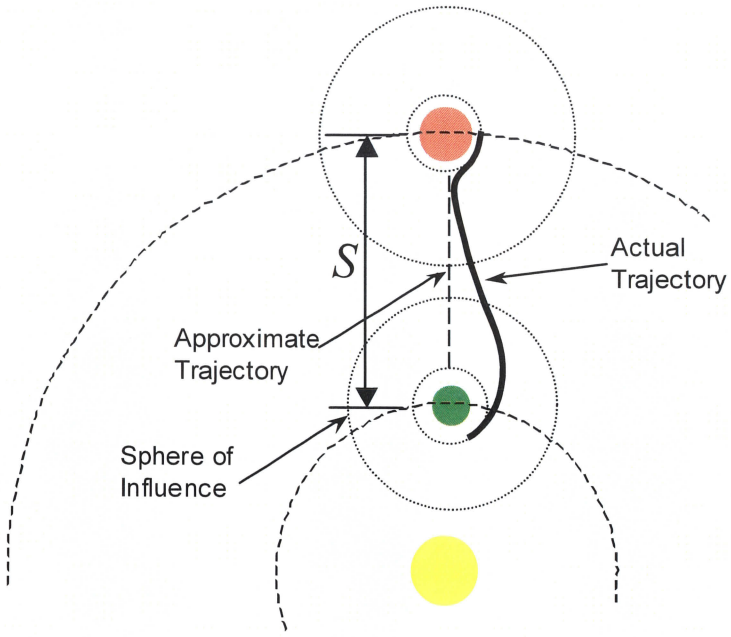

Figure 3.11 Straight line approximation for medium thrust trajectories

The first approximation covered here is the Moeckel-Shepherd-Williams equations. Moeckel took the basic kinematic relations for straight line acceleration taught in sophomore dynamics classes and converted the independent variables to those more appropriate for in-space vehicles [34], namely, specific impulse and specific power. He also showed that for constant acceleration the straight line approximation optimized to burn times that are 2/3 the trip time for rendezvous missions (1/3 acceleration, 1/3 deceleration). This assumption will be prevalent in the models described below.

Shepherd used a similar relation to calculate the optimal relationship between specific power and specific impulse [35]. Williams refined the techniques by the others and applied the results to fly-by, rendezvous and round-trip missions [36]. In each case the solutions assumed no gravity losses and a straight-line trajectory. Additionally, the options assume that the propulsion system is continually operating. This assumption will

always yield the shortest time of flight for a given set of vehicle parameters and distance. The thrust profile accelerates the vehicle to roughly a middle point on the trajectory, where the vehicle would flip over and decelerate until reaching its destination. Velocity produced by acceleration right before the flip maneuver would be destroyed by deceleration right after the flip yielding minimal benefit. Thus acceleration/deceleration near the mid-point of the trajectory produces a small decrease in the time of flight at the expense of a large amount of required propellant. The same time of flight may be better achieved with a larger sized propulsion system and a coast phase. Therefore neglecting coast phases in the trajectory tends to yield non-optimal solutions.

Finally, this approximation uses a derived optimal relationship between I_{sp} and α. This relationship limits the use of the approximation since frequently the optimal specific power, or specific impulse, is not physically achievable. Additionally, there are other considerations in propulsion system or vehicle design that may make it desirable to operate at points that are not optimal for a given mission. One such example is a vehicle that is designed to handle a range of mission concepts. This option is one that the high performing medium thrust systems are well suited for.

The Moeckel-Shepherd-Williams approximation yields an achievable payload mass fraction for a given vehicle ΔV and other performance parameters.

$$\frac{m_L}{m_i} = \frac{1 + V_e^{\,2}/V_c^2}{\left[\left(\Delta V / V_c\right)\left(2V_e / V_c\right)\right] \cdot \left(1 + V_c^{\,2}/V_e^2\right) + 1} - \frac{V_e^{\,2}}{V_c^2} \qquad (3.109)$$

Here the exhaust velocity V_e is produced using ideal expansion and therefore is equal to $g_0 I_{sp}$. The parameter V_c is the characteristic velocity of the vehicle as defined by

Moeckel, is a function of trip time, t and specific power. The trip time is a function of these parameters plus distance as defined below.

$$\frac{S}{ct} = \frac{1 - V_e^{\,2} / V_c^2}{1 + V_e^{\,2} / V_c^2}; V_c = \sqrt{2\eta_j t / \alpha} \tag{3.110}$$

One should be careful when using the term characteristic velocity. Several of the authors' in the 1950's and 1960's literature refer to the ΔV as the characteristic velocity or characteristic speed. The more recent literature uses characteristic velocity as defined above in non-dimensional variables. The characteristic velocity was shown by Shepherd to have several interesting properties. One was that the ΔV cannot exceed 0.805 of the characteristic velocity. Another is that there is an optimum value for the ratio of exhaust velocity to characteristic velocity. The value varies with the mission requirements but ranges from 0.5 to 0.805. Since the exhaust velocity is proportional to specific impulse and the characteristic velocity is proportional to specific power, the fact that there is an optimum value suggests that there is a specific impulse at which point performance is maximized and a higher specific impulse will degrade that performance. This is counterintuitive given the history of chemical propulsion systems where improving specific impulse is a very high priority. However, this phenomenon is well understood and well accepted. Also the optimum specific impulse is a function of the specific power. Propulsion systems with higher specific powers have a higher optimal specific impulse. The exact relation between optimal specific impulse and specific depends on the assumptions made in calculating performance.

Borowski derived a similar solution as part of an effort to compare several medium thrust systems of interest [10]. This is also a straight-line approximation without

gravity losses, but does allow for a non-optimal specific impulse and specific power. The time of flight relation derived by Borowski is

$$t_m = \frac{I_{sp}}{T/W_f}\left[\frac{1}{\beta} - 1\right]. \tag{3.111}$$

Similarly the distance equation is

$$D = \frac{g_0 {I_{sp}}^2}{T/W_f}\left[\frac{1}{\sqrt{\beta}} - 1\right]^2. \tag{3.112}$$

Borowski used an initial thrust to vehicle mass as a parameter. This ratio is related to both specific impulse and specific power as can be seen in equation (3.37). This method does not have an explicit relation for mass ratio or payload ratio. Such a relation was calculated assuming a ΔV and using other methods.

Thio incorporated coast time in his derivation [37]. Specifically, he assumed that one third of the time of flight was devoted to acceleration, one-third was devoted to coast and one third devoted to deceleration. This method also lacks a specific relationship for payload ratio. The time of flight relation is shown below without proof.

$$\tau = \frac{3}{2}\left[\frac{2S^2}{(P_{jet}/m_f)(m_f/m_i)}\right]^{1/3}. \tag{3.113}$$

Cole derived a linearized computational model to calculate interplanetary trajectories [38]. This model assumes a linear ramp in velocity, which indicates a constant acceleration. Coast times are built into the model as well. This model is illustrated in Figure 3.12. This code still assumes a straight-line approximation without gravity losses.

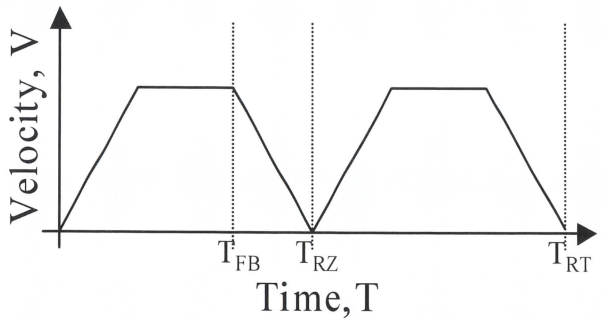

Figure 3.12 Linearized computational model diagram

Polsgrove and Adams (the author of this treatise) started with the derivations done by Shepherd above and removed the relation between optimal I_{sp} and α [15]. The result was a more complicated equation for time of flight,

$$\tau = \frac{S}{g_o I_{sp}} \left(\frac{1 - \left(1 - \frac{2F}{g_o{}^2 I_{sp}{}^2} \frac{P_{jet}}{m_i} \right)}{\left(1 - \frac{2F}{g_o{}^2 I_{sp}{}^2} \frac{P_{jet}}{m_i} \right) \left(\ln\left(1 - \frac{2F}{g_o{}^2 I_{sp}{}^2} \frac{P_{jet}}{m_i} \right) - 1 \right) + 1} \right). \tag{3.114}$$

Note that including non-optimal I_{sp} and α introduces a new variable, $\frac{P_{jet}}{m_i}$, which is the ratio of jet power to initial mass. This ratio is related to the thrust to initial weight ratio and specific impulse though equation (3.37). The payload ratio is also determined using these variables as defined below.

$$\frac{m_L}{m_o} = 1 - \frac{2F}{g_o^2 I_{sp}^2} \frac{P_{jet}}{m_i} - \frac{1}{\alpha} \frac{P_{jet}}{m_i}. \tag{3.115}$$

Investigation of equation (3.114) reveals that the equation could be simplified considerably if the logarithmic term in the denominator could be simplified. A binomial

expansion immediately presents itself. Skipping the intermediate steps it can be shown that equation (3.114) simplifies to

$$TOF = \sqrt{\frac{g_o I_{sp} S}{2\frac{P_{jet}}{m_i}}} \quad (3.116)$$

Equation (3.115) is not affected by this expansion. However for the expansion to be accurate the following relation must be true.

$$2F\frac{P_{jet}}{m_i} << g_o{}^2 I_{sp}^2 \quad (3.117)$$

Unfortunately, this condition is frequently not satisified; thus, the full derivation must be used. All other assumptions relating to Moeckel-Shepherd-Williams equations still hold, so this approximation is still of limited use.

It is worthwhile to consider development of guidance schedules for launch vehicles. A launch vehicle trajectory could be considered to be a special case of a medium thrust trajectory. Most launch trajectories require periods of both burning and coasting, but the burn times are significant compared to the overall mission time. Thompson [39] derives a schedule for thrust angle using calculus of variations and assuming a flat non-rotating earth and ignoring drag losses.

$$\tan\alpha = \left(1 - \frac{t}{t_b}\right)\tan\gamma_i \quad (3.118)$$

where the angle α varies linearly over the time of the burn. A nearly exact duplicate of this equation was derived independently by Ehricke [40].

Clearly, there are several areas in the medium thrust approximation that require further attention. First none of the techniques above have been applied to a planetary escape case. Only Cowell's method requiring numerical integration is suitable for such application. Second gravitational losses must be reintroduced to enable an accurate estimate. If one was to develop an approximate closed-form solution incorporating gravitational losses it would very helpful to both the propulsion and trajectory/performance communities. The approximation would assist propulsion engineers and scientists guide development of their concepts, yielding insight into selecting between options at the subsystem level that would ultimately improve specific impulse or specific power. The desire in the propulsion community is apparent in that so many have devoted their time to develop the approximations above. The benefit to the trajectory community is equally apparent. An approximation that incorporates gravitational losses would necessarily have a more realistic flight path and guidance schedule. Such an approximation, if it handled all of the first order variables for the trajectory, could initialize a full numerical integration code. This code would then have a much higher likelihood of optimizing the trajectory considering second order effects without crashing. Such an approximation would save the analyst the days and weeks required attempting to create an initial trajectory from scratch and thus greatly accelerate analysis time.

3.9 Uses of Analytic Approximations

It has already been mentioned that approximate techniques hold considerable interest in the propulsion community and have benefits for the trajectory community as

well. It is instructive to investigate the literature to see how these techniques are being applied and could be applied. Several studies and papers are described below that are related to these techniques.

Gilland described use of a low thrust approximation for Lunar and Mars missions [41]. The approximation was used to trade optimal I_{sp} and α for nuclear electric propulsion systems for these missions. Here we see an attempt to use these approximations to drive propulsion system design and perform trade studies on the numerous options that exist for NEP systems.

Many of the medium thrust systems proposed employ fusion reactions as the power source. Fusion systems use the concept of gain as a performance parameter. Gain is the amount of power derived by the fusion system divided by the amount of power needed to sustain the system. Thus, powers greater than unity are necessary to sustain a fusion reaction. Chakrabarti et al. investigated the effect of gain on propulsion performance [42]. He used the Borowski relationship for medium thrust non-optimal I_{sp}, α approximation. These calculations attempted to define the sensitivity of gain on propulsion system performance. This relationship is of high interest as its definition could resolve a conflict between the space flight and energy communities. High gain is essential for cost effective power generation using fusion sources. However it is not clear whether high gain is necessary for efficient fusion propulsion.

Borowski used his derivation described above to compare a variety of Fusion/Antiproton systems [10]. His analysis incorporated mission performance and fuel costs using his medium thrust non-optimal I_{sp}, α approximation and drew conclusions on the relative capability and worthiness of development of these systems. Here, we see use

of approximate techniques to make determinations on the relative worthiness of several propulsion systems to meet the demands of several mission concepts.

The author led a multi-disciplinary team that generated several conceptual vehicles that would carry a crew and relevant equipment to Jupiter's moon Callisto and back [43]. Finding a design point for such a mission proved to be a challenge. It was necessary to perform parametric studies of trajectories to define a suitable mission time of flight. A study ground rule required that the crew be exposed to microgravity for one year total or less. Initial cases used a time of flight of one year to avoid inclusion of artificial gravity systems. The result was a propellant dominated vehicle and retrograde trajectories on both the inbound and outbound legs. The next iteration assumed a 1 ½ year mission time, which allowed departure from, and arrival at Earth when Earth's velocity vector was pointed optimally. Finally after a parametric study, it was determined that a mission time of approximately 1-¾ years offered the best trade between use of Earth's velocity and the additional time for acceleration. In the final analysis, the difference between a 1 year and 1 ½ year mission was a halving of the initial mission mass. Going to a 1-¾ year mission decreased initial mass another 25% approximately. Finally the jet power level for the 1-¾ year mission was 1-2 GW. The 1 year mission had a power level of 4-5 GW. For comparable missions using nuclear electric propulsion (NEP) and a nearly 5-year trip time, the jet power level was 30-40 MW. Obviously there is a rapidly increasing (i.e., exponential) jet power level trend with decreasing trip time. Significant savings may have been discovered if a case with a 2-½ to 2-¾ year trip time had been executed. Such a case would have had slightly less propellant mass due to

lower acceleration requirements but substantial decrease in jet power and subsequently propulsion, power and thermal masses.

CHAPTER 4

METHODOLOGY

Clearly the literature demonstrates that several investigators have attempted to develop medium thrust approximations for their own purposes. These purposes are generally to guide propulsion system development and to accelerate trajectory analysis. However these techniques are also inadequate to the task because they require too many assumptions that introduce inaccuracies or they require numerical solutions that do not give insight into global responses.

Thus the intent of this dissertation is to develop an analytical approximation to the two-body problem that is more representative of the physical problem. Thus there must be proof that the results from this approximation compare well to actual solutions. Finally, the use of this approximation must be clearly demonstrated so that the communities for which it was developed embrace it. The results from this dissertation are thereby broken into the three chapters, derivation, computation and application. The chapter on derivation starts with the two-body approximation to the equations of state. A dimensionless-pi analysis breaks down the equations of state and vehicle mass relations into basic dimensionless variables. These dimensionless variables are applied in development of the approximation. Four approaches have been identified for approximation development. These four, optimal control theory, calculus of variations, geometric curve fitting and bounding of differential equations, are applied one at a time until a satisfactory result appears.

A satisfactory result is simply a relationship that calculates payload ratio, time of flight, and the position vector as a function of time or true anomaly. These equations are depicted as

$$\frac{m_L}{m_o} = fcn\left(I_{sp}, \alpha, etc.\right), \tag{4.1}$$

$$T = fcn\left(I_{sp}, \alpha, etc.\right), \tag{4.2}$$

$$r = r(\upsilon), \tag{4.3}$$

$$\upsilon = \upsilon(t). \tag{4.4}$$

These relations would be sufficient to drive design of the propulsion system for a given mission. The position vector will have several inaccuracies but will give the general outline of the actual trajectory that can be used with further analysis.

The results from the derivation chapter must be validated before the analytical approximation can be used. This chapter compares the analytical approximation against several analytical codes used in the industry. The variance between the approximation and the codes is calculated. The uncertainty propagation method is also applied to the approximation to estimate the error created in use of the analytical approximation.

Finally, the application chapter demonstrates uses of the analytical approximation. The approximation is shown to converge with low thrust and high thrust approximations in the limit. The results of the dimensionless-pi analysis from the analytical chapter are shown to accelerate trajectory analysis. Finally the relationship between specific impulse and specific power is shown and how this relationship can drive propulsion system selection and design for given missions.

CHAPTER 5

DERIVATION OF TWO-BODY APPROXIMATION

5.1 Introduction

Derivation of a new algorithm is a time intensive process. It is made more complicated by the principles of orbital mechanics (*r, V, TOF*) are being combined with performance values and design variables for the vehicle in question (α, I_{sp}, T, M_i, M_f, etc.). As was seen in Chapter 3, high thrust solutions keep these variables uncoupled, that is, the mission analyst solves the appropriate orbital mechanics problem which generates a ΔV, which is then included in the vehicle performance analysis. For low thrust solutions, the vehicle performance variables are more tightly included in the orbital mechanics analysis, and for medium thrust solutions, the orbital mechanics has been simplified to triviality (straight line approximation, 1/3 coast, 2/3 thrust time, etc.). That simple solution is integrated with the vehicle analysis, giving an easy solution but one with a high probability of error.

The equations of motion are nonlinear and first order; when accelerative forces are included, it becomes second order. The equations of motion combined with the vehicle performance equations generate a daunting number of overall variables. Therefore, the first step in this derivation will be to create non-dimensional variables to cover all the pertinent factors for the medium thrust two-body problem. The non-dimensional variables will be incorporated into the more pertinent high and low thrust solutions shown in Chapter 3. Next the equations of motion, combined with the vehicle

performance equations will be converted to the non-dimensional variables. The four solution methods will be applied to the non-dimensional equations one at a time until one of the solution methods yields a satisfactory result. That result will be evaluated against computational results.

5.2 Issues Regarding Optimal Thrust and Acceleration

Chapter 3 discussed the prevalent derivation in the literature that indicates that optimal thrust requires minimization of the integral $\int_0^{t_b} a^2 dt$. Previous authors have suggested that a constant acceleration over the life of the burn will give a minimum. But a constant thrust profile will yield a lower *J*. Given a constant thrust, the acceleration over the burn time can be found as

$$a = \frac{T}{M_i - m't} \tag{5.1}$$

Some algebra will convert the above to

$$a = g_0 \frac{T/W_i}{1 - T/W_i \dfrac{t}{I_{sp}}} \tag{5.2}$$

Figure 5.1 illustrates the graphs of both a and a^2 assuming constant thrust and constant acceleration. It is clear that constant thrust gives a smaller *J*. It is not clear why the myth of constant acceleration has been perpetuated by some in the literature.

However, minimization of this integral does not address a couple of issues. First it maximizes final mass instead of payload mass. This integral does not anticipate that the final mass could be maximized by increasing the propulsion system mass (at the

expense of the payload mass) to increase the final mass. Second, the integral does not anticipate the need to meet a particular ΔV. Now in practical use a computer model will attempt to minimize the integral after a solution to the mission requirements is found. However it makes sense to attempt to derive this integral to first maximize payload mass and second to constrain the solution to meet a particular ΔV after losses are accounted.

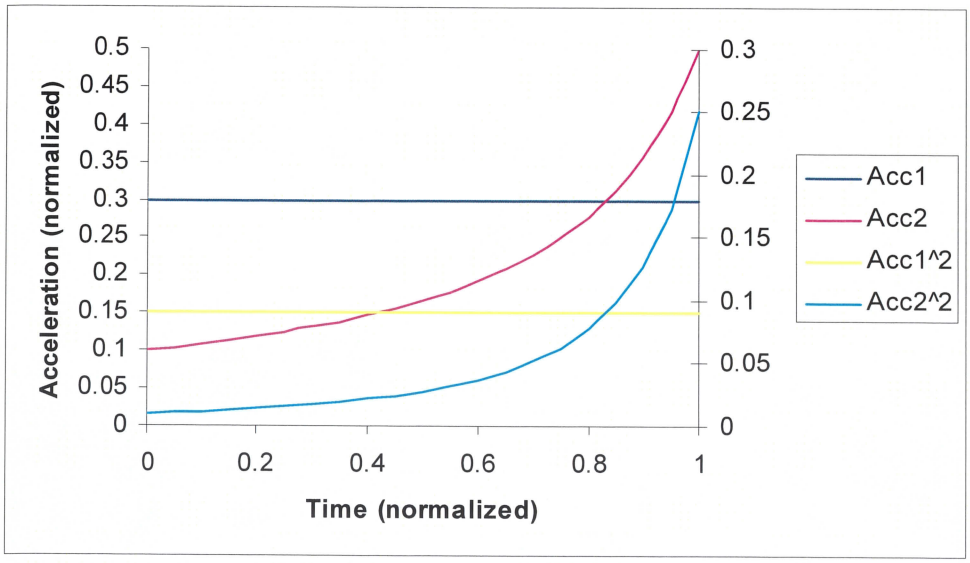

Figure 5.1 Plots of acceleration and acceleration^2 vs. time

Starting from the definition of thrust

$$F = -\dot{m}V_e = Ma, \tag{5.3}$$

and using the definition of specific power for this treatise,

$$\alpha = \frac{P_{jet}}{\eta_{tot} m_{prop}} = \frac{\dot{m}V_e^{\,2}}{2\eta_{tot} m_{prop}}. \tag{5.4}$$

Substituting the two equations above and solving for exit velocity yields

$$V_e^{\,2} = \frac{\eta_{tot}\alpha m_{prop}}{\dot{m}} = \left(\frac{-Ma}{\dot{m}}\right)^2 . \tag{5.5}$$

Solving for mass and integrating over time

$$-\int_0^{t_b} \frac{\dot{m}}{M^2} dt = \int_0^{t_b} \frac{a^2}{2\eta_{tot}\alpha m_{prop}} dt . \tag{5.6}$$

Evaluating the integral and noting that the vehicle mass is M_i at $t = 0$ and M_f at $t = t_b$ yields

$$\frac{1}{M_f} = \frac{1}{M_i} + \frac{1}{2\eta_{tot}\alpha m_{prop}} \int_0^{t_b} a^2 dt . \tag{5.7}$$

But the objective is to maximize the payload mass. So noting that the final mass is

$$M_f = m_{prop} + m_{inert} + m_{pay} . \tag{5.8}$$

And for convenience, defining

$$J = \frac{1}{2\eta_{tot}\alpha} \int_0^{t_b} a^2 dt , \tag{5.9}$$

the combination of the last three equations yields

$$m_{pay} = \left(\frac{1}{M_i} + \frac{J}{m_{prop}}\right)^{-1} - m_{prop} - m_{inert} . \tag{5.10}$$

Dividing through by the initial mass yields

$$\frac{m_{pay}}{M_i} = \frac{m_{prop}}{m_{prop} + M_i J} - \frac{m_{prop}}{M_i} - \frac{m_{inert}}{M_i} . \tag{5.11}$$

The definitions of payload ratio and structural mass fraction may be used to obtain the equation,

$$\lambda = \frac{1}{1 + \dfrac{J}{m_{prop} / M_i}} - \frac{m_{prop}}{M_i} - \varepsilon \tag{5.12}$$

Note that to maximize the payload ratio, J must still be minimized. J can be evaluated using its definition and the definition of constant thrust as given in equation (5.13).

$$J = \frac{1}{2\eta_{tot}\alpha} \int_0^{t_b} \left(\frac{T/W_i}{1 - T/W_i \dfrac{t}{I_{sp}}} \right)^2 dt \tag{5.13}$$

Evaluating under the integral yields

$$J = \frac{1}{2\eta_{tot}\alpha} g_0 I_{sp}{}^2 \left(\frac{T/W_i}{1 - T/W_i \dfrac{t_b}{I_{sp}}} - T/W_i \right) \tag{5.14}$$

Recalling that $t_b/I_{sp} = \tau$, the relation from Section 5.2 that compares τ with the initial and final thrust to weight can be incorporated. That equation can be rewritten as

$$\frac{T/W_i}{T/W_f} = 1 - \frac{T/W_i}{\tau} \tag{5.15}$$

Substituting into equation (5.14) and simplifying yields

$$J = \frac{g_0 I_{sp}{}^2}{2\eta_{tot}\alpha} \left(T/W_f - T/W_i \right) dt \tag{5.16}$$

It is worthwhile to pause here and explore the definition of propulsion system thrust to weight. Propulsion system thrust to weight can be defined from first principles as

$$\left.\frac{T}{W}\right|_{prop} = \frac{2\eta_{tot}\alpha}{I_{sp}g_0^{\,2}} \tag{5.17}$$

Therefore

$$J = \frac{T/W_f - T/W_i}{T/W_{prop}} \tag{5.18}$$

It is tempting to say that now this relation must be minimized, but recall that the payload fraction equation involved the ratio of propulsion system mass to initial mass. For constant thrust that ratio can be written as the ratio of propulsion system thrust to weight to initial thrust to weight. Putting that and the previous equation back into the payload fraction equation yields

$$\lambda = \frac{1}{1+\dfrac{\dfrac{T/W_f - T/W_i}{T/W_{prop}}}{\dfrac{T/W_i}{T/W_{prop}}}} - \frac{T/W_i}{T/W_{prop}} - \varepsilon \tag{5.19}$$

And reducing the above equation yields

$$\lambda = \frac{T/W_i}{T/W_f} - \frac{T/W_i}{T/W_{prop}} - \varepsilon \tag{5.20}$$

Which is just equation (5.11) again divided by initial mass. This trivial result suggests that the construct J is not terribly relevant for maximizing payload fraction. However, that result should be confirmed by attempting to optimize the payload fraction

equation that uses J and the ratio of propulsion to initial mass as variables. Defining a new convenience variable

$$b = \frac{m_{prop}}{M_i} \tag{5.21}$$

The derivatives of the payload fraction equation are

$$\frac{\partial \lambda}{\partial b} = \frac{1}{\left(1+\frac{J}{b}\right)^2}\frac{J}{b^2} - 1 \tag{5.22}$$

$$\frac{\partial \lambda}{\partial J} = \frac{-1}{\left(1+\frac{J}{b}\right)^2}\frac{1}{b} \tag{5.23}$$

The optimal solutions for J and b will be the ones where both derivatives equal zero. Working with the first equation yields

$$\frac{-b}{J} = \frac{-1}{\left(1+\frac{J}{b}\right)^2}\frac{1}{b} \tag{5.24}$$

But the term on the right equals equation (5.23) which is also set to zero. Therefore the equations are both satisfied only when

$$\frac{b}{J} = 0 \quad or \quad \frac{1}{\left(1+\frac{J}{b}\right)^2} = 0 \tag{5.25}$$

Since propulsion system mass and initial mass are finite, this first term can only be achieved by maximizing J. And that is contrary to what is written in the literature. The second term is not possible to satisfy as both J and b are positive.

A test for whether the above stationary point is either a maximum or minimum point is found by considering

$$\frac{\partial^2 f}{\partial x^2}\cdot\frac{\partial^2 f}{\partial y^2} > \left(\frac{\partial f}{\partial x \partial y}\right)^2 . \tag{5.26}$$

The relevant second derivatives are

$$\frac{\partial^2 \lambda}{\partial b^2} = \frac{2}{\left(1+\frac{J}{b}\right)^3}\frac{J^2}{b^4} - \frac{2}{\left(1+\frac{J}{b}\right)^2}\frac{J}{b^3} \tag{5.27}$$

$$\frac{\partial^2 \lambda}{\partial J^2} = \frac{2}{\left(1+\frac{J}{b}\right)^3}\frac{1}{b^2} \tag{5.28}$$

$$\frac{\partial^2 \lambda}{\partial b \partial J} = \frac{-2}{\left(1+\frac{J}{b}\right)^3}\frac{J}{b^3} + \frac{1}{b^2\left(1+\frac{J}{b}\right)^2} . \tag{5.29}$$

Substituting those derivatives into equation (5.26) yields

$$\left(\frac{1}{\left(1+\frac{J}{b}\right)^2}\frac{J^2}{b^2} - \frac{1}{\left(1+\frac{J}{b}\right)}\frac{J}{b}\right)\frac{1}{\left(1+\frac{J}{b}\right)^4}\frac{J^4}{b^4} > \left(\frac{1}{\left(1+\frac{J}{b}\right)^2}\frac{J^2}{b^2} - \frac{1}{\left(1+\frac{J}{b}\right)}\frac{J}{b} + 1\right)\frac{1}{\left(1+\frac{J}{b}\right)^4}\frac{J^4}{b^4} . \tag{5.30}$$

The outside terms and the first two terms in parentheses cancel, leaving 0>1. Since that is not true, this is not a maximum or minimum. All that is left is a saddle point, and that can be seen in the figure below.

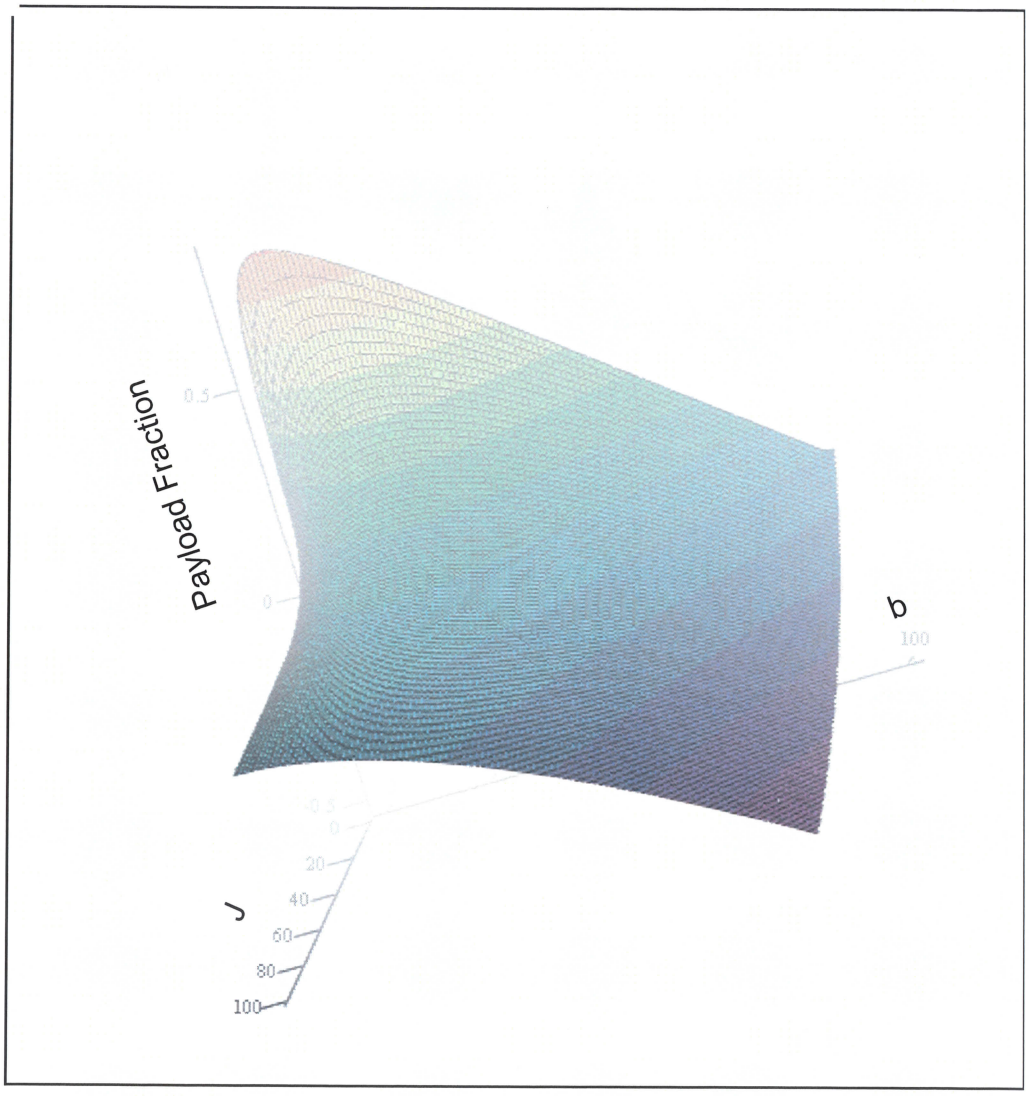

Figure 5.2 Payload fraction as a function of *J* (extending downward) and the ratio of propulsion system mass to initial mass (extending left to right)

The figure shows that near minimal *J* and near minimal *b* is desired to maximize payload fraction. It is worthwhile to explode the corner of the graph to get a better idea of the location of the peak payload mass fraction. Figure 5.3 below is that exploded view; this time as a contour plot to better locate the peak payload fraction.

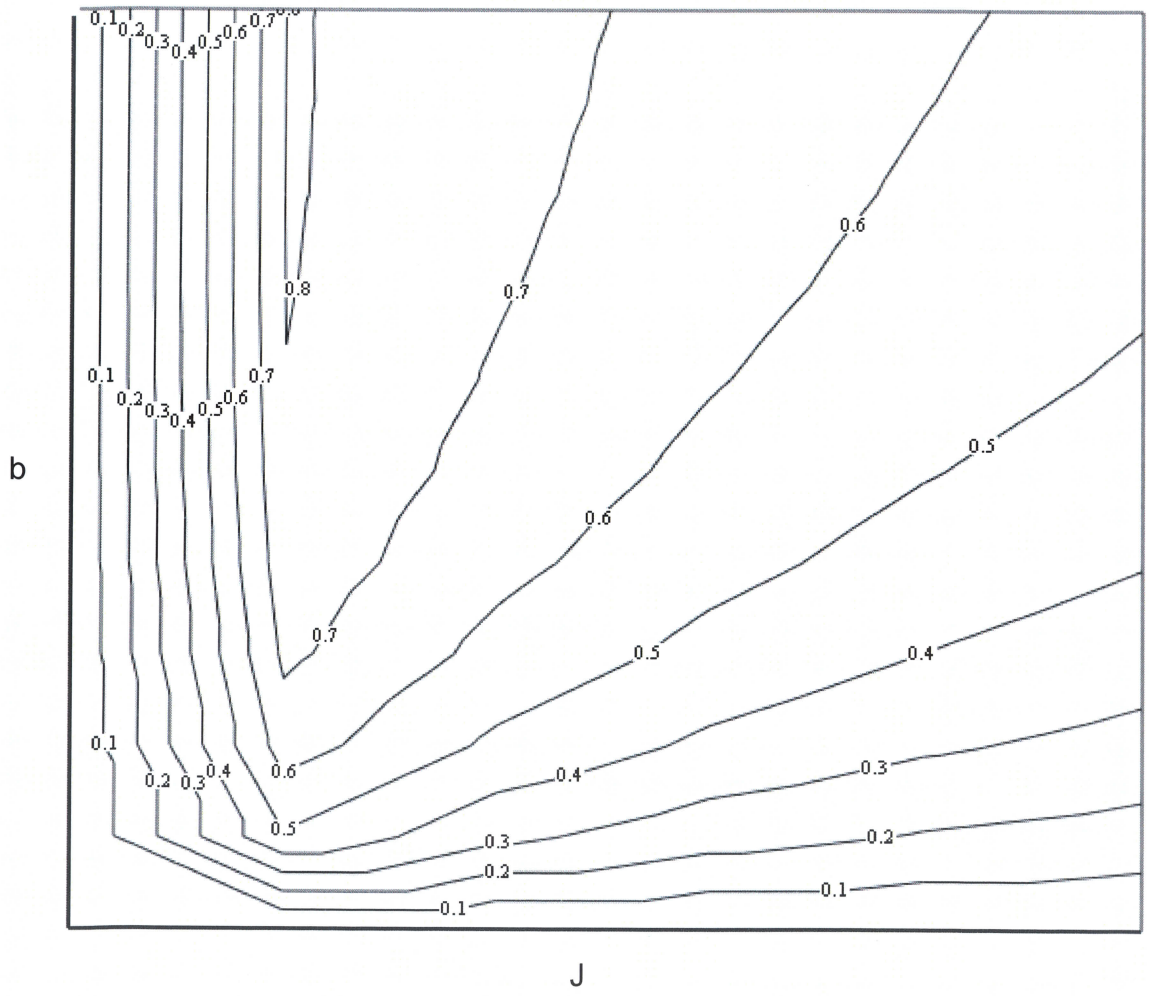

Figure 5.3 Exploded view of Figure 5.2 near origin. X-axis is *J*, y-axis is *b*. Contour values are for payload fraction

From this plot, it is clear that near minimal *J* while also near minimal *b* will give the highest payload fraction. The two variables are connected, and they will be constrained by other mission requirements as will be seen shortly. It is also clear that the stated objective of several algorithms in the low thrust literature to completely minimize *J* will not maximize payload fraction. A complete minimization of *J* would result in zero

payload mass fraction. In practice, the ability of low thrust systems to minimize J is limited, and so it is likely that such systems would never achieve such a low J as to cross over to the back side of this peak. However, the higher performance of the medium thrust systems would have a greater chance of crossing this peak; therefore, it is important to remember that near minimization of J, not complete minimization is desired.

The above analysis does not address the issue of maintaining the ΔV requirement. As noted earlier, a constant acceleration over a given burn time will not yield the same ΔV as a linearly varying acceleration, even if the average acceleration is the same. A desire to keep J to a minimum and b very low has conflicting requirements. A low J implies a short burn time which would be achieved by a large propulsion system. Such a system would result in a larger b. In either case, the total ΔV produced by the spacecraft is represented by

$$\Delta V_{vehicle} = \int_0^{t_b} a dt = g_0 I_{sp} \ln\left(\frac{M_i}{M_f}\right), \tag{5.31}$$

as was found in Chapter 3. So the total ΔV developed by a spacecraft, minus the relevant losses was defined in Chapter 3 as

$$\Delta V = g_0 I_{sp} \ln\left(\frac{M_i}{M_f}\right) - \int_0^{t_b} g \sin\gamma dt - \int_0^{t_b} \frac{F_{vac}}{M}(1-\cos\alpha')dt, \tag{5.32}$$

where, of course, the gravitational acceleration is

$$g = \frac{\mu}{r^2}. \tag{5.33}$$

The term on the left represents the minimum or ideal ΔV to meet the mission requirements. The first term on the right is of course the ΔV the vehicle is capable of

producing. The final two terms are the losses to gravity and steering respectively. The desire is to minimize the ΔV loss the vehicle experiences during the trajectory. That loss has to be constrained such that the total ΔV meets the mission requirements plus the minimal losses.

Several attempts were made using different techniques to reduce equation (5.32). Unfortunately, all were unsuccessful in determining an analytical approximation of the appropriate guidance schedule that would solve the equation above. These attempts are documented in Appendix C. Documenting these failed attempts should assist others attempting to solve this same problem.

The author did have some success with curvefitting an empirical solution. This solution is documented here. It meets the minimum requirements to develop an analytical approximation for performance of medium thrust vehicles. Furthermore, development of the empirical solution has grounding in fundamental theory.

The author created a simple backwards differencing numerical integrator to test solutions and look for trends. As expected, under most circumstances, accelerating along the velocity vector tended to give a near optimal solution, minimizing the ΔV loss. Consideration of equation (5.32) shows that the last term on the right will go to zero if acceleration is constrained along the velocity vector. If so, then calculation of the next to last term, the gravity loss term, is all that is needed to calculate the gravity loss for the system.

Trend analysis of variation of flight path angle and radius magnitude for tangential thrust trajectories revealed that the following approximation was suitable for the gravity loss term.

$$\Delta V_{grav} = \int_0^{t_b} \frac{\mu}{\left(r_i + \left(\frac{t}{t_b} \right)^2 \left(r_f - r_i \right) \right)^2} \left(\frac{t}{t_b} \right)^{3/2} \sin(\gamma_f) dt \tag{5.34}$$

After considerable reduction of the integral and algebra with the above equation, it becomes possible to write

$$\Delta V_{grav} = \left[\frac{\sqrt{2}}{\frac{8}{a}} \left(\begin{array}{l} a \sin\left(\sqrt{2} \left(\frac{r_i}{r_f} a \right) \right) \\ + \ln\left(\sqrt{1 - \frac{r_i}{r_f}} + \sqrt{2} \left(\frac{r_i}{r_f} a \right) + \sqrt{\frac{r_i}{r_f}} \right) \end{array} \right) - \frac{r_i}{2 r_f} \right] \frac{\mu t_b \sin(\gamma_f)}{r_i^2 a^4} \tag{5.35}$$

where

$$a = \left(1 - \frac{r_i}{r_f} \right)^{0.25} \tag{5.36}$$

This equation requires an estimate of the final flight path angle. The user can specify that angle, but to get to that angle for a certain velocity and radius may require acceleration not along the velocity vector. Intuitively, one would expect the variation in flight path angle to be a function of both specific impulse and thrust to weight as well as burn time. So an empirical curvefit of the final flight path angle came out to be

$$\gamma_f = 30 \deg \frac{TW_i}{10^{-4}} \left(\frac{1000 \sec}{I_{sp}} \right)^{0.125} \left(\frac{t_b}{100 day} \right)^2 \tag{5.37}$$

Now, all the equations are defined that are required to solve for a given maneuver. An attempt was made to reconfigure the above equations with the non-dimensional numbers found in Appendix E, but it was not successful.

$$\Delta V_{grav} = \int_0^{t_b} \frac{\mu}{\left(r_i + \left(\frac{t}{t_b} \right)^2 \left(r_f - r_i \right) \right)^2} \left(\frac{t}{t_b} \right)^{3/2} \sin(\gamma_f) dt \tag{5.34}$$

After considerable reduction of the integral and algebra with the above equation, it becomes possible to write

$$\Delta V_{grav} = \left[\frac{\sqrt{2}}{\frac{8}{a}} \left(\begin{array}{l} a \sin\left(\sqrt{2} \left(\frac{r_i}{r_f} a \right) \right) \\ + \ln\left(\sqrt{1 - \frac{r_i}{r_f}} + \sqrt{2} \left(\frac{r_i}{r_f} a \right) + \sqrt{\frac{r_i}{r_f}} \right) \end{array} \right) - \frac{r_i}{2 r_f} \right] \frac{\mu t_b \sin(\gamma_f)}{r_i^2 a^4} , \tag{5.35}$$

where

$$a = \left(1 - \frac{r_i}{r_f} \right)^{0.25} . \tag{5.36}$$

This equation requires an estimate of the final flight path angle. The user can specify that angle, but to get to that angle for a certain velocity and radius may require acceleration not along the velocity vector. Intuitively, one would expect the variation in flight path angle to be a function of both specific impulse and thrust to weight as well as burn time. So an empirical curvefit of the final flight path angle came out to be

$$\gamma_f = 30 \deg \frac{TW_i}{10^{-4}} \left(\frac{1000 \sec}{I_{sp}} \right)^{0.125} \left(\frac{t_b}{100 day} \right)^2 . \tag{5.37}$$

Now, all the equations are defined that are required to solve for a given maneuver. An attempt was made to reconfigure the above equations with the non-dimensional numbers found in Appendix E, but it was not successful.

The algorithm for the solution is as follows. Determine the ΔV ideal required from Lambert's problem or the semi-tangential transfer problem. Select a burn time, specific impulse, specific power, final thrust to weight and total efficiency for the propulsion system.

Calculate propulsion system thrust using the previously defined

$$\left.\frac{T}{W}\right|_{prop} = \frac{2\eta_{tot}\alpha}{I_{sp}g_0{}^2} \tag{5.17}$$

Iterate the next three equations to compute a new burn time, ΔV loss, and thrust to weight

$$\gamma_f = 30\deg\frac{TW_i}{10^{-4}}\left(\frac{1000\sec}{I_{sp}}\right)^{0.125}\left(\frac{t_b}{100day}\right)^2 \tag{5.37}$$

$$\Delta V_{grav} = \left[\frac{\sqrt{2}}{\frac{8}{a}}\left(\begin{array}{l} a\sin\left(\sqrt{2}\left(\frac{r_i}{r_f}a\right)\right) \\ +\ln\left(\sqrt{1-\frac{r_i}{r_f}}+\sqrt{2}\left(\frac{r_i}{r_f}a\right)+\sqrt{\frac{r_i}{r_f}}\right)\end{array}\right)\right]-\frac{r_i}{2r_f} \tag{5.35}$$

$$\frac{1}{\left.\frac{T}{W}\right|_i}-\frac{1}{\left.\frac{T}{W}\right|_f}=\frac{1}{\tau_{Isp}} \tag{5.15}$$

$$\Delta V_{vehicle} = \int_0^{t_b} a dt = g_0 I_{sp}\ln\left(\frac{M_i}{M_f}\right) = \Delta V_{ideal} + \Delta V_{loss} \tag{5.38}$$

Results of this algorithm against algorithms previously defined in the literature are given in the next chapter.

The derivation of this equation required the assumption that the jet power was constant. This is a reasonable assumption as it makes sense that while the engine is on

use of all the power produced is desired. If parts of the trajectory did not use the full power of the engine for the entire burn time, then it is possible that by reducing the power at the peak could increase payload mass by reducing propulsion system mass. That mass would be lost in part by higher ΔV losses (and therefore more propellant required) over a longer burn time.

Given that jet power is constant, then it is clear that if thrust or specific impulse is held constant, the other must be constant as well. This is clear from a cursory examination of equation (3.10), repeated here for convenience.

$$P_{jet} = \frac{1}{2} g_o I_{sp} F \tag{5.39}$$

Unfortunately a number of the derivations covered in Chapter 3 neglect this axiom for convenience. However this requirement can have a profound influence on the performance of a vehicle.

Constant thrust and specific impulse is the norm for most propulsion systems in use today. Chemical propulsion systems do throttle back during launch trajectories (to reduce the aerodynamic and vibrational loads on the vehicle or to maintain a maximum acceleration for crew health and comfort or payload requirements). However for in-space trajectories, throttling the propulsion system is rarely desired. Throttling the propulsion system results in lower thrust, power and specific impulse. Since the energy source for a chemical propulsion system is the propellant itself, injecting less propellant means less power is available for the jet. And, less mass in the combustion chamber means lower combustion pressures. The completeness of the chemical reaction is generally a strong function of combustion pressure.

Throttling of electric propulsion systems is difficult. Adjusting the voltage and current delivered to a propulsion system will change the number of ionized atoms and the velocity by which they are ejected from the thruster. That is good; fewer atoms means a lower mass flow rate and a lower thrust while higher voltages means higher exit velocities and therefore higher specific impulses. However, the materials and propellants used impose strong restrictions on how much these parameters can be varied. A given propellant will require a certain minimum energy to ionize each atom, too low a current will dissipate that current into heat and not create the needed ions. High voltages are limited by materials and the need to accelerate the atoms without having them strike and erode the potential grids. And of course transforming incoming power into current and voltage imposes a loss on the system due to resistance in the transformer and lines to the thruster. Higher currents will dissipate more power meaning less is delivered to the propellant.

For these reasons, the assumption of constant thrust and specific impulse is very good for current propulsion systems.

5.3 Analytic Comparison of Medium Thrust Model to Existing Models

An investigation of the new algorithm shows that the algorithm agrees with known high and low thrust equations. Consider the main equations, repeated below for convenience,

$$\gamma_f = 30\deg \frac{TW_i}{10^{-4}} \left(\frac{1000\sec}{I_{sp}} \right)^{0.125} \left(\frac{t_b}{100day} \right)^2 \tag{5.37}$$

$$\Delta V_{grav} = \left[\frac{\frac{\sqrt{2}}{8}}{a} \left(\begin{array}{l} a \sin\left(\sqrt{2} \left(\frac{r_i}{r_f} a \right) \right) \\ + \ln\left(\sqrt{1 - \frac{r_i}{r_f}} + \sqrt{2} \left(\frac{r_i}{r_f} a \right) + \sqrt{\frac{r_i}{r_f}} \right) \end{array} \right) - \frac{r_i}{2 r_f} \right] \frac{\mu t_b \sin(\gamma_f)}{r_i^2 a^4} \tag{5.35}$$

For a high thrust solution, the gravity losses should approach zero as the burn time goes to zero. The limit as burn time approaches zero of the flight path angle is indeterminate. As burn time goes down, the initial thrust to weight goes up. The time term will vary faster, due to it being squared, but the burn time varies roughly three orders of magnitude for most trajectories of note, varying from 0 seconds to about a thousand days for the longest practical burn times. While varying over this range, the thrust to weight can easily range from 10 to 10^{-8}. So the variation of that term can be expected to be roughly proportional to the change of the time term squared.

However the ΔV_{loss} equation varies with the flight path angle and the burn time, all other parameters being the same. Since the flight path angle remains finite (which is consistent with high thrust theory), the limit as burn time goes to zero would also drive the losses to zero. Which is also consistent with high thrust theory.

Comparison to low thrust models is a little more complex. The nature of low thrust models implies low variation in flight path angle. These trajectories are generally spiral trajectories, which due to their shape have a slow variation in the radial direction. The flight path angle empirical relation is consistent with low thrust theory. The changes from the empirical base of the equation are burn times perhaps one order of magnitude from the base. The thrust to weight can easily drop faster than the two orders of magnitude change in the time squared. Again the flight path angle is expected to be

finite, given the near proportional nature of the change in thrust to weight and burn time, but the flight path angle should approach zero. All of this is consistent with the nature of low thrust trajectories.

The ΔV_{loss} equation is also consistent with low thrust theory. A low thrust trajectory can double or triple the required ΔV because of losses over the ideal requirement. The flight path angle is still expected to be finite and non-zero; however, the burn time is increasing substantially. Therefore a greater ΔV_{loss} is expected.

5.4 Geometric Representation of a Thrust Trajectory

All non-thrusting orbits about a central body are conic sections; that is, a circle, ellipse, parabola or hyperbola is defined by the intersection of a plane with a right circular cone. Varying the inclination of the plane that cuts the cone will define the shape of the conic section, as well as define whether the section is an ellipse, parabola, or hyperbola. Consider Figure 5.4 below from Vallado [6] that illustrates the possible orbits created by these intersections.

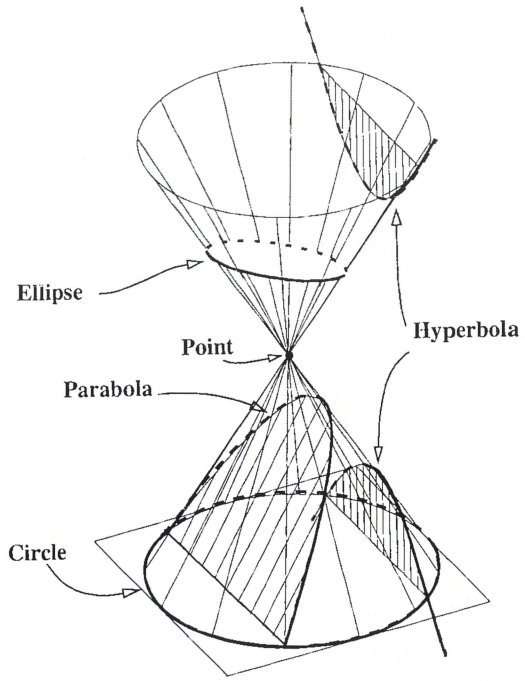

Figure 5.4 Intersection of cone and plane to create conic sections. From Vallado [6]

Given that orbits are conic sections, one is tempted to wonder what the physical representation of the cone and plane are. The author pondered this for a while, and conducted some research to see if another has tried to answer this question. No research was found. After some thought, the author believes that the cone could be replaced with a paraboloid (parabola of revolution). The paraboloid should be more appropriate because the $1/r^2$ nature of the gravitational forces of the central body. The question is will the intersection of a plane and a paraboloid will also yield the familiar conic sections defining the respective orbits? This is determined by calculating the intersection of the right circular paraboloid and an arbitrary plane. The equation for a plane in three-dimensional space is

$$C_1x + C_2y + C_3z = C_4 . \tag{5.40}$$

The equation for a paraboloid is given as

$$z = C_5\left(x^2 + y^2\right). \tag{5.41}$$

Solving equation (5.40) for z and setting it equal to equation (5.41) yields

$$\frac{C_4 - C_1x - C_2y}{C_3} = C_5\left(x^2 + y^2\right) . \tag{5.42}$$

Simple algebra reduces the above to

$$C_3C_5x^2 + C_3C_5y^2 + C_1x + C_2y + C_4 = 0 . \tag{5.43}$$

The equation for an ellipse is

$$Ax^2 + Bxy + Cy^2 + Dx + Ey + F = 0 , \tag{5.44}$$

where

$$B^2 < 4AC . \tag{5.45}$$

It is useful to note that the equations for parabolas and hyperbolas also follow the format of equation (5.44), where for them the criteria is, respectively,

$$B^2 = 4AC \tag{5.46}$$

$$B^2 > 4AC . \tag{5.47}$$

So at first blush, it seems equation (5.43) is a form of equation (5.44) and that as long as the criterion given in equation (5.45) is met, then the cross section of a paraboloid and an plane is an ellipse. However equation (5.44) is an equation in two dimensions and equation (5.43) represents the intersection of the paraboloid and plane in

three dimensions. Since the representation of ellipses, parabolas and hyperbolas are defined as the intersection of a plane and cone projected into two-dimensional coordinates with respect to the plane, it is important to conduct a coordinate transformation on equation (5.43) so that it is defined in two-dimensional terms.

First note that the position vector for any point along the curve defined in equation (5.43) is given as

$$\vec{r} = x\hat{i} + y\hat{j} + z\hat{k} \tag{5.48}$$

The normal to the plane is given as

$$\vec{n} = C_1\hat{i} + C_2\hat{j} + C_3\hat{k} \tag{5.49}$$

Imagine a plane parallel to the plane intersecting the paraboloid but also passing through the origin. The position vector for the curve also, by definition, passes through the origin. If the position vector is subtracted by the projection of the position vector onto the normal of the plane passing through the origin, the result will be a position vector that defines the intersection curve projected onto the plane intersecting the origin. This position vector will also always be in the plane of the plane intersecting the origin. Note that the normal for the plane remains the same for the plane intersecting the paraboloid and the plane intersecting the origin as they were defined to be parallel. Therefore the projection of the position vector onto the normal becomes

$$\vec{n} \cdot \vec{r} = C_1 x\hat{i} + C_2 y\hat{j} + C_3 z\hat{k} \tag{5.50}$$

Therefore the vector subtraction of the projection from the position vector itself is

$$\vec{r} - \vec{n} \cdot \vec{r} = (1 - C_1)x\hat{i} + (1 - C_2)y\hat{j} + (1 - C_3)z\hat{k} \tag{5.51}$$

Since all terms are multiplied by a constant, it should make sense that the projection onto the plane intersecting the origin maintains the same structure as equation (5.43). Additionally now that the plane intersects the origin the coordinate transformation to a two-dimensional coordinate system referenced to the plane intersecting the origin will require one angular rotation about a vector that is normal to both the plane normal and the normal to the x-y plane in the three-dimensional coordinate system (i.e., $\hat{k}$). Rotating about a single vector for coordinate transformation is a mainstay of quaternion analysis. Suffice it to say the coordinate transformation will change the constants but not the structure of equation (5.43). Thus intersection of a plane and paraboloid creates circles, ellipses, parabolas and hyperbolas, as expected.

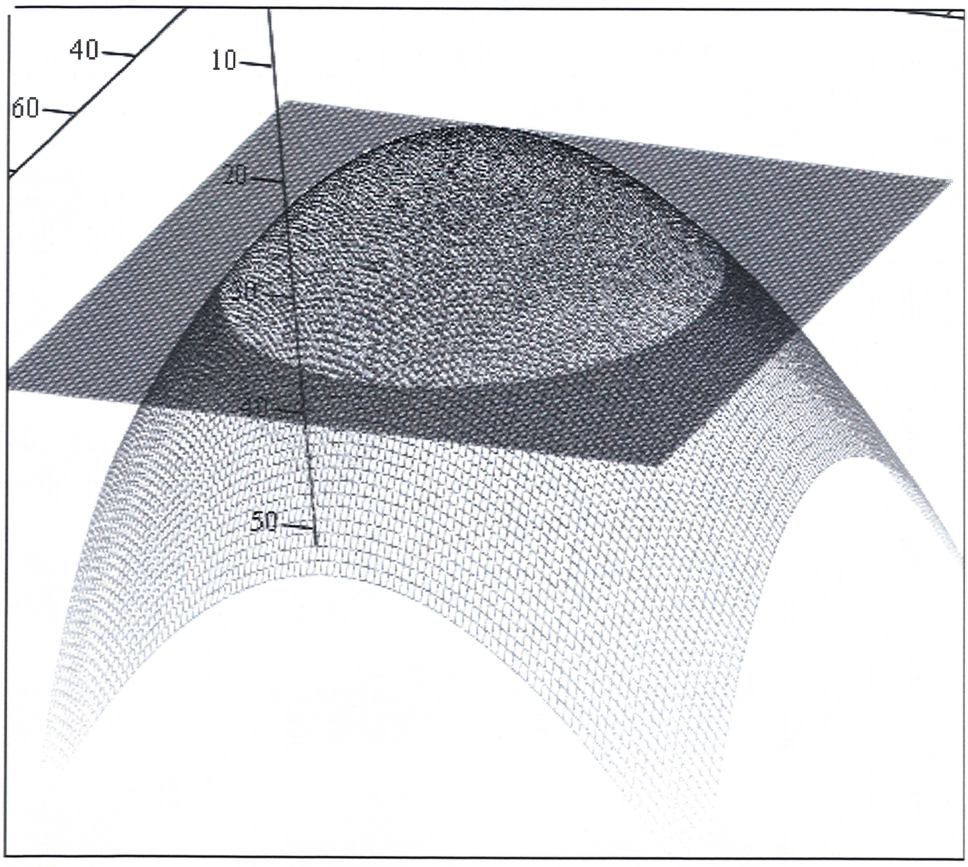

Figure 5.5 Intersection of a plane and a paraboloid of revolution

Applying a ΔV to a spacecraft is tantamount to rotating the plane. The plane obviously has to rotate around the spacecraft which is constrained to always being on the surface of the paraboloid and the plane simultaneously. An impulsive ΔV in the tangential direction will rotate the plane down; that is, the line constrained to the plane connecting the spacecraft and going through the z-axis will move downward. If the ΔV is applied in any other direction, a combination of change downward (pitch) and rotating about the line between the spacecraft and z-axis (yaw). A plane intersection after a ΔV maneuver is shown below.

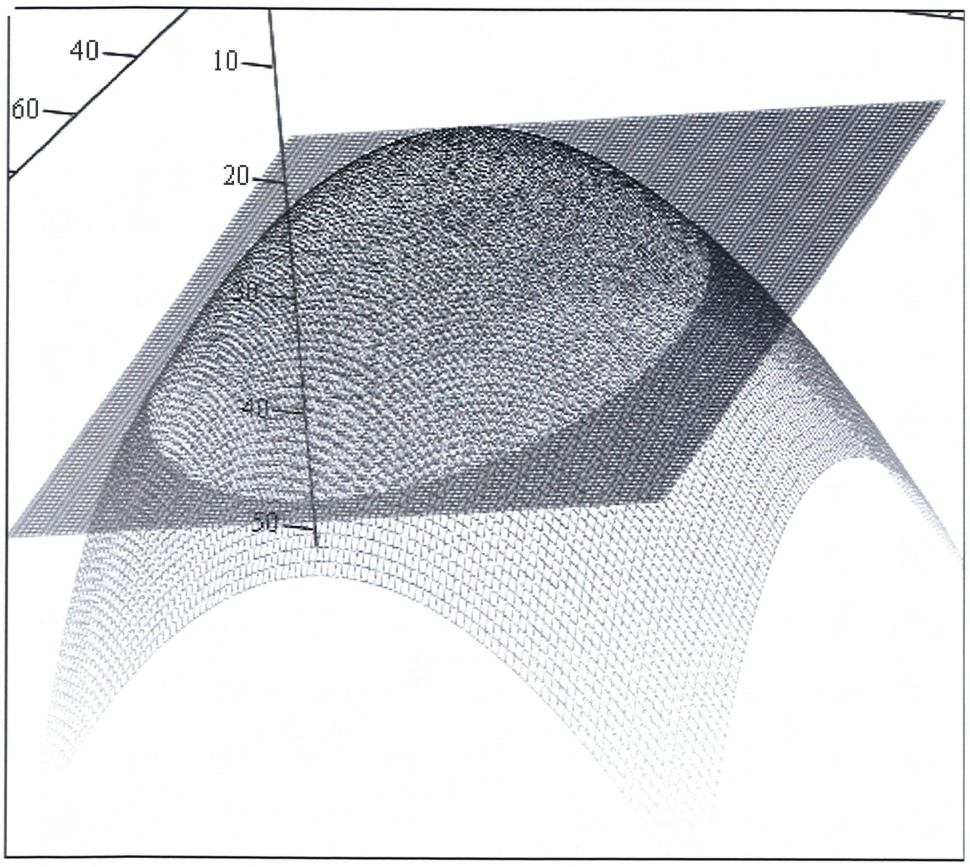

Figure 5.6 Intersection after ΔV maneuver changing pitch of the plane

This paraboloid and plane concept is very useful for describing a number of phenomena related to orbit transfer. Consider the Hohmann transfer. Long regarded as the most efficient of orbital transfers, it still is the most efficient and widely used transfer mechanism in most situations. Only the bi-elliptic (and now the new maneuver) have the possibility to be more efficient, and then only in some special circumstances.

The Hohmann transfer is illustrated with the paraboloid and plane concept as follows. The plane is perpendicular to the z-axis and intersects the paraboloid at a point where the radius at each point equals the initial radius of the spacecraft orbit. At the

moment of the first burn, the plane is pitched downward until the intersection of the plane and the paraboloid touches the desired radius of the final orbit. The spacecraft coasts around the resulting elliptical orbit until it has reached the point where the plane intersects the paraboloid at the desired orbit and then the plane is pitched again. The pitch angle here is sufficient to restore the plane to perpendicular to the z-axis. The difference in the gradient of the paraboloid is the source that describes the difference in ΔV requirements between the first and second maneuver.

The bi-elliptic transfer is known to be more efficient than the Hohmann transfer when the ratio of the change in orbital radii exceeds approximately 11.94. Again consider the plane and paraboloid concept. Here the plane is rotated to a point much farther than would have been required for the Hohmann transfer. Going farther down the paraboloid is easier the further the plane is rotated because at higher angles further rotation of the plane moves the intersection points much further down the plane. Noting that the ΔV change is proportional to the angular change of the plane swinging down to lower points on the paraboloid can be done for little cost. The new intersection points represent the intermediate ellipse of the bi-elliptic. The second maneuver brings the periapse of the intermediate ellipse up to the radius of the desired final orbit. The rotation of the plane at this point can be done at little cost because the long length created by the steep angle from the first maneuver means a small change in angle will sweep a large distance on the paraboloid. And, finally, the last maneuver for the bi-elliptic will raise the plane back up so that it is perpendicular to the z-axis at the final radius.

The new maneuver is also explained with this concept. For this maneuver, the spacecraft is attempting to achieve escape velocity, or fall off the edge of the paraboloid.

Reaching that status directly would be a simple exercise in rotating the plane downward a sufficient angle. With the new maneuver, a lower total rotation can be had by first rotating the plane upward towards the apex of the paraboloid. At a higher point on the paraboloid, a second rotation can move the plane off the edge of the paraboloid, or reach escape with a lower total rotation than using the direct option. And the break-even point between the two maneuvers is defined by whether the total rotation angle is sufficient to rotate towards the apex. If so, that corresponds to a ΔV equal to the initial orbital velocity which was calculated earlier to be the break-even point between the new and direct maneuver.

Finally the author believes that with time and effort the representation here could be used to improve on the approximation techniques already derived. Consider a continuous thrusting trajectory. Starting from a circular orbit, if a small thrust increment is applied along the velocity vector, then at the time step that corresponds to the thrust increment the plane will have changed through a small angle. The spacecraft will also have traveled during that time, moving to a new true anomaly. Now if the spacecraft was to apply another velocity increment at this point, it would have several options. To continue to thrust along the velocity vector would of course be near optimal for achieving the desired final orbit. However because the spacecraft has clocked along its trajectory to a new point, it is no longer opposite the point on the other side of the orbit that is closest to the desired final orbit. So to do another tangential burst would move the new opposite point towards the final orbit. The previous final point would also move towards the final orbit, but it won't travel as much as the new opposite point. It is better that the plane be rotated with pitch and a slight yaw. That will cause the original opposite point to

continue to travel the furthest distance towards the target final orbit. One can envision a trajectory etched on the side of the paraboloid where at each point the trajectory was optimized to minimize the total angular change required for the plane. Solving for this optimal path would translate to an optimal trajectory for the spacecraft. It should be noted however, that a globally optimal path might travel in non-locally optimal directions. For instance, a medium thrust version of the bi-elliptic would probably have the spacecraft traveling across the side of the paraboloid for the first maneuver, then straight down the side of the parabola on the other side, and then finally back up the first side.

Whether or not the plane and paraboloid analogy ever produces an algorithm for trajectory optimization, it has value as a teaching and visualization tool. The author intends to continue developing this concept as it seems to have considerable power to explain a host of phenomena regarding orbit transfer and mission analysis. Other geometries should be considered to create the most accurate reflection of orbital mechanics. A funnel, represented by an asymptotic line revolved about the z-axis may better represent the overall gravitational potential of the central body.

CHAPTER 6

COMPUTATIONAL RESULTS

6.1 Introduction

The algorithm generated in the last chapter has to be confirmed against proven methods before it can be deemed ready for use. This chapter is organized into several parts. The first few sections compare the algorithm against existing high, low and medium thrust performance solutions. The ability of the algorithm to predict payload fraction and mission time from mission requirements are compared to both computational and analytical results in the literature and computational results generated by the author. Next calculations are made determining the goodness of fit of the analytical result to the existing results. Using the analytical equation and the goodness of fit results, an uncertainty propagation analysis is conducted. This analysis identifies the major sources of error of which any user of the algorithm should be aware and should minimize. Finally some sample cases are plotted. The projected trajectory of the algorithm in this treatise is compared to existing trajectory models.

6.2 Comparison to High Thrust Solutions

High thrust analysis is very mature, with the appropriate equations having been in the literature for over a century. The algorithm was compared to curves generated using the semi-tangential transfer defined in Chapter 3.

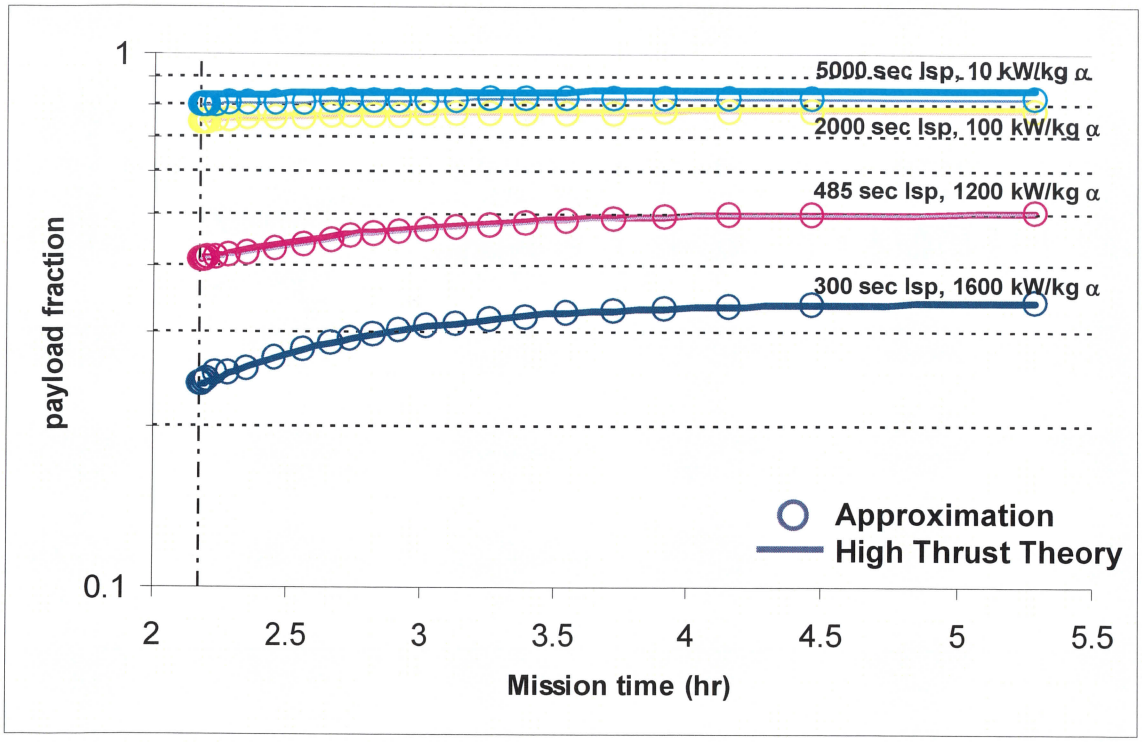

Figure 6.1 Comparison of the analytical approximation to the high thrust solution

6.3 Comparison to Low Thrust Solutions

Several low thrust solutions are employed to compare against the algorithm created in Chapter 5. The models covered in Chapter 3, created by Tsien and Levin, are plotted here. Note that these models assume either radial, centrifugal or tangential thrust uniformly and do not attempt to optimize the trajectory. Additionally, the formulation by Edelbaum and the ChebyTOP algorithm, also covered in Chapter 3 are plotted here.

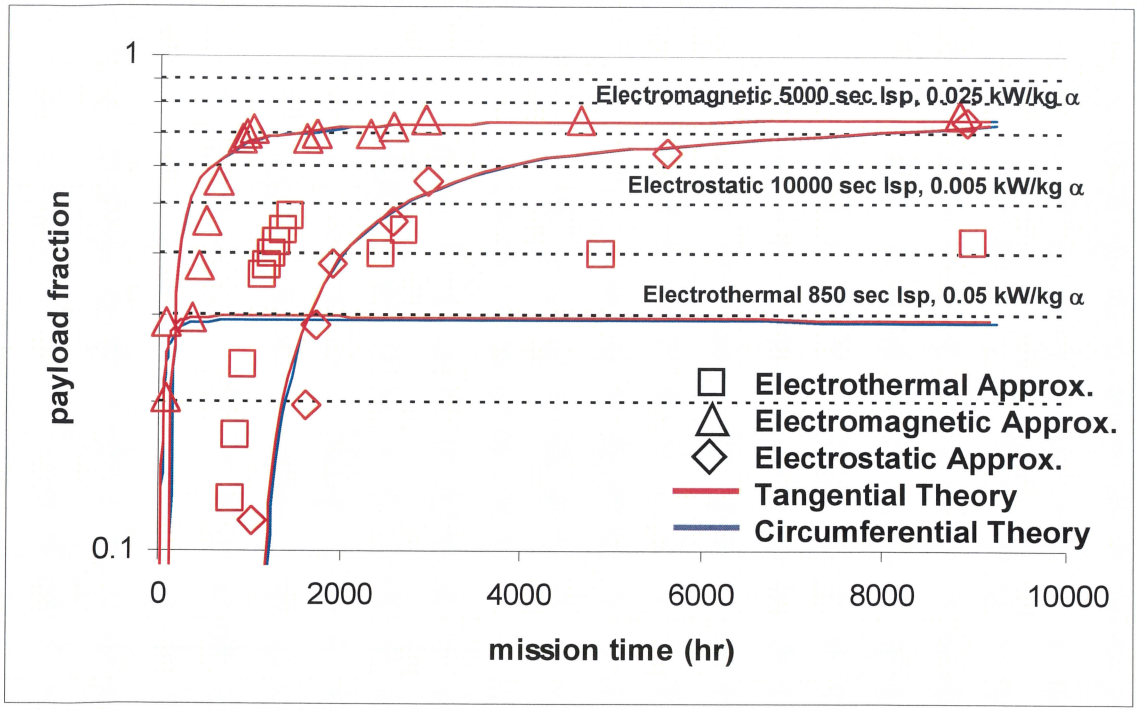

Figure 6.2 Comparison of analytical approximation to low thrust solutions

6.4 Statistical Analysis of Goodness of Fit

The variance between the analytical model and numerical solutions must be measured. The t-test for goodness of fit is documented in several texts [44]. The general standard for this test is that a probability of χ of 95% or better means the null hypothesis can be rejected; that is, the hypothesis that the two sets of data are not correlated. The results of this analysis are shown in Table 6.1 for all of the cases considered in Sections 6.2 to 6.4.

Table 6.1 Results of χ^2 test for analytical approximation

System	χ_0^2	P-value	(Yates)χ_0^2	P-value	*G-test*	P-value
High Thrust (T/W 110, Isp 300 sec)	0.0002	100.0	20.9496	58.42	0.0103	100.0
High Thrust (T/W 55, Isp 485 sec)	0.0012	100.0	12.97	95.26	0.1753	100.0
High Thrust (T/W 10, Isp 2,000 sec)	0.0009	100.0	7.65	99.89	0.2554	100.0
High Thrust (T/W 0.04, Isp 5,000 sec)	0.0277	100.0	6.247	99.98	1.4630	100.0
Electrothermal(α=0.05 kW/kg, Isp 850 sec)	1.7086	100.0	8.5617	96.90	1.539	100.0
Electromagnetic(α=0.02 5kW/kg, Isp 5,000 sec)	0.2124	100.0	8.3199	91.03	0.8136	100.0
Electrostatic (α=0.005 kW/kg, Isp 10,000 sec)	0.0907	100.0	7.9726	33.50	0.5737	99.91

Note: Electric propulsion systems compared to the circumferential model.

As can be seen from this table, the analytical approximation gives excellent agreement with high thrust systems. Agreement with the low thrust electric propulsion system performance was also good. However these results must be taken with a grain of salt. The chi-squared test is considered by some to not be accurate when expected values

are under 5 [45]. The Yates criterion is used in such cases to compensate for this effect. However the Yates criterion is known to overcompensate in correcting the error generated by the low expected values. Here the table shows that the 300 sec Isp option does not reject the hypothesis but the other high thrust options do. Scrutiny of Figure 6.1 shows that the expected and measured values for the 300 sec option seem to have as good agreement as for the higher specific impulse options. It seems that the lower expected value (payload fraction) for the 300 sec option is the difference that causes the Yates criterion to give a lower probability of agreement. This is also borne out by the fact that the probability given by the Yates criterion trends upward with increasing specific impulse (and therefore increasing payload fraction). Finally the table lists the results using the G-test [46]. Here again the G-test suggests excellent agreement with expected values. But the G-test also has difficulty with low expected values. The G-test replaces the Chi-squared test in cases with small sample sizes. Given that the number of points considered in this analysis total 24, it made sense to confirm that the G-test and Chi-Squared test gave similar probabilities, which they do.

However, looking at the figure in Chapter 5, it is clear that the fit is not nearly as good for these propulsion systems. The analytical approximation broke down, requiring much longer burn times to produce the same ΔV as was required by the approximations of Tsien and Levin. The best explanation is that these propulsion systems were pushing the limits of performance to do the Earth escape mission and therefore were too far from norm to be well approximated by the algorithm developed here. Despite this, it appears that the analytical approximation is sufficient to model high thrust and most low thrust

trajectories. Establishing the accuracy at these extremes of performance suggests that the approximation will give good results in the medium thrust range as well.

6.5 Uncertainty Analysis to Results using Proposed Solution

It is instructive to evaluate the new algorithm and its predictive capabilities in the context of uncertainty propagation. The uncertainty calculations will reveal which factors are most important in driving the uncertainty of the performance estimates. The methodology used here is that described in Coleman and Steele [47].

For a given equation that is a function of several independent variables

$$r = r\left(X_1, X_2, X_3, ...X_j\right). \tag{6.1}$$

An estimate of the uncertainty for a given equation can be found as

$$U_r{}^2 = \left(\frac{\partial r}{\partial X_1}\right)^2 U_{X_1}{}^2 + \left(\frac{\partial r}{\partial X_2}\right)^2 U_{X_2}{}^2 + \left(\frac{\partial r}{\partial X_3}\right)^2 U_{X_3}{}^2 + ... + \left(\frac{\partial r}{\partial X_j}\right)^2 U_{X_j}{}^2 , \tag{6.2}$$

where U_X is the uncertainty of variable X and the partial differential term for each variable is the uncertainty multiplication factor (UMC) for that variable. This equation will be applied systematically to each governing equation in calculation of vehicle performance.

In this analysis, only bias errors are considered. No random errors are considered because all of the sources of uncertainty are contained inside equations with explicit variables. If this analysis was being conducted for a particular mission and a particular vehicle, there would be random errors in measurement of the appropriate celestial values and vehicle performance parameters.

Under consideration is the estimate of payload fraction for a given mission. So repeating equation (5.20) for convenience, the payload fraction is found as

$$\lambda = \frac{1}{MR} - \frac{T/W\big|_i}{T/W\big|_{prop}} - \varepsilon \tag{5.20}$$

Applying the uncertainty propagation equation yields

$$U_\lambda{}^2 = \frac{1}{MR^4} U_{MR}{}^2 + \frac{1}{T/W\big|_{prop}{}^2} U_{T/W_i}{}^2 + \frac{T/W\big|_i{}^2}{T/W\big|_{prop}{}^4} U_{T/W_{prop}}{}^2 + U_\varepsilon{}^2 \tag{6.3}$$

Next the uncertainties for each of the terms in the equation above must be evaluated. First is the evaluation of required initial mass once given the final mass. That mass ratio is given by the ideal rocket equation, repeated below.

$$MR = e^{\frac{\Delta V_{ideal}+\Delta V_{loss}}{g_o I_{sp}}} = e^{\frac{\Delta V_{ideal}}{g_o I_{sp}}} e^{\frac{\Delta V_{loss}}{g_o I_{sp}}} \tag{3.14}$$

Applying the uncertainty equation to the above yields

$$U_{MR}{}^2 = \frac{1}{g_o{}^2 I_{sp}{}^2} e^{\frac{2(\Delta V_{ideal}+\Delta V_{loss})}{g_o I_{sp}}} U_{\Delta V_{ideal}}{}^2 + \frac{1}{g_o{}^2 I_{sp}{}^2} e^{\frac{2(\Delta V_{ideal}+\Delta V_{loss})}{g_o I_{sp}}} U_{\Delta V_{loss}}{}^2 + \ldots \tag{6.4}$$
$$\frac{(\Delta V_{ideal}+\Delta V_{loss})^2}{g_o{}^4 I_{sp}{}^2} e^{\frac{2(\Delta V_{ideal}+\Delta V_{loss})}{g_o I_{sp}}} U_{g_0}{}^2 + \frac{(\Delta V_{ideal}+\Delta V_{loss})^2}{g_o{}^2 I_{sp}{}^4} e^{\frac{2(\Delta V_{ideal}+\Delta V_{loss})}{g_o I_{sp}}} U_{Isp}{}^2$$

There are a number of variables in the above equation that are sources of uncertainty. Both the ideal and loss ΔV variables are shown as well as the gravitational constant and the specific impulse. The loss term can be expected to dominate here as the specific impulse is generally well understood for a given propulsion system and the ideal ΔV and gravitational constant can be calculated to a high level of accuracy.

Next is the uncertainty represented by the propulsion system thrust to weight term. Repeated for convenience is equation (5.17) below.

$$\left.\frac{T}{W}\right|_{prop} = \frac{2\eta_{tot}\alpha}{I_{sp}g_0{}^2} \tag{5.17}$$

Applying equation (6.2) to the above yields

$$U^2_{T/W_{prop}} = \left(\frac{2\alpha}{I_{sp}g_0{}^2}\right)^2 U^2_{\eta_{tot}} + \left(\frac{2\eta_{tot}}{I_{sp}g_0{}^2}\right)^2 U^2_{\alpha} + \left(\frac{2\eta_{tot}\alpha}{I_{sp}{}^2 g_0{}^2}\right)^2 U^2_{I_{sp}} + \left(\frac{2\eta_{tot}\alpha}{I_{sp}g_0{}^3}\right)^2 U^2_{g_0} \tag{6.5}$$

Again the uncertainty in the gravity term can be expected to give a low contribution. The contribution of the propulsion system total efficiency should be the next lowest contribution because the uncertainty of the total efficiency is limited to a value between 0 and 1, same as the total efficiency itself. So the uncertainties of the specific power and specific impulse variable are expected to combine to make up the major contribution of the propulsion system thrust to weight uncertainty.

Rolling the uncertainties from propulsion system thrust to weight and mass ratio equation (6.3) requires that the terms will be multiplied by the UMF for propulsion system thrust to weight and mass ratio, respectively. Mass ratio is generally a number greater than but close to unity. From equation (6.3) it seems clear that the uncertainty in payload fraction and therefore the capabilities of the vehicle are a strong function of the accuracy of the loss ΔV. Note that the UMF for ΔV loss will go up exponentially as the total ΔV requirement for the mission goes up. That suggests that accuracy is more difficult to attain for low thrust missions as it is for medium or high thrust missions. This problem is further exacerbated by considering the other terms in equation (6.3). Note that the uncertainty for initial and final thrust to weight is also multiplied by the inverse of the propulsion system thrust to weight. Clearly low thrust systems, which will have much lower propulsion system thrust to weights than medium and high thrust systems, will

have considerably higher UMF than would their medium and high thrust counterparts. This agrees with the results of the last section, where accuracy was obtained at the high thrust level but not as much at the low thrust level. This gives further confidence that the algorithm as stated will give good results in the medium thrust range.

Further clarity is obtained by comparing several sample cases. Below lists the pertinent independent variables for a typical high, low and medium thrust mission.

Table 6.2 Independent variables and typical values for high, low, and medium thrust missions to escape low Earth orbit

Variable	*% error*	*High*	*Low*	*Medium*
Specific Power, α (kW/kg)	5	1650	0.025	100
Total Efficiency, η_{tot}	1	1	1	1
Specific Impulse, I_{sp} (sec)	1	320	5000	77,000
Gravitational constant, g_0 (m/sec^2)	0.1	9.807	9.807	9.807
ΔV_{ideal} (km/sec)	1	3	3	3
ΔV_{loss} (km/sec)	10	0.1	3	1
Initial T/W, T/W_i	10	0.4	0.000007	0.0001
Tankage mass fraction, e	10	0.1	0.1	0.1

Given the data above, the uncertainty contributions for each variable and for each scenario (High, Low and Medium thrust) can be calculated. These contributions are illustrated in Figure 6.3. First it is important to note that the specific impulse and

gravitational constant variables contribute to the payload mass fraction uncertainty through uncertainties in both the mass ratio and propulsion system thrust to weight. The contribution through both variables to payload mass fraction uncertainty is represented in the figure. Second it is important to note that there is still some dependence between initial thrust to weight and ΔV_{loss} in that higher thrust to weight would mean lower burn time and potentially lower ΔV_{loss}. However the connection between the variables is connected through integration of the gravitational loss term. Evaluating that connection would require more data than is readily available. The examples in Table 6.2 were evaluated so that that the relationship between ΔV_{loss} and initial thrust to weight were optimized.

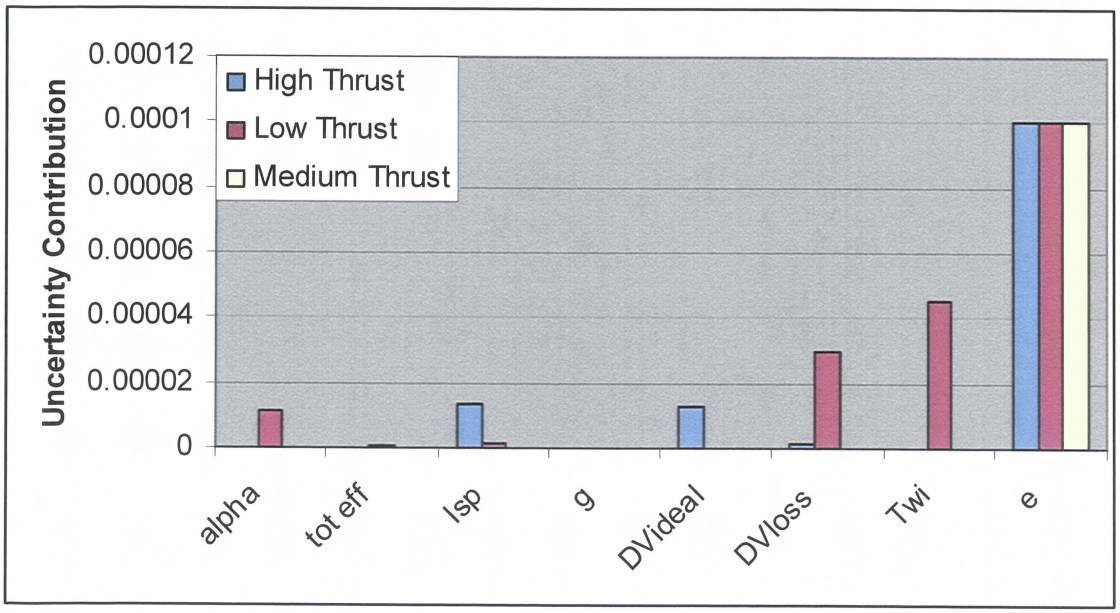

Figure 6.3 Uncertainty contributions to payload mass fraction for independent variables under the considered scenarios

Several points can be gleaned from this figure. First and most important is that the major contribution in the uncertainty for payload mass fraction is the uncertainty in tankage mass fraction. Thus, it suggests that the efforts made in the literature (including this treatise) have not paid sufficient attention to reducing the uncertainty contributed by tankage mass fraction. In fact in many analyses the tankage mass fraction is either ignored or rolled into the payload mass fraction.

The next highest contribution depends on the scenario considered. For high thrust systems, the highest uncertainty comes from specific impulse and the estimate of the required ideal ΔV. For low thrust systems, the contribution comes from the initial thrust to weight, specific power and ΔV_{loss}. It is interesting that the variables that represent the weaknesses of the high and low thrust systems, respectively, also are the major contributors to the uncertainties in their performance. Thus, when a vehicle designer is using either type of propulsion system, he/she must be cautious is pressing the limits of performance in trying to achieve a given mission. For example in the above case, if the propulsion designer working on an earth escape system decides to use a low thrust system, accuracy in estimating ΔV_{loss} is critical in accurately calculating performance. But the analyst will also work to reduce ΔV_{loss} before other variables because it has a greater impact on performance.

Finally, contributions to medium thrust propulsion system performance uncertainty are very small relative to similar contributions for the medium and high thrust systems. The only medium thrust contribution of note is the aforementioned contribution by the tankage mass fraction. This collaborates the premise that uncertainties in performance from ΔV_{loss} have less effect on the estimate of medium thrust performance.

Which implies again that since the algorithm developed herein had strong correlation with high thrust scenarios and relatively good correlation with low thrust scenarios, it can be expected to have correlation with medium thrust scenarios as good or better than the low thrust scenarios.

CHAPTER 7

CONCLUSIONS AND RECOMMENDATIONS

A review of the literature illustrates two points of major importance. First, many authors over the last 60 years have devoted considerable time developing relationships to quickly calculate vehicle performance for launch vehicle and in-space trajectories. Second is that those relationships still involve considerable assumptions and have limited use and accuracy. This dissertation summarizes the author's effort to bring some additional organization and new insight to this problem.

Chapter 5 contains a development a new set of non-dimensional variables specifically intended to facilitate mission analysis, trajectory optimization and vehicle design. The latter half of Chapter 5 includes extensive derivation of the core component of this thesis, a new medium thrust relationship. In the course of investigating possible guidance algorithms, a new maneuver was discovered. This maneuver, an offshoot of the Oberth Effect, allows for more efficient escape maneuvers from solar orbit.

Several mathematical approaches were attempted in development of this algorithm. While the attempts did not meet with success, there is some value in delineating failed approaches. Some options include using calculus of variations to optimize a trajectory. Hypergeometric functions were used to give as generic a polynomial expansion as possible for modeling the trajectory. These approaches are described in Appendix C. During the course of these events, a new extension of the

isoparametric problem was developed. This extension has application to optimization problems cast in the form of second order partial differential equations of two variables.

This relationship is compared to existing models in the literature in Chapter 6. The performance estimation for low, medium and high thrust systems is plotted against the performance estimated by the algorithm in this treatise. Additionally the projected trajectories are compared to both analytical and computational results. A goodness of fit analysis suggests that the medium thrust analysis predicts performance with good accuracy. The medium thrust algorithm is more accurate with high thrust systems than low thrust systems. Using the predictive capability of the medium thrust algorithm, an uncertainty analysis of the system suggests that the medium thrust algorithm can predict performance within 10 percent.

There is a long list of items to be considered in efforts following this one. The analysis of the slingshot maneuver would benefit from being extended to orbit to orbit transfer. The current analysis is applicable mainly to escape or fly-by scenarios. A more rigorous proof of the necessity to operate the propulsion system at full power is suggested.

Inclination changes were not addressed in this treatise. For escape maneuvers, inclination is rarely a strong factor in mission requirements. However most orbit to orbit transfers involve a rendezvous with a target and that frequently implies an inclination change. For transfers from planet to planet in the solar system, the inclination change is very small. But as was pointed out in the uncertainty analysis in Chapter 6, even small changes in inclination can have a significant effect on mission requirements.

The treatise here only assumes two-body motion. A natural extension of this treatise would be to employ the patched conic approximation for motion under the influence of three bodies. This would allow for approximate techniques to calculate missions starting at LEO and rendezvous with another planet or other celestial body.

The algorithm given within does not anticipate starting from non-circular orbits. Future work should address that deficiency. Other regimes that the algorithm should be applied to is non-constant thrust systems such as variable specific impulse systems or propulsions systems that have a drop off with distance from the sun, such as solar sails or solar electric propulsion systems.

Future work should also consider broadening the application of this algorithm to problems other than orbital mechanics. Electromagnetic environments also experience a $1/r^2$ change in potential. Application of these equations may simplify some equations in plasma physics and optics.

The medium thrust algorithm derived herein has been shown to be relatively accurate over a wide range of application. It should prove to assist in trajectory analysis and will facilitate NASA conceptual design studies.

APPENDICES

Appendix A

CELESTIAL CONSTANTS USED IN THIS TREATISE

The gravitational constants in the table below are referenced from the Northrop-Grumman Space Data book [48].

Table A.1 Celestial constants

Body	Gravitational Parameter (km3/sec2)	Semi-major axis (AU)	Equatorial Radius (km)
Sol	$1.32712 \cdot 10^{11}$	n/a	$1.392 \cdot 10^{6}$
Mercury	$2.18 \cdot 10^{4}$	0.387	$2.44 \cdot 10^{3}$
Venus	$3.249 \cdot 10^{5}$	0.723	$6.05 \cdot 10^{3}$
Earth	$3.986 \cdot 10^{5}$	1.000	$6.38 \cdot 10^{3}$
Mars	$4.293 \cdot 10^{4}$	1.524	$3.40 \cdot 10^{3}$
Jupiter	$1.267 \cdot 10^{8}$	5.203	$7.15 \cdot 10^{4}$
Saturn	$3.792 \cdot 10^{7}$	9.539	$6.03 \cdot 10^{4}$
Uranus	$5.788 \cdot 10^{6}$	19.190	$2.56 \cdot 10^{4}$
Neptune	$6.8 \cdot 10^{6}$	30.060	$2.48 \cdot 10^{4}$

Other pertinent constants

Astronautical Unit, $AU = 149.6 \cdot 10^{6}$ km

Speed of light in a vacuum, $c = 299{,}792{,}458$ m/sec

Gravitational constant, $g_0 = 9.807$ m/s^2

Appendix B

CONSERVATION OF ENERGY FOR THE NEW MANEUVER

For convenience, the specific mechanical energy or vis-visa equation is repeated here.

$$\xi = \frac{V^2}{2} - \frac{\mu}{r} = \frac{-\mu}{2a} . \tag{B.1}$$

Starting from a circular orbit, the initial specific orbital energy can be found by noting $a = r_0$. The masses of the various components must also be calculated. Given a particular $\Delta V_1, \Delta V_3$ and *Isp*, the masses of the spacecraft, ejected mass of the first burn, and ejected mass of the second burn are

$$\frac{M_f}{M_i} = e^{-\frac{\Delta V_1 + \Delta V_3}{g_0 I_{sp}}} \tag{B.2}$$

$$\frac{M_{\Delta V_1}}{M_i} = 1 - e^{-\frac{\Delta V_1}{g_0 I_{sp}}} \tag{B.3}$$

$$\frac{M_{\Delta V_3}}{M_i} = \frac{M_{\Delta V_1}}{M_i} - e^{-\frac{\Delta V_3}{g_0 I_{sp}}} = 1 - e^{-\frac{\Delta V_3}{g_0 I_{sp}}} - e^{-\frac{\Delta V_1}{g_0 I_{sp}}} . \tag{B.4}$$

Repeated applications of the vis-visa equation to the spacecraft, first ejected mass and second ejected mass will give the specific mechanical energy of each component after the slingshot or inverse bi-elliptic maneuver. The specific mechanical energy for the spacecraft was derived in Chapter 5 to be

$$\xi_3 = \left(V_1^{\,2} - 2\frac{\mu}{r_0} \right) \cdot \left(\frac{1}{2} - \frac{\Delta V_3}{V_1} \right) + \frac{\Delta V_3^{\,2}}{2} \quad , \tag{B.5}$$

where

$$V_1 = \sqrt{\frac{\mu}{r_0}} - \Delta V_1 \quad . \tag{B.6}$$

The specific mechanical energy for the two slugs of propellant are

$$\xi_{\Delta V_1} = \frac{\left(V_0 + g_0 I_{sp} \right)^2}{2} - \frac{\mu}{r_0} \tag{B.7}$$

$$\xi_{\Delta V_3} = \frac{\left(V_2 - g_0 I_{sp} \right)^2}{2} - \frac{\mu}{r_2} \quad . \tag{B.8}$$

Note that the term $g_0 I_{sp}$ equals the exhaust velocity under the assumption in this treatise that propellant exhaust is fully expanded against a vacuum. Thus the velocity term is simply the velocity of the rocket combined with the velocity of the exhaust combined with the appropriate term to indicate whether the thrust with or against the velocity vector.

Multiplying each of these specific energies against the relevant masses and summing will give the total mechanical energy of spacecraft plus the two ejected masses. However it makes sense to simplify the specific mechanical energy of the last burn first. Solving for r_2 and V_2 requires the same principles as in Chapter 5.

The difference in mechanical energies must be equal to power delivered to the spacecraft. Noting that the jet power equation is found as

$$P_{jet} = \frac{1}{2}\dot{m}V_e^2 \quad , \tag{B.9}$$

substituting for exit velocity and assuming constant thrust yields

$$P_{jet} = \frac{1}{2}\frac{m_p}{t_b}\left(g_0 I_{sp}\right)^2 \quad . \tag{B.10}$$

So the jet energy is simply the jet power over the burn time

$$E_{jet} = \frac{1}{2}m_p\left(g_0 I_{sp}\right)^2 \quad . \tag{B.11}$$

And this energy has to exceed the difference in energy from the final to initial condition of the spacecraft and ejected masses.

Appendix C

UNSUCCESSFUL ATTEMPTS TO DETERMINE AN OPTICAL GUIDANCE SCHEDULE

The isoperimetric function applies here. Its first application was to prove that maximum area that can be contained by a closed line of a given length takes the form of a circle. This method is used to find the maxima or minima of an integral based on a particular constraint which is also an integral. Here the equation to maximize is the one that calculates the payload fraction. It is again

$$\lambda = \frac{M_f}{M_i} - \frac{m_{prop}}{M_i} - \varepsilon \quad . \tag{C.1}$$

This equation requires maximization in stages. For instance maximization of the first term above suggests minimization of the ΔV requirement. However the ΔV must be minimized in such a way that the ΔV still met the minimum requirements for the mission.

The ΔV requirement can be constrained using the isoperimetric constraint to the integral J in the payload fraction equation. So

$$I = \int_0^{t_b} \frac{\mu}{r^2}\sin\gamma + a(1-\cos\alpha')dt + \lambda_l\left[\Delta V_{ideal} - \int_0^{t_b} a - \frac{\mu}{r^2}\sin\gamma - a(1-\cos\alpha')dt\right], \tag{C.2}$$

where λ_l is a Lagrangian multiplier. The loss mechanisms in the integral on the left are to be minimized. The Lagrangian multiplier on the right multiplies a zero term, which is that the integral must sum to equal the ideal ΔV requirement. The integral resolves to

$$I = \lambda_l \Delta V_{ideal} + \int_0^{t_b} (1 + \lambda_i) \left[\frac{\mu}{r^2} \sin\gamma + a(1 - \cos\alpha') \right] - a dt \tag{C.3}$$

The ΔV requirement to the mission requirements can be calculated using high thrust relationships. The most general solutions for coplanar transfer between two orbits are solutions to Lambert's problem. Consider Figure C.1.

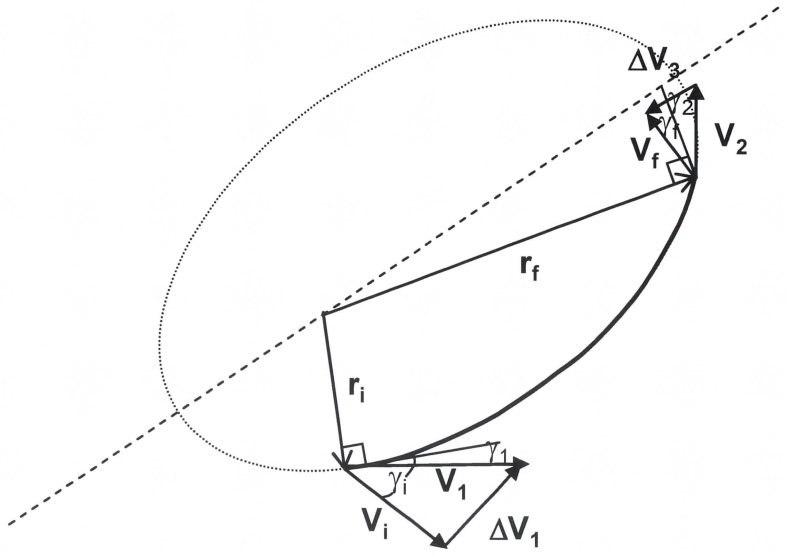

Figure C.1 Lambert's problem

The angle between the initial and final radii is defined by the dot product between the two vectors.

$$\cos(\Delta\nu) = \frac{\vec{r}_i \cdot \vec{r}_f}{|\vec{r}_i||\vec{r}_f|} = \frac{x_i x_f + y_i y_f}{r_i r_f} \tag{C.4}$$

An equation for the semi-major axis must be found to determine required ΔV between the initial and final points. For a semi-tangential transfer, the initial orbit is circular. For the

Lambert's problem, the initial and final positions are more arbitrary. Equations for both situations are derived.

For the semi-tangential, the angle between radii was also defined in Chapter 3 as

$$\cos(\Delta\nu) = \frac{1}{e}\left[\frac{a(1-e^2)}{r_f} - 1\right]. \tag{C.5}$$

While the eccentricity is given as

$$e = 1 - \frac{r_i}{a}. \tag{C.6}$$

Setting the equations equal to one another and inserting the equation above for eccentricity yields

$$\frac{x_i x_f + y_i y_f}{r_i r_f} = \frac{1}{1-\frac{r_i}{a}}\left[\frac{a\left(1-\left(1-\frac{r_i}{a}\right)^2\right)}{r_f} - 1\right]. \tag{C.7}$$

After some algebra, this equation reduces to

$$a = \frac{(x_i x_f + y_i y_f) r_i - r_i^3}{r_i r_f + x_i x_f + y_i y_f - 2r_i^2}. \tag{C.8}$$

Since the initial orbit is circular, the initial position can be arbitrarily set to x_i=0 and y_i=-r_i. The above equation reduces to

$$a = \frac{r_i^2 + y_f r_i^2}{2r_i - r_f + y_f}. \tag{C.9}$$

For Lambert's problem, it is simple to define the chord that connects the initial and final radii. It is

$$c = \sqrt{r_i^{\,2} + r_f^{\,2} - 2r_i r_f \cos(\Delta\nu)} \quad . \tag{C.10}$$

Recalling equation (C.4) the equation above becomes

$$c = \sqrt{r_i^{\,2} + r_f^{\,2} - 2r_i r_f \left(x_i x_f + y_i y_f\right)} \quad . \tag{C.11}$$

Using the chord definition, the semi-major axis is found as

$$a = \frac{r_i + r_f + c}{4} \quad . \tag{C.12}$$

With either scenario finding the semi-major axis of the transfer ellipse allows for calculation of the total ΔV required to maneuver from the initial to final point. The velocity along the transfer ellipse after the first maneuver is

$$V_1 = \sqrt{\frac{2\mu}{r_i} - \frac{2\mu}{a}} \quad . \tag{C.13}$$

And similarly, for the velocity before the second maneuver is

$$V_2 = \sqrt{\frac{2\mu}{r_f} - \frac{2\mu}{a}} \quad . \tag{C.14}$$

The flight path angles required at points 1 and 2 are calculated as

$$V_2 = \sqrt{\frac{2\mu}{r_f} - \frac{2\mu}{a}} \quad . \tag{C.15}$$

The initial flight path angle and final flight path angle are defined by the initial and final radii and velocities defined in the problem. Thus the ΔV required for the maneuver is simply found by using the law of cosines.

$$\Delta V_1 = \sqrt{V_i^{\,2} + V_1^{\,2} - 2V_i V_1 \cos(\gamma_1 - \gamma_i)} \tag{C.16}$$

$$\Delta V_3 = \sqrt{V_f^2 + V_2^2 - 2V_f V_2 \cos(\gamma_f - \gamma_2)} \tag{C.17}$$

The sum of these two maneuvers is the least expensive way to get from an initial radius and velocity to a final radius and velocity.

The ideal ΔV requirement is now defined. The next step is to investigate methods to minimize equation (C.3). The integral on the right should be minimized. Complicating that effort is noting that a, r, γ, α' are all related. Consider the figure below that illustrates the relevant vectors and angles. It should be clear (and was implied in the original derivation of equation (C.3) that $\sin\gamma$ and $\cos\alpha'$ are angles that relate the orientation of the radius, velocity and acceleration vectors. Thus an examination of the figure shows that

$$|\vec{r}||\vec{V}|\sin\gamma = \vec{r}\cdot\vec{V} \tag{C.18}$$

and

$$|\vec{V}||\vec{a}|\cos\alpha' = \vec{V}\cdot\vec{a} \tag{C.19}$$

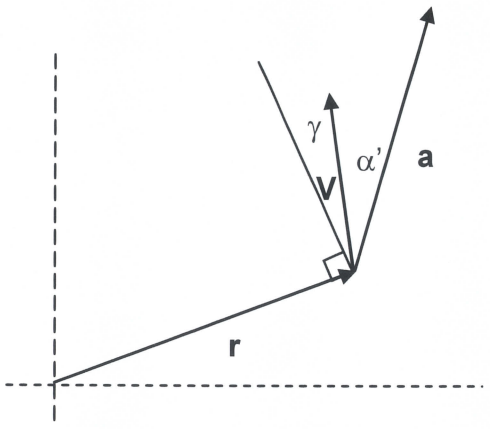

Figure C.2 Relationship between *r*, *V* and *a*

So equation (C.3) reflects a second-order, non-linear differential equation, which contains relations between radius, velocity and acceleration. Clearly, some simplification is required to make solution of this problem more tractable. The author tried several techniques, without success.

However the simplification that did produce results is documented here. The theory is as follows. At any given point along the propulsive trajectory, the optimal thrust direction is that one where the line of apsides does not change along the trajectory and the semi-major axis is gradually extended towards the target final orbit. The reasons behind this hypothesis are outlined in a later section.

Imagine a point along a thrusting trajectory where the optimal thrust angle is desired. In Figure C.3 below, this point is defined by the r and V vectors.

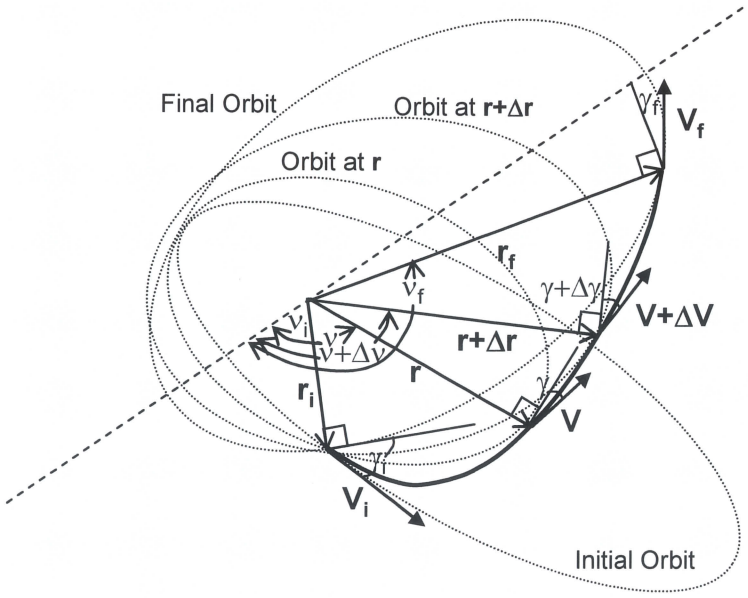

Figure C.3 Differential change in trajectory from initial to final position

Based on the theorem above, the difference between the current flight path angle and the flight path angle desired to increase the semi-major axis along the line of apsides is desired. So the difference in the flight path angles is

$$\alpha' = \gamma - \gamma_f \,. \tag{C.20}$$

Of course the flight path angle is defined

$$\alpha' = \cos^{-1}\left(\frac{H}{rV}\right) - \gamma_f \,. \tag{C.21}$$

Angular momentum is a function of eccentricity and semi-major axis, so

$$\alpha' = \cos^{-1}\left(\frac{\sqrt{\left(1-e^2\right)\mu a}}{rV}\right) - \gamma_f \,. \tag{C.22}$$

And the eccentricity can be replaced with

$$\alpha' = \cos^{-1}\left(\frac{\sqrt{\left(1-\left(\frac{r_f - r}{r\cos(\nu) - r_f\cos(\nu_f)}\right)^2\right)\mu a}}{rV}\right) - \gamma_f \,. \tag{C.23}$$

The semi-major axis was defined earlier by the chord between the initial and final radii

$$\alpha' = \cos^{-1}\left(\frac{\sqrt{\left(1-\left(\frac{r_f - r}{r\cos(\nu) - r_f\cos(\nu_f)}\right)^2\right)\mu\sqrt{r^2 + {r_f}^2 - 2rr_f\cos(\Delta\nu)}}}{rV}\right) - \gamma_f \,. \tag{C.24}$$

This equation can be rearranged to get

$$\alpha' = \cos^{-1}\left(\frac{\sqrt{\left(\left(\cos(\nu) - \frac{r_f}{r}\cos(\nu_f)\right)^2 - \left(\frac{r_f}{r} - 1\right)^2\right)\frac{\mu}{r_f}\left[\frac{r}{r_f} + 1 + \sqrt{\left(\frac{r}{r_f}\right)^2 + 1 - 2\frac{r}{r_f}\cos(\Delta\nu)}\right]}}{\left(\frac{r}{r_f}\cos(\nu) - \cos(\nu_f)\right)}\right) - \gamma_f \quad \text{(C.25)}$$

Taking the limit as r approaches r_f and V approaches V_f.

$$\alpha' = \cos^{-1}\left(\frac{\sqrt{\left(\left(\cos(\nu) - \cos(\nu_f)\right)\right)^2\left[2 + \sqrt{2 - 2\cos(\Delta\nu)}\right]}}{\left(\cos(\nu) - \cos(\nu_f)\right)}\right) - \gamma_f \quad \text{(C.26)}$$

Applying some basic trigonometric relations reduces the above equation to

$$\alpha' = \cos^{-1}\left(\frac{\sqrt{2}}{2}\sqrt{1 + \sin\left(\frac{\Delta\nu}{2}\right)}\right) - \gamma_f \quad \text{(C.27)}$$

Applying this new guidance schedule to equation (C.3) yields

$$\alpha' = \cos^{-1}\left(\frac{\sqrt{2}}{2}\sqrt{1 + \sin\left(\frac{\Delta\nu}{2}\right)}\right) - \gamma_f \quad \text{(C.28)}$$

Consider the definition of radius, velocity and acceleration. The resulting equation becomes

Current isometric theory extends to applications of second-order ordinary differential equations and first order partial differential equations of two independent variables. Extending the isoperimetric theory to cover second-order partial differential equations was required. The proof is a straightforward extension of current theory and is defined in Appendix D. The resulting equation is given as

$$I = \int F(t, x, x', x'', y, y', y'') + \lambda G(t, x, x', x'', y, y', y'')dt \quad \text{(D.6)}$$

This integral is minimized when

$$\frac{\partial f}{\partial x} - \frac{d}{dx}\frac{\partial f}{\partial y'} + \frac{d^2}{dx^2}\frac{\partial f}{\partial y''} = 0 \quad \text{(C.29)}$$

For the integral in (C.3), the definitions are

$$x = t, \quad y = r \quad y' = V \quad y'' = a \quad \text{(C.30)}$$

From this, the derivatives to be plugged into (C.29) become

$$\frac{\partial f}{\partial x} = \frac{2\lambda_l \mu}{r^3}\sin\gamma \quad \text{(C.31)}$$

$$\frac{\partial f}{\partial y'} = 0 \quad \text{(C.32)}$$

$$\frac{d^2}{dx^2}\frac{\partial f}{\partial y''} = 2a'' \quad \text{(C.33)}$$

Substituting back into (C.29) yields

$$\frac{2\lambda_l \mu}{r^3}\sin\gamma + 2a'' = 0 \quad \text{(C.34)}$$

Integrating acceleration twice with respect to time yields

$$a = \frac{\lambda_l \mu}{r}\sin\gamma + C_1 t + C_2 \quad \text{(C.35)}$$

Defining the acceleration due to thrust as

$$a_T = C_1 t + C_2, \quad \text{(C.36)}$$

the Lagrangian multiplier is defined as

$$\lambda_l = \frac{a_T}{\frac{\mu}{r}\sin\gamma} \tag{C.37}$$

There are three constants to be defined here, C_1, C_2 and λ_l. The first two constants are easily found by realizing the initial and final accelerations are given by $\frac{F}{g_0 M_i}$ and $\frac{F}{g_0 M_f}$. The Lagrangian multiplier is defined by realizing that ΔV for the mission must remain constant. Thus returning to equation (5.32) and making some of the substitutions conducted earlier yields

$$\Delta V = \int_0^{t_b} -\frac{\mu}{r^2}\sin\gamma + a\cos\alpha' \, dt \tag{C.38}$$

Substituting equation (C.37) gives

$$\Delta V = \int_0^{t_b} -\frac{a_T}{r\lambda_l} + a\cos\alpha' \, dt \tag{C.39}$$

Consider the definition of radius, velocity and acceleration. The resulting equation becomes untractable when applied to the series of equations shown above. At this point the author abandoned this approach.

Appendix D

EXTENSION OF THE ISOPERIMETRIC PROBLEM TO SECOND ORDER DIFFERENTIAL EQUATIONS AND FUNCTIONS OF TWO VARIABLES

The proof given here extends the proofs given in [49] for calculus of variations using second order derivatives and the isoperimetric problem involving only first order derivatives.

The isoparametric problem finds the extrema of a given integral (as in calculus of variations) but also while meeting a subsidiary constraint. Thus the equation

$$J(y)=\int_a^b F(x,y,y')dx \tag{D.1}$$

is either maximized or minimized subject to the constraint that

$$K(y)=\int_a^b G(x,y,y')dx \tag{D.2}$$

must equal a given constant L. Following standard isoparametric theory, this result can be extended to functions that contain both first and second derivatives of y. Euler's equation gives for a function

$$F(x,y,y',y''), \tag{D.3}$$

the extrema can be found to satisfy

$$F_y-\frac{d}{dx}F_{y'}\frac{d^2}{dx^2}F_{y''}=0 \tag{D.4}$$

Thus the isoparametric problems for second order differentials is simply

$$F_y - \frac{d}{dx}F_{y'} \frac{d^2}{dx^2}F_{y''} - \lambda\left[G_y - \frac{d}{dx}G_{y'} \frac{d^2}{dx^2}G_{y''}\right] = 0 \quad , \tag{D.5}$$

which is similar in form to the isoparametric form for first order differentials. Now the problem to solve here is

$$I = \int_0 F(t, x, x', x'', y, y', y'') + \lambda G(t, x, x', x'', y, y', y'')dt \quad . \tag{D.6}$$

So applying equation (D.4) to this problem yields

$$\frac{d}{dt}F - \frac{d}{dt}F_{x'} + \frac{d^2}{dt^2}F_{x''} - \lambda\left[\frac{d}{dt}G - \frac{d}{dt}G_{x'} + \frac{d^2}{dt^2}G_{x''}\right] = 0 \tag{D.7}$$

and

$$\frac{d}{dt}F - \frac{d}{dt}F_{y'} + \frac{d^2}{dt^2}F_{y''} - \lambda\left[\frac{d}{dt}G - \frac{d}{dt}G_{y'} + \frac{d^2}{dt^2}G_{y''}\right] = 0 \quad . \tag{D.8}$$

Subtracting the two equations yields

$$-\frac{d}{dt}\left(F_{x'} - F_{y'}\right) + \frac{d^2}{dt^2}\left(F_{x''} - F_{y''}\right) = \lambda\left[-\frac{d}{dt}\left(G_{x'} - G_{y'}\right) + \frac{d^2}{dt^2}\left(G_{x''} - G_{y''}\right)\right] \quad . \tag{D.9}$$

And integrating yields

$$-\left(F_{x'} - F_{y'}\right) + \frac{d}{dt}\left(F_{x''} - F_{y''}\right) = \lambda\left[-\left(G_{x'} - G_{y'}\right) + \frac{d}{dt}\left(G_{x''} - G_{y''}\right)\right] + C \quad . \tag{D.10}$$

This equation was used in attempts to derive a analytical solution for the two-body problem. Those attempts are documented in Appendix C.

Appendix E

NON-DIMENSIONAL ANALYSIS

E.1 Non-dimensional Analysis

The Buckingham-Pi analysis method is applied here to determine non-dimensional variables that may simplify the medium thrust two-body problem. The Buckingham-Pi theory is not discussed here, it can be found easily in standard texts in fluid mechanics [50].

If we consider the equations from Chapter 3 that are of interest here, we can develop a table of variables that will be important to this analysis. Table E.1, shown below lists each of those variables. It is important to note the fundamental dimensions that are important to the medium thrust two-body problem, a scan of the table reveals that there are three: mass (M), length (L), and time (θ). Given that the table shows 8 generic variables, in actuality there are many more when the subscripts of the individual variables are included. The Buckingham-Pi analysis tells us that the number of non-dimensional variables will equal the number of variables minus the three fundamental dimensions. Note that these are generic variables, meaning where noted there would be a subscript further indicating what this variable represents. However, for the purposes of non-dimensional analysis, those subscripts are largely ignored here.

Table E.1 List of pertinent variables for trajectory analysis

Variable	Description	SI Units	English Units	Fundamental Dimensions
M, m	Mass (with subscript)	kg	lbm	M
t, Isp	Time (with subscript) or specific impulse	sec	sec	θ
F	Thrust	N, kg-m/s^2	lbf, slug-ft/s^2	MLθ^{-2}
g_0, $\left\|\ddot{\vec{r}}\right\|$	Gravitational constant at earth surface, local gravitational acceleration	m/s^2	ft/s^2	Lθ^{-2}
$\left\|\vec{r}\right\|$	Radius (with subscript)	m, km	ft, nm	L
μ	Gravitational parameter	km^3/s^2	ft^3/s^2	L$^3\theta^{-2}$
P_{jet}	Jet power	W, kg-m^2/s^2	BTU/s	ML$^2\theta^2$
$\left\|\vec{V}\right\|$	Magnitude of velocity (with subscript)	m/s, km/s	ft/s, nm/s	Lθ^{-1}

Including the development of all of the non-dimensional variables in this treatise would be unnecessarily time consuming. Instead the derivation of the first non-dimensional variable is included below.

Before starting, three variables have to be selected as the standard variables that are potentially included in each non-dimensional variable. Selected are the thrust, *F*, the

burn time, t_b, and the instantaneous magnitude of the velocity, V. These variables are used because the three combined include each of the fundamental dimensions, and the author intuitively expects these variables to be of especially high importance in the later derivations.

For example the dimensionless variable including initial mass is shown in the equation below.

$$\pi_1 = M_i^a F^b t_b^c V^d . \tag{E.1}$$

In terms of fundamental dimensions, the equation can be rewritten as

$$\pi_1 = M^a \left(ML\theta^{-2}\right)^b \theta^c \left(ML^{-1}\right)^d . \tag{E.2}$$

The exponents a, b, c and d must be selected so that the underlying dimensions cancel out. We can then write three equations for mass, length and time, each equation incorporating a, b, c and d. In matrix form, the system of equations is

$$\mathbf{Ax} = \mathbf{0}, \tag{E.3}$$

where

$$\mathbf{A} = \begin{bmatrix} 1 & 1 & 0 & 0 \\ 0 & 1 & 0 & 1 \\ 0 & -2 & 1 & -1 \end{bmatrix} \tag{E.4}$$

and

$$\mathbf{x} = \begin{bmatrix} a \\ b \\ c \\ d \end{bmatrix}. \tag{E.5}$$

Using Gauss-Jordan elimination, **A** can be written as

$$\mathbf{A} = \begin{bmatrix} 1 & 1 & 0 & 0 \\ 0 & 1 & 0 & 1 \\ 0 & 0 & 1 & 1 \end{bmatrix}. \tag{E.6}$$

We still have three equations for four unknowns. It is important to note though that there are actually an infinite number of solutions that give a non-dimensional variable. All that is required is that the proportions of the exponents *a*, *b*, *c* and *d* remain the same. Therefore the simplest solution is to assume one of the variables is 1 and solve for the rest. So assuming d = 1 the solution for **x** is

$$\mathbf{x} = \begin{bmatrix} 1 \\ -1 \\ -1 \\ 1 \end{bmatrix}. \tag{E.7}$$

Applying these exponents to equation (E.2) yields

$$\pi_1 = M_i^1 F^{-1} t_b^{-1} V^1 = \frac{M_i V}{t_b F}. \tag{E.8}$$

Using a similar method, the table of all non-dimensional variables is given in Table E.2.

Table E.2 List of non-dimensional variables

Non-dimensional variable(s)	Equation	Pertinent variable(s)
$\pi_1 \rightarrow \pi_5$	$= \frac{MV}{t_b F}$	$M_i, M_f, m_L, m_{prop}, m_p$
$\pi_6 \rightarrow \pi_8$	$= \frac{t_b}{t_m}$	t_m, t_c, I_{sp}

Table E.2 Cont.

Non-dimensional variable(s)	Equation	Pertinent variable(s)
π_9, π_{10}	$= \frac{V}{g_0 t_b}$	$g_0, \lvert\dddot{\vec{r}}\rvert$
π_{11}	$= \frac{V^3 t_b}{\mu}$	μ
π_{12}	$= \frac{FV}{P_{jet}}$	P_{jet}
π_{13}	$= \frac{V t_b}{\lvert\vec{r}\rvert}$	$\lvert\vec{r}\rvert$

One of the most useful aspects of non-dimensional variables is the underlying meaning of the ratios in the variable. For instance the Reynolds number is the ratio of inertial to viscous forces acting inside the fluid. Thus for low Reynolds numbers we can assume viscous flows dominate and any perturbances are quickly dampened giving a laminar flow. Similarly the Mach number ratios the local velocity to the speed of sound. Once the Mach number exceeds unity, we know that there is supersonic flow and shock waves and expansion waves will set up if the flow is turned.

The physical meaning of the non-dimensional variables in Table E.2 is not immediately apparent in almost all cases. Therefore it makes sense to create new non-dimensional variables that are more meaningful by multiplying and dividing the current ones. Since the creation of new non-dimensional variables is somewhat intuitive, each one created is documented in the following paragraphs.

Starting with the first non-dimensional variable, we can create

$$\pi_{14} = \frac{\pi_9}{\pi_1} = \frac{V}{g_0 t_b} \frac{t_b F}{M_i V} = \frac{F}{g_0 M_i} \quad \text{(E.9)}$$

This is clearly the initial thrust-to-weight of the vehicle and is expected to be a major consideration in any analytical derivation. Similarly, final thrust-to-weight, propulsion system thrust-to-weight, etc., can be similarly derived by replacing the first non-dimensional variable with the second, third, etc., that is shown in Table E.2. The end result is a new thrust to weight with the appropriate mass term. This dimensionless number is quite prevalent in the literature, the author found it first used by Moeckel [51].

Another new variable is created by dividing π_9 through with π_8

$$\pi_{17} = \frac{\pi_9}{\pi_8} = \frac{V}{g_0 t_b} \frac{t_b}{I_{sp}} = \frac{V}{g_0 I_{sp}} \quad \text{(E.10)}$$

which if the difference in velocities is taken from final to initial, this would be the term in the ideal rocket equation.

It is already clear from the literature that for optimal performance of medium thrust systems there is a clear relation between specific impulse and specific power. Since the term above involves specific impulse, it would be very useful to have a similar term for specific power. So starting with the non-dimensional variables in Table E.2, one gets

$$\pi_{18} = \frac{1}{\pi_4 \pi_{12}} = \frac{F t_b}{m_{prop} V} \frac{P_{jet}}{FV} = \frac{t_b P_{jet}}{m_{prop} V^2} \quad \text{(E.11)}$$

Recalling the definition of specific power from Chapter 3 and recasting yields

$$m_{prop} = \frac{P_{jet}}{\eta_{tot}\alpha} \quad \text{(E.12)}$$

Substituting (E.11) into (E.12) yields

$$\pi_{18} = \frac{t_b P_{jet}}{\frac{P_{jet}}{\eta_{tot}\alpha}V^2} = \frac{t_b \eta_{tot}\alpha}{V^2} \quad \text{(E.13)}$$

Dividing through by π_{17} and π_8 yields

$$\pi_{19} = \frac{1}{\pi_{18}\pi_{17}\pi_8} = \frac{V^2}{t_b\eta_{tot}\alpha}\frac{g_0 I_{sp}}{V}\frac{t_b}{I_{sp}} = \frac{V}{\eta_{tot}\alpha/g_0} \quad \text{(E.14)}$$

This term is the vehicle velocity divided by a form of the characteristic velocity. The characteristic velocity is defined by Sutton [2], but an earlier version was defined by Moeckel [51].

And so the change in this variable will equal the change in velocity delivered to the vehicle divided by the jet power produced per unit weight of the propulsion system.

Vehicle acceleration can be related to local gravitational acceleration by

$$\pi_{21} = \frac{\pi_1}{\pi_{10}} = \frac{t_b\left|\ddot{\vec{r}}\right|}{V}\frac{M_i V}{F t_b}\frac{1/g_0}{1/g_0} = \frac{\left|\ddot{\vec{r}}\right|/g_0}{F/M_i g_0} \quad \text{(E.15)}$$

This non-dimensional number stands to be very important in evaluating when a mission concept is operating in the low, medium or high thrust regime.

The non-dimensional number π_{11} looks difficult, but it can be cast into a more useful form by

$$\pi_{22} = \frac{\pi_{11}}{\pi_{13}^{\,2}} = \frac{V^3 t_b}{\mu}\left(\frac{\left|\vec{r}\right|}{V t_b}\right)^2 = \frac{\left|\vec{r}\right|^2 V}{\mu t_b} \quad \text{(E.16)}$$

Still it is unclear what this non-dimensional variable represents. Further modification results in

$$\pi_{23} = \frac{\pi_{11}\pi_{12}}{\pi_{22}\pi_{13}} = \frac{M_i V}{F t_b} \frac{FV}{P_{jet}} \frac{\mu t_b}{|\vec{r}|^2 V} \frac{|\vec{r}|}{V t_b} = \frac{M_i \mu / |\vec{r}|}{t_b P_{jet}} \tag{E.17}$$

Note here that the top is just the negative of the gravitational potential and the bottom is the total jet energy delivered over the burn time. So this term can relate the change in potential energy with the burn.

The non-dimensional numbers π_{12}, and π_{13} do not require further modification. From Table E.2, it is clear that π_{12} is the ratio of the change in kinetic energy with jet power (if a difference between the initial and final velocity is used). Furthermore π_{13} is simply a status variable for the nominal orbit. It should prove useful as a single variable to indicate the orbital status of the vehicle during analysis. One reference for non-dimensional variables recognizes this as the Thompson number [52]. Moeckel [51] defines this as the propulsion-time number.

Table E.3 below shows all of the new dimensionless variables, their physical meanings, and the equations that define them. Also shown are new variable names assigned to them to give them meaning in the later analysis.

The first entry uses a subscript to designate the numerator of the non-dimensional variable. Specific impulse is shown, but a generic time variable, mission time or coast time could be applied as well.

Table E.3 List of non-dimensional numbers and their physical meanings

Name	π_X	Equation	Physical Meaning
τ_{Isp}	π_8	$= \frac{I_{sp}}{t_b}$	When combined with T/W it becomes a ratio of the exhaust velocity to acceleration over burn time
ψ	π_{12}	$= \frac{FV}{P_{jet}}$	$\psi_f - \psi_i = \frac{\text{change in kinetic energy}}{\text{jet power}}$
β	π_{13}	$= \frac{Vt_b}{\lvert\vec{r}\rvert}$	$= \frac{\text{distance traveled over burn time}}{\text{radius from center of dominant body}}$
$\left.\frac{T}{W}\right\rvert_i$	π_{14}	$= \frac{F}{g_0 M_i}$	= initial vehicle thrust to weight
$\left.\frac{T}{W}\right\rvert_f$	π_{15}	$= \frac{F}{g_0 M_f}$	= final vehicle thrust to weight
$\left.\frac{T}{W}\right\rvert_{prop}$	π_{16}	$= \frac{F}{g_0 m_{prop}}$	= propulsion system thrust to weight
γ	π_{17}	$= \frac{V}{g_0 I_{sp}}$	$\gamma_f - \gamma_i$ = exponent in ideal rocket equation
δ	π_{20}	$= \frac{V}{\eta_{tot}\alpha / g_0}$	$\delta_f - \delta_i = \frac{\text{change in velocity}}{\text{jet power per unit mass of propulsion system}}$
ς	π_{21}	$= \frac{\lvert\dddot{\vec{r}}\rvert / g_0}{F / M_i g_0}$	$= \frac{\text{gravitational acceleration in g's}}{\text{initial thrust acceleration in g's}}$
$/\phi$	π_{23}	$= \frac{M_i \mu / \lvert\vec{r}\rvert}{t_b P_{jet}}$	$= \frac{\text{gravitational potential energy}}{\text{energy delivered by jet during burn}}$

E.2 Relationships between Non-Dimensional Variables

Given the number of non-dimensional variables shown in the table above, it makes sense to apply some of the definitions and governing equations in Chapter 3 and see if these variables are related to each other. Noting that the difference between the initial mass and the final mass is the propellant mass, we can show

$$M_i - M_f = m_p \,. \tag{E.18}$$

Or by multiplying through with the gravitational constant over the thrust,

$$\frac{M_i g_0}{F} - \frac{M_f g_0}{F} = \frac{m_p g_0}{F} \,, \tag{E.19}$$

noting that the thrust equation can be defined as

$$F = \dot{m} V_e = \frac{m_p}{t_b} g_0 I_{sp} \,. \tag{E.20}$$

Combining equations (E.19) and (E.20) yields

$$\frac{M_i g_0}{F} - \frac{M_f g_0}{F} = \frac{m_p g_0}{F} \frac{F t_b}{m_p g_0 I_{sp}} = \frac{t_b}{I_{sp}} \,. \tag{E.21}$$

Using our non-dimensional variable definitions gives

$$\frac{1}{\left.\frac{T}{W}\right|_i} - \frac{1}{\left.\frac{T}{W}\right|_f} = \frac{1}{\tau_{Isp}} \,. \tag{E.22}$$

Next look at the definition of specific power. Starting with the equation from Chapter 3, substituting the definitions of δ and ψ yields

$$\alpha = \frac{V g_0}{\eta_{tot} \delta} = \frac{P_{jet}}{\eta_{tot} m_{prop}} \frac{FV}{P_{jet} \psi} \,. \tag{E.23}$$

Canceling terms and a little algebra give

$$\frac{\psi}{\delta} = \frac{F}{m_{prop} g_0} = \left.\frac{T}{W}\right|_{prop} . \tag{E.24}$$

Conservation of vehicle masses is given as

$$M_i = M_f + m_p = m_{prop} + m_s + m_L + m_p . \tag{E.25}$$

There are several definitions that are commonly found in the literature that are pertinent here. They are the definitions of mass ratio, *MR*, inert mass fraction, ε, and payload fraction, λ,

$$MR = \frac{M_i}{M_f} \tag{E.26}$$

$$\varepsilon = \frac{m_s}{M_i} \tag{E.27}$$

and

$$\lambda = \frac{m_L}{M_i} , \tag{E.28}$$

respectively. Multiplication of equation (E.25) by the gravitational constant, dividing by thrust, including the definitions above and performing a little algebra yields

$$\frac{1}{MR} = \frac{\left.T/W\right|_i}{\left.T/W\right|_{prop}} + \varepsilon + \lambda . \tag{E.29}$$

The ideal rocket equation, defined in Chapter 3 can be recast as

$$\frac{\Delta V}{g_0 I_{sp}} = \ln\left(\frac{M_i}{M_f}\right) . \tag{E.30}$$

Noting the definition of mass ratio and for γ yields

$$\gamma_f - \gamma_i = \ln(MR) \quad . \tag{E.31}$$

The two-body equation was defined in Chapter 3. It is repeated here as

$$\ddot{\vec{r}} = -\frac{\mu}{r^3}\vec{r} \quad . \tag{E.32}$$

Since $\ddot{\vec{r}}$ and $\vec{r}$ are the only vectors in the equation we note that they must be in parallel and additionally parallel with the unit vector $\frac{\vec{r}}{|\vec{r}|}$. Eliminating the vectors from the equation yields

$$\left|\ddot{\vec{r}}\right| = -\frac{\mu}{r^2} \quad . \tag{E.33}$$

Substituting the definitions of ϕ, β and ψ gives

$$\varsigma \frac{T}{W}\bigg|_i g_0 = -\frac{\mu}{r^2}\frac{\phi P_{jet} t_b}{\frac{\mu}{r} M_i}\frac{\beta r}{V t_b}\frac{FV}{P_{jet}\psi} \quad . \tag{E.34}$$

Canceling terms gives

$$\varsigma \frac{T}{W}\bigg|_i g_0 = -\frac{\phi\beta}{\psi}\frac{F}{M_i} \quad . \tag{E.35}$$

The thrust to weight term cancels with the term left over on the right and so the non-dimensional two-body equation becomes

$$\varsigma = -\frac{\phi\beta}{\psi} \quad . \tag{E.36}$$

The jet power coming from the engine exhaust is defined as

$$P_{jet} = \frac{1}{2}\dot{m}V_e^2 \quad . \tag{E.37}$$

Substituting the definitions for thrust and specific impulse gives

$$P_{jet} = \frac{1}{2}(\dot{m}V_e)V_e = \frac{1}{2}Fg_0 I_{sp} \quad \text{(E.38)}$$

Substituting ψ on the right hand side gives

$$\frac{FV}{\psi} = \frac{1}{2}Fg_0 I_{sp} \quad \text{(E.39)}$$

The thrust terms cancel, bringing the velocity term over to the right side and recalling the definition of γ means the equation above reduces to

$$\psi = 2\gamma \quad \text{(E.40)}$$

During a burn, the mass of the vehicle will reduce by the amount of propellant mass going through the propulsion system and out the exhaust. Therefore, we can expect the final thrust to weight to be higher than the initial thrust to weight. Frequently there is a considerable change between the initial and final thrust to weight. It is convenient to define an average thrust to weight that we can use for calculations across the burn. Since in a choked nozzle the mass flow through the nozzle reaches a constant maximum, we might be tempted to assume that the mass flow rate is a constant and therefore the best average between the initial and final thrust to weight is an algebraic average. However, after many calculations, the author decided on using a geometric mean of the two thrust to weights in these calculations. The geometric mean is defined as

$$\chi = \sqrt{\frac{T}{W}\bigg|_i \frac{T}{W}\bigg|_f} \quad \text{(E.41)}$$

Why the geometric mean? The geometric mean can be shown to be the algebraic mean of the log of all the values to be averaged. Or in this case, equation (E.41) is given as

$$\chi = \exp\left(\frac{\ln\left(\left.\frac{T}{W}\right|_i\right) + \ln\left(\left.\frac{T}{W}\right|_f\right)}{2}\right). \tag{E.42}$$

The logarithmic nature of the ideal rocket equation implies that the geometric mean will prove to be more useful here.

E.3 Relationship between *r* and *V*

Given that $\vec{r}$ is the position vector and $\vec{V}$ is the velocity vector, they are related to one another as

$$\left|\dot{\vec{r}}\right| = V. \tag{E.43}$$

Note that this is just the relationship between the magnitudes of radius and velocity, and does not attempt to relate the respective vectors. It would seem that the dimensionless variables these variables are based on could be related using the above equation. Recasting the equation for β gives

$$r = \frac{Vt_b}{\beta}. \tag{E.44}$$

Taking the first derivative with respect with time, we get

$$\dot{r} = V = \frac{\dot{V}t_b}{\beta} - \frac{Vt_b}{\beta^2}\dot{\beta}. \tag{E.45}$$

The derivative of V is an issue here. It can be eliminated by using the derivative of one of the non-dimensional variables based on V. Working with γ yields

$$V = \gamma g_0 I_{sp}. \tag{E.46}$$

The first derivative gives

$$\dot{V} = \dot{\gamma} g_0 I_{sp} \,. \tag{E.47}$$

Substituting (E.47) into (E.45)

$$V = \frac{\dot{\gamma} g_0 I_{sp} t_b}{\beta} - \frac{V t_b}{\beta^2} \dot{\beta} \,. \tag{E.48}$$

Solving for V yields

$$V = \frac{\dot{\gamma} g_0 I_{sp} t_b \beta}{\beta^2 + t_b \dot{\beta}} \,. \tag{E.49}$$

Substituting β back into the equation yields

$$\frac{\beta}{t_b} + \frac{\dot{\beta}}{\beta} = \frac{\dot{\gamma}}{\gamma} \,. \tag{E.50}$$

This is interesting but not very helpful as of yet. The derivative of ϕ may yield some results. It is

$$\dot{\phi} = -\frac{\mu M_i}{r^2 t_b P_{jet}} \dot{r} \,. \tag{E.51}$$

The only non-dimensional variable we have that can cancel out the gravitational parameter is ϕ. Therefore dividing by ϕ yields

$$\frac{\dot{\phi}}{\phi} = -\frac{\dot{r}}{r} \,. \tag{E.52}$$

Noting equation (E.44) and the definition of β gives

$$\frac{\dot{\phi}}{\phi} = -\frac{V}{r} = -\frac{\beta}{t_b} \,. \tag{E.53}$$

This can be substituted back into equation (E.50) to get

$$\frac{\dot{\beta}}{\beta} = \frac{\dot{\phi}}{\phi} + \frac{\dot{\gamma}}{\gamma} . \tag{E.54}$$

Integrating the above and taking the exponent of the results yields

$$\beta = A\phi\gamma . \tag{E.55}$$

This derivation looks useful until we realize that β is a function of V/r, ϕ is a function of $1/r$ and γ is a function of V. The equation can still be proven useful once the constant of integration is found, but this equation does not really incorporate the concept of equation (E.43). After all we could have written the same equation directly without referencing equation (E.43) by noting of what the functions β, ϕ, and γ were.

Solving for the constant of integration requires substituting the definitions for β, ϕ, and γ.

$$\frac{Vt_b}{r} = A\frac{V}{g_0 I_{sp}}\frac{M_i \mu / r}{t_b P_{jet}} . \tag{E.56}$$

Canceling terms and noting the definition for P_{jet} yields.

$$A = \frac{g_0 {t_b}^2 I_{sp}}{M_i \mu}\left(\frac{1}{2} F g_0 I_{sp}\right) . \tag{E.57}$$

Noting the definition of initial thrust to weight gives

$$A = \frac{{g_0}^3 {t_b}^2 {I_{sp}}^2}{2\mu}\left.\frac{T}{W}\right|_i . \tag{E.58}$$

Incorporating the definition of τ yields

$$A = \frac{{g_0}^3 {I_{sp}}^4}{2\mu {\tau_{Isp}}^2}\left.\frac{T}{W}\right|_i . \tag{E.59}$$

This constant does not have an obvious physical meaning. As noted above, the relationship between β, ϕ, and γ could have been noted without the efforts of equations (E.44) to (E.55). Other efforts to relate the time rate of change to velocity were not successful. Therefore it seems that this relationship is the only one available.

E.4 Application of Non-dimensional Variables to High Thrust Equations

Since the eventual medium thrust two-body problem will have to be compared to the existing literature, including current methods for solving high thrust problems, it makes sense to apply the non-dimensional variables derived earlier in this chapter to the equations for high thrust two-body problem. Recall from Chapter 3 that the vis-visa equation is given as

$$\xi = \frac{V^2}{2} - \frac{\mu}{r} \,. \tag{E.60}$$

We expect an equation in this form that uses only the non-dimensional variables defined in this chapter. The obvious and easiest method would be to substitute the variable definitions into the above equation and simplify. In observing the above equation, it is apparent that the last term on the right will need to be converted to ϕ. So multiplying through by the appropriate variables,

$$\xi \frac{M_i}{t_b P_{jet}} = \frac{M_i V^2}{2 t_b P_{jet}} - \frac{M_i \frac{\mu}{r}}{t_b P_{jet}} \,. \tag{E.61}$$

We can factor the first term on the right to

$$\xi \frac{M_i}{t_b P_{jet}} = \frac{1}{2} \frac{V}{g_0 I_{sp}} \frac{FV}{P_{jet}} \frac{g_0 M_i}{F} \frac{I_{sp}}{t_b} + \phi \,. \tag{E.62}$$

And applying all the pertinent non-dimensional variable definitions, the result is

$$\xi' = \xi \frac{M_i}{t_b P_{jet}} = \frac{\psi \tau_{Isp} \gamma}{2 \frac{T}{W}\Big|_i} + \phi \quad \text{(E.63)}$$

where the term on the right is redefined as a non-dimensional specific mechanical energy of the orbit. Since the initial mass and burn time stay constant over the burn, and P_{jet} is assumed to remain constant (partially by virtue of constant mass flow rate), the non-dimensional specific mechanical energy will remain constant for a given orbit. Note that it will not stay constant during thrusting maneuvers, but that is consistent with the use of this equation before the non-dimensional variables were applied.

Similarly, the conservation of angular momentum equation was derived in Chapter 3 as

$$H = \vec{r} \times \vec{V} = rV \cos \tilde{\gamma} \quad \text{(E.64)}$$

The inclusion of β suggests itself here as only it and ϕ have the radius variable, and ϕ will introduce the gravitational parameter, which no other non-dimensional variable has.

$$H = \frac{V^2 t_b}{\beta} \cos \tilde{\gamma} \quad \text{(E.65)}$$

The velocity squared term was eliminated in the vis-visa equation too; similar non-dimensional variables may work here too.

$$H = \frac{FV}{P_{jet}} \frac{V g_0 m_{prop}}{P_{jet}} \frac{F}{g_0 m_{prop}} \frac{P_{jet^2} t_b}{F^2 \beta} \cos \tilde{\gamma} \quad \text{(E.66)}$$

Bringing the last term on the right before the cosine term to the left hand side of the equation and applying the definition of the non-dimensional variables yields

$$H' = H\frac{F^2}{P_{jet}{}^2 t_b} = \frac{\psi\delta}{\beta}\frac{T}{W}\bigg|_{prop}\cos\tilde{\gamma} \tag{E.67}$$

Substituting equations (E.24) and (E.40) into the above gives

$$H' = \frac{4\gamma^2}{\beta}\cos\tilde{\gamma} \tag{E.68}$$

E.5 Application of Non-dimensional Variables to Low Thrust Equations

Historically, the creators of most low thrust approximation techniques found it convenient to non-dimensionalize their equations during the derivation process. However, it is still convenient to convert these equations to the non-dimensional numbers used in this treatise, if only to make comparison of results easier in the succeeding chapters. Equations (3.50) – (3.52) defined the equations of motion in non-dimensional polar coordinates. These equations are easily converted using the non-dimensional numbers defined in this chapter.

$$\frac{\partial^2\beta}{\partial\tau^2} = F_t\frac{\beta\gamma\tau_{Isp}}{\beta_0} + \frac{\beta^2}{\beta_0}\left(\frac{\partial\theta}{\partial\tau}\right)^2 - \frac{\beta^3\gamma\tau_{Isp}}{\beta_0{}^3} \tag{E.69}$$

$$\frac{\partial}{\partial\tau}\left(\beta\frac{\partial\theta}{\partial\tau}\right) = F_r\sqrt{\frac{\gamma\tau_{Isp}}{\beta_0}} \tag{E.70}$$

Tsien's solution to this problem with thrust in the radial direction is given as

$$\tau = \sqrt{\frac{2}{\chi}}\left[\frac{\sqrt{2(\chi+1)}}{2\chi+1} + F\left(\frac{1}{\sqrt{8\mu'}}, \cos^{-1}\frac{2\chi-1}{2\chi+1}\right) + E\left(\frac{1}{\sqrt{8\chi}}, \cos^{-1}\frac{2\chi-1}{2\chi+1}\right)\right] \tag{E.71}$$

$$\lambda = \exp\left(-\frac{\chi}{\tau_{Isp}}\right) - \varepsilon - \frac{T/W\big|_i}{T/W\big|_{prop}}, \tag{E.72}$$

where χ is the geometric mean of the vehicle thrust to weight.

Tsien's solution for the circumferential direction is now

$$\frac{\chi}{\tau_{Isp}} = \ln\left(\frac{m_o}{m_f}\right). \tag{E.73}$$

Which when solved for the payload fraction will yield the same result as equation (E.74). Similarly Levin's solution for tangential thrust is

$$\frac{\chi}{\tau_{Isp}} = \ln\left(\frac{m_o}{m_f}\right). \tag{E.74}$$

In each case, χ represents the average acceleration in g's that Tsien and Levin used in their calculations. Since χ is a vehicle thrust to weight, it can also be interpreted as acceleration in g's. These equations are only applicable for take-off from Earth's orbit.

$$\frac{\chi}{\tau_{Isp}}\sqrt{\frac{1}{\left.\frac{T}{W}\right|_i \xi}} = \ln\left(\frac{m_o}{m_f}\right) \tag{E.75}$$

$$\lambda = \exp\left(-\frac{\chi}{\tau_{Isp}}\sqrt{\frac{1}{\left.\frac{T}{W}\right|_i \xi}}\right) - \varepsilon - \frac{\left.T/W\right|_i}{\left.T/W\right|_{prop}}. \tag{E.76}$$

Here, the term in the square root normalizes the equation for the new gravitational field based on a given acceleration in multiples of Earth g's.

E.6 Application of Non-Dimensional Variables to Medium Thrust Equations

Again the developers of medium thrust relations found it convenient to define several dimensionless variables in the process of their derivations. Several variables occur in more than one of these derivations. It is worthwhile to discuss them here before continuing on to the conversion of the models in the literature.

The first parameter is the ratio of the exit velocity to the characteristic velocity as defined below.

$$\frac{V_e}{V_c} = \frac{g_0 I_{sp}}{\sqrt{2\eta_{tot} t_b \alpha}} \quad \text{(E.77)}$$

Applying the appropriate non-dimensional variables gives

$$\frac{V_e}{V_c} = \sqrt{\frac{\delta}{\gamma}\frac{\tau_{Isp}}{2}} \quad \text{(E.78)}$$

The characteristic velocity has been defined in several sources and is discussed in Chapter 3.

The next variable to be considered is the ratio of ΔV to characteristic velocity. It is defined as

$$\frac{\Delta V}{V_c} = \frac{V_f}{\sqrt{2\eta_{tot} t_b \alpha}} - \frac{V_i}{\sqrt{2\eta_{tot} t_b \alpha}} \quad \text{(E.79)}$$

Again applying the non-dimensional variables defined in Section 5.1 yields

$$\frac{\Delta V}{V_c} = \left(\sqrt{\frac{\delta_f \gamma_f}{2}} - \sqrt{\frac{\delta_i \gamma_i}{2}} \right) \sqrt{\tau_{Isp}} \quad \text{(E.80)}$$

As noted in Chapter 3 many of the medium thrust concepts use a distance between points as a parameter. The distance is generally divided by the burn time and exhaust velocity. Since the distance between points is usually radially oriented from orbit to orbit as shown in Figure 3.11, the dimensionless number is defined here as

$$\frac{S}{c t_b} = \left(r_f - r_i\right) \frac{1}{g_0 I_{sp} t_b} \quad \text{(E.81)}$$

Substituting the appropriate dimensionless variables yields

$$\frac{S}{ct_b} = \frac{\gamma_f}{\beta_f} - \frac{\gamma_i}{\beta_i} \tag{E.82}$$

With these definitions, the conversion of the medium thrust relations defined in Chapter 3 can be converted to the non-dimensional variables defined in this treatise.

First is the Moeckel-Shepherd-Williams equations. The payload fraction and distance-time equations were defined in Chapter 3 and are repeated here for convenience.

$$\frac{m_L}{m_i} = \frac{1 + V_e^{\,2}/V_c^2}{\left[(\Delta V/V_c)(2V_e/V_c)\right]\left[1 + \left(V_e^{\,2}/V_c^2\right)^{-1}\right] + 1} - \frac{V_e^{\,2}}{V_c^2} \tag{3.119}$$

$$\frac{S}{ct} = \frac{1 - V_e^{\,2}/V_c^2}{1 + V_e^{\,2}/V_c^2}; V_c = \sqrt{2\eta_j t/\alpha} \tag{3.120}$$

Applying equations (E.78) and (E.80) to the above yields

$$\lambda = \frac{1 + \frac{\delta}{\gamma}\frac{\tau_{Isp}}{2}}{\left[\left(\sqrt{\frac{\delta_f^{\,3}}{2}} - \sqrt{\frac{\delta_i^{\,3}}{2}}\right)\sqrt{\tau_{Isp}^{\,3}}\right]\left[1 + \frac{2\gamma}{\delta\tau_{Isp}}\right] + 1} - \frac{\delta}{\gamma}\frac{\tau_{Isp}}{2} \tag{E.83}$$

Similarly the distance equation becomes

$$\frac{\gamma_f}{\delta_f} - \frac{\gamma_i}{\delta_i} = \frac{1 - \frac{\delta}{\gamma}\frac{\tau_{Isp}}{2}}{1 + \frac{\delta}{\gamma}\frac{\tau_{Isp}}{2}} \tag{E.84}$$

Borowski's relationships were shown in Chapter 3 as

$$t_m = \frac{I_{sp}}{T/W_f}\left[\frac{M_i}{M_f} - 1\right] \tag{3.121}$$

$$D = \frac{g_0 {I_{sp}}^2}{T/W_f}\left[\sqrt{\frac{M_i}{M_f}} - 1\right]^2 . \tag{3.122}$$

Substituting the appropriate non-dimensional variables yields

$$\lambda = \left[\sqrt{\left(\frac{\gamma_f}{\beta_f} - \frac{\gamma_i}{\beta_i}\right)\frac{T/W_f}{\tau_{Isp}} + 1}\right]^{-2} - \varepsilon - \frac{T/W_i}{T/W_{prop}} \tag{E.85}$$

$$\tau_m = \left(\frac{\gamma_f}{\beta_f} - \frac{\gamma_i}{\beta_i}\right) + 2\sqrt{\left(\frac{\gamma_f}{\beta_f} - \frac{\gamma_i}{\beta_i}\right)\frac{\tau_{Isp}}{T/W_f}} . \tag{E.86}$$

Finally the Polsgrove-Adams relations were shown in Chapter 3. Those equations were defined as

$$\tau = \frac{S}{g_o I_{sp}}\left(\frac{1 - \left(1 - \frac{2F}{{g_o}^2 {I_{sp}}^2}\frac{P_{jet}}{m_i}\right)}{\left(1 - \frac{2F}{{g_o}^2 {I_{sp}}^2}\frac{P_{jet}}{m_i}\right)\left(\ln\left(1 - \frac{2F}{{g_o}^2 {I_{sp}}^2}\frac{P_{jet}}{m_i}\right) - 1\right) + 1}\right) \tag{3.123}$$

$$\frac{m_L}{m_o} = 1 - \frac{2F}{g_o^2 I_{sp}^2}\frac{P_{jet}}{m_i} - \frac{1}{\alpha}\frac{P_{jet}}{m_i} . \tag{3.124}$$

Again applying the non-dimensional variables and the relations above yield

$$\lambda = \left[\sqrt{\left(\frac{\gamma_f}{\beta_f} - \frac{\gamma_i}{\beta_i}\right)\frac{T/W_f}{\tau_{Isp}} + 1}\right]^{-2} - \varepsilon - \frac{T/W_i}{T/W_{prop}} \tag{E.87}$$

$$\tau_m = \left(\frac{\gamma_f}{\beta_f} - \frac{\gamma_i}{\beta_i}\right)\left[\frac{1 - \lambda + \frac{T/W_i}{T/W_{prop}}}{\left(\lambda + \frac{T/W_i}{T/W_{prop}}\right)\left(\ln\left(\lambda + \frac{T/W_i}{T/W_{prop}}\right) - 1\right) + 1}\right] . \tag{E.88}$$

Appendix F

ACCIDENTAL DERIVATION OF A NEW MANEUVER

F.1 Derivation

As was noted in Chapter 3, there are a variety of thoughts regarding optimum thrust angle. Most low thrust models assume thrust along the tangential path. However, a review of the launch vehicle literature also contained in Chapter 3 illustrates that thrusting along the tangent line is not generally the optimal solution. Launch vehicle trajectories can be considered special cases of medium thrust trajectories. Launch trajectories have a continuous thrust profile which prevents high thrust trajectory solutions to be applied. And the thrust levels for launch trajectories are much higher than are typical for low thrust trajectories. Also launch trajectories tend to have a coast phase after the vehicle has left the atmosphere and a final burn when the launch vehicle reaches the apex of its trajectory to insert into a parking orbit.

Thus the issue of thrust angle must be resolved as a part of development of an analytical medium thrust trajectory approximation. One notable comment reviewed in Chapter 3 indicates that the instantaneous rate of change of kinetic energy is proportional to both acceleration and velocity. Therefore, if a vehicle in a particular parking orbit was to steer into a lower orbit where it would reach a higher velocity and therefore a greater change in kinetic energy for the given vehicle thrust (and acceleration). It seems non-

intuitive that more energy could be gained from the same thrust if the accelerating vehicle is traveling at a faster initial velocity.

As a thought experiment, the author considered a maneuver where the spacecraft would decelerate from an initial circular orbit dropping into an orbit with a lower specific mechanical energy. When the vehicle reaches the periapse of the new orbit, it accelerates. Can such a maneuver produce a higher specific orbital energy than a direct burn from the initial circular orbit? A sketch of the maneuver is illustrated below. For this treatise the maneuver is referred to as the inverse bi-elliptic, as it maneuvers closer to the central body in an attempt to achieve a higher orbit more cheaply than a direct Hohmann transfer. The bi-elliptic, of course, achieves the same result by achieving a much higher orbit before inserting into the final orbit. When used to escape the gravitational effects of the central body, the maneuver will be referred to in this treatise as the new maneuver for reasons discussed at the end of this section.

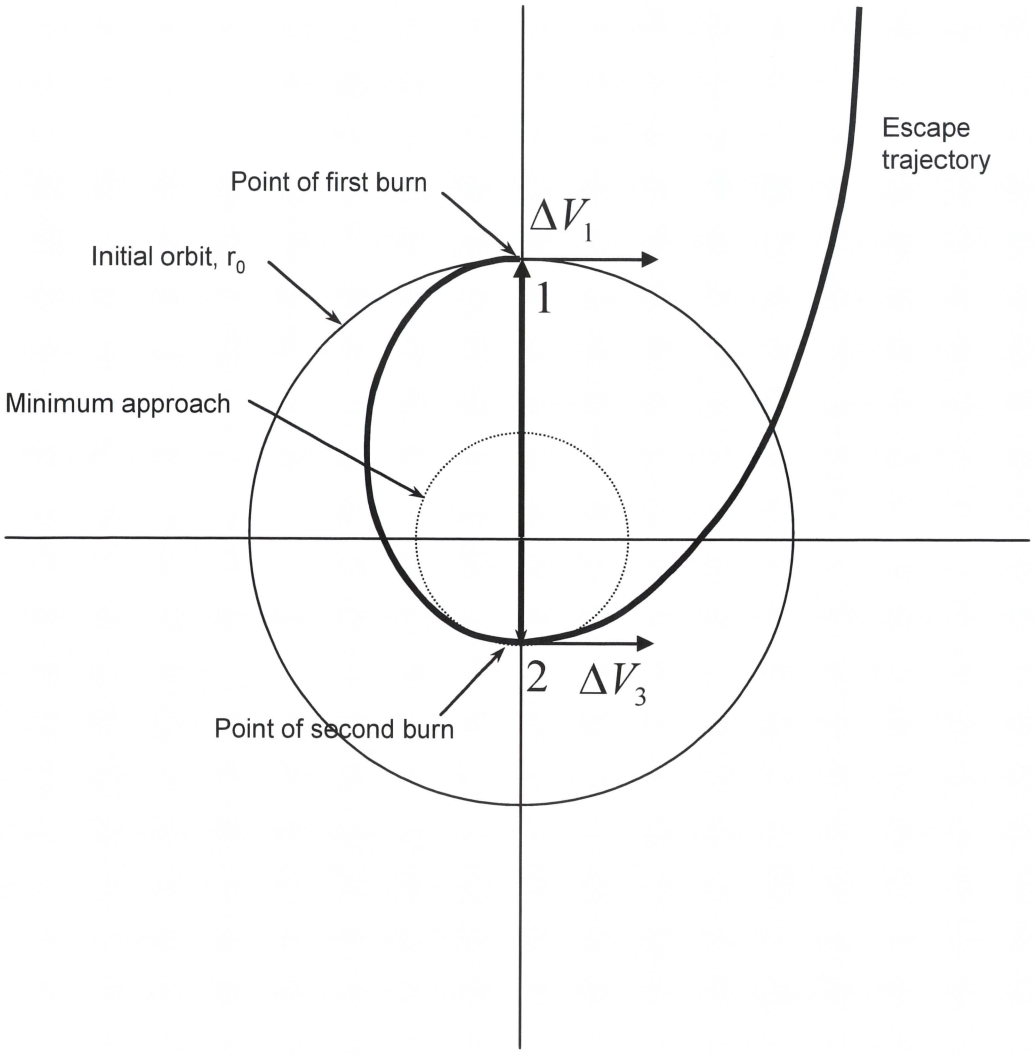

Figure F.1 New maneuver

Using the equations derived in Chapter 3, an equation can be derived for specific mechanical energy for the maneuver. For purposes of this analysis, the comparison is the specific mechanical energy achieved after the second burn at periapse without consideration of a third final circularization burn (the slingshot option.) Starting with equation (3.17) and designating the second burn at periapse as ΔV_3, the specific mechanical energy equation becomes

$$\xi_3 = \frac{(V_2 + \Delta V_3)^2}{2} - \frac{\mu}{r_3}. \tag{F.1}$$

The maneuver is made at periapse and is assumed here to be an impulse burn so $r_3 = r_2$. The periapse point is given by the definition of semi-major axis as

$$r_2 = 2a_1 - r_1. \tag{F.2}$$

The semi-major axis can be calculated by the specific mechanical energy of the orbit before the ΔV_3 burn.

$$a_1 = -\frac{\mu}{2\xi_1}. \tag{F.3}$$

Finally the velocity at point 2 can be calculated from the vis-visa equation too.

$$V_2 = \sqrt{\frac{2\mu}{r_2} - \frac{\mu}{a_2}}. \tag{F.4}$$

Note that since no maneuver happens between points 1 and 2, then $a_1 = a_2$. Substituting all the above into the specific mechanical energy equation and reducing the algebra yields

$$\xi_3 = \frac{\left(\sqrt{\frac{-2\mu}{\frac{\mu}{\xi_1} + r_1} + 2\xi_1} + \Delta V_3\right)^2}{2} + \frac{\mu}{\frac{\mu}{\xi_1} + r_1}. \tag{F.5}$$

The specific energy of the orbit at position 1 can be defined from the conditions at position 1.

$$\xi_1 = \frac{V_1^2}{2} - \frac{\mu}{r_1}. \tag{F.6}$$

Substituting the above into the specific mechanical energy equation above yields

$$\xi_3 = \frac{\left(\sqrt{\frac{-2\mu}{\frac{\mu}{\sqrt{\frac{V_1^2}{2}-\frac{\mu}{r_1}}}+r_1}+2\sqrt{\frac{V_1^2}{2}-\frac{\mu}{r_1}}}+\Delta V_3\right)^2}{2}+\frac{\mu}{\frac{\mu}{\sqrt{\frac{V_1^2}{2}-\frac{\mu}{r_1}}}+r_1}. \tag{F.7}$$

Some simple algebra reduces the equation to

$$\xi_3 = \frac{\left(\sqrt{\frac{4\mu^2+r_1^2V_1^4-4\mu r_1V_1^2}{r_1^2V_1^2}}+\Delta V_3\right)^2}{2}+\frac{\mu r_1V_1-2\mu^2}{r_1^2V_1^2}. \tag{F.8}$$

The radius before the burn and after are the same, or $r_0 = r_1$. Finally the initial velocity can be found as

$$V_0 = \sqrt{\frac{\mu}{r_0}}. \tag{F.9}$$

Again note that the burn the vehicle makes to depart the initial circular orbit ΔV_1 is assumed to be instantaneous. Substituting all the above into the specific mechanical energy yields

$$\xi_3 = \frac{\left(\sqrt{\dfrac{4\mu^2 + r_0^{\,2}\left(\sqrt{\dfrac{\mu}{r_0}} - \Delta V_1\right)^4 - 4\mu r_0\left(\sqrt{\dfrac{\mu}{r_0}} - \Delta V_1\right)^2}{r_0^{\,2}\left(\sqrt{\dfrac{\mu}{r_0}} - \Delta V_1\right)^2}} + \Delta V_3 \right)^2}{2} + \frac{\mu r_0\left(\sqrt{\dfrac{\mu}{r_0}} - \Delta V_1\right) - 2\mu^2}{r_0^{\,2}\left(\sqrt{\dfrac{\mu}{r_0}} - \Delta V_1\right)^2} \tag{F.10}$$

Note that the ΔV_1 maneuver opposes the initial velocity of the spacecraft. Define the convenience variable

$$V_1 = \sqrt{\frac{\mu}{r_0}} - \Delta V_1 \tag{F.11}$$

After considerable algebraic reduction, the equation for specific mechanical energy becomes

$$\xi_3 = \left(V_1^{\,2} - 2\frac{\mu}{r_0} \right) \cdot \left(\frac{1}{2} - \frac{\Delta V_3}{V_1} \right) + \frac{\Delta V_3^{\,2}}{2} \tag{F.12}$$

Here the final specific mechanical energy is a function of the radius of the initial orbit and the magnitude of the ΔV maneuvers only.

The specific mechanical energy for the direct burn option is simpler to derive. Noting that the starting velocity has been defined previously, the specific mechanical energy yields

$$\xi_3 = \frac{\left(\sqrt{\dfrac{\mu}{r_0}} + \Delta V_1 + \Delta V_3 \right)^2}{2} - \frac{\mu}{r_0} \tag{F.13}$$

Setting the two equal to one another will yield the breakeven point between the direct option and the new option

$$\frac{\left(\sqrt{\frac{\mu}{r_0}}+\Delta V_1+\Delta V_3\right)^2}{2}-\frac{\mu}{r_0}=\left(V_1{}^2-2\frac{\mu}{r_0}\right)\cdot\left(\frac{1}{2}-\frac{\Delta V_3}{V_1}\right)+\frac{\Delta V_3{}^2}{2} \tag{F.14}$$

Squaring out the terms yields

$$V_1{}^2-2V_1\Delta V_3+\frac{4\mu\Delta V_3}{V_1 r_0}=\frac{\mu}{r_0}+2\Delta V_1\sqrt{\frac{\mu}{r_0}}+\Delta V_1{}^2+2\Delta V_1\Delta V_3 \tag{F.15}$$

Substituting for V_1 and after considerable algebra the equation reduces to

$$\Delta V_1+\Delta V_3=\sqrt{\frac{\mu}{r_0}} \tag{F.16}$$

Thus the new maneuver can produce a greater specific mechanical energy for a given ΔV budget than a direct burn but only when the total budget exceeds the initial velocity in the initial orbit. So the ΔV budget must be considerable before the slingshot maneuver is worthwhile. For instance, starting from a circular orbit around the sun at a distance equal to earth's orbit, the ΔV budget equal to the initial circular velocity is sufficient to completely escape the solar system with a V_∞ of about 17.5 km/sec. However, the ΔV budget is well within the range of many missions of interest to NASA. For instance, the interstellar precursor mission presents the challenge of traveling 1000 astronomical units (AU) within 50 years, the career lifetime of the average engineer or scientist. The escape velocity above will deliver a spacecraft to the required distance in over 110 years, so clearly a slingshot maneuver would be useful for this mission.

Finally a class of mission that has received attention by NASA in recent years is the deflection or fragmentation of asteroids and comets that are on a collision course with Earth. The ΔV imparted to an oncoming asteroid is very low, on the order of 1-100 cm/sec [53]. This ΔV is sufficient to deflect most asteroids provided that the impulse is applied to the asteroid early enough. Current deflection methods require 2-50 years between application of the impulse and the projected collision date. Therefore the device that will impart the impulse to the asteroid must intercept or rendezvous with the asteroid with all haste. Given that, the ΔV requirement to intercept an incoming asteroid is generally on the order of 10-30 km/s [54]. The ΔV requirement to rendezvous can be as high as 70 km/sec. Both values are well within the range necessary to make the new maneuver economical.

If the new maneuver is more economical, it makes sense to figure out the optimal split in ΔV's between the first and second burn to maximize the final specific mechanical energy. The specific mechanical energy is a function of two variables ΔV_1 and ΔV_3. But we can relate the two variables by noting

$$\Delta V_1 + \Delta V_3 = \Delta V_t, \tag{F.17}$$

where the total change in velocity ΔV_t, should be held constant. We can then apply the chain rule to the desired derivative.

$$\frac{d\xi}{d\Delta V_1} = \frac{\partial \xi}{\partial \Delta V_1}\frac{\partial \Delta V_1}{\partial \Delta V_1} + \frac{\partial \xi}{\partial \Delta V_3}\frac{\partial \Delta V_3}{\partial \Delta V_1}. \tag{F.18}$$

So noting that

$$\frac{\partial \Delta V_1}{\partial \Delta V_1} = 1 \quad , \tag{F.19}$$

and equation (F.17) yields

$$\frac{\partial \Delta V_3}{\partial \Delta V_1} = -1 \quad . \tag{F.20}$$

Working from equation (F.10) the derivative with respect to ΔV_1 yields

$$\frac{\partial \xi_3}{\partial \Delta V_1} = \left(2V_1(-r_0)\right)\left(\frac{1}{2r_0} - \frac{\Delta V_3}{V_1 r_0}\right) + \left(r_0 V_1^{\,2} - 2\mu\right)\frac{\Delta V_3}{V_1^{\,2} r_0^{\,3/2}}\left(-\sqrt{r_0}\right) \quad . \tag{F.21}$$

Simplifying yields

$$\frac{\partial \xi_3}{\partial \Delta V_1} = \left(-r_0 V_1^{\,3} + \Delta V_3 r_0 V_1^{\,2} - 2\mu \Delta V_3\right)\frac{1}{r_0 V_1^{\,2}} \quad . \tag{F.22}$$

The derivative with respect to ΔV_3 is

$$\frac{\partial \xi_3}{\partial \Delta V_3} = \frac{-\left(V^{\,2} - 2\mu\right)}{a'\sqrt{r_0}} + \Delta V_3 \quad . \tag{F.23}$$

Plugging these derivatives into the chain rule above gives

$$\frac{d\xi_3}{d\Delta V_1} = \left(-r_0 V_1^{\,3} + \Delta V_3 r_0 V_1^{\,2} - 2\mu \Delta V_3\right)\frac{1}{r_0 V_1^{\,2}}(1) + \left(\frac{-\left(r_0 V_1^{\,2} - 2\mu\right)}{r_0 V_1} + \Delta V_3\right)(-1) \quad . \tag{F.24}$$

After some algebra, the equation becomes

$$\frac{d\xi_3}{d\Delta V_1} = \frac{2\mu}{r_0 V_1^{\,2}}\Delta V_3 - \frac{2\mu}{r_0 V_1} = 0 \quad . \tag{F.25}$$

Substituting (F.10) and doing more algebraic reduction gives an interesting result

$$\Delta V_1 + \Delta V_3 = \sqrt{\frac{\mu}{r_0}} \quad . \tag{F.26}$$

This result is the same as the break even point between the new and the direct option. But it isn't clear whether this is a local minimum or maximum. Taking the second derivative requires another application of the chain rule. Assigning

$$\frac{d\xi}{d\Delta V_1} = f(\Delta V_1, \Delta V_3) \tag{F.27}$$

So then

$$\frac{d^2\xi}{d\Delta V_1^{\,2}} = \frac{df}{d\Delta V_1} = \frac{\partial f}{\partial \Delta V_1}\frac{\partial \Delta V_1}{\partial \Delta V_1} + \frac{\partial f}{\partial \Delta V_3}\frac{\partial \Delta V_3}{\partial \Delta V_1} \tag{F.28}$$

The derivative with respect to ΔV_1 gives

$$\frac{\partial f}{\partial \Delta V_1} = \frac{(-2)-2\mu}{V_1^{\,3} r_0^{\,3/2}}\left(-\sqrt{r_0}\right)\Delta V_3 - \frac{2\mu}{-V_1^{\,2} r_0^{\,3/2}}\left(-\sqrt{r_0}\right) \tag{F.29}$$

Simplifying yields

$$\frac{\partial f}{\partial \Delta V_1} = \frac{4\mu}{V_1^{\,3} r_0}\Delta V_3 - \frac{2\mu}{V_1^{\,2} r_0} \tag{F.30}$$

The derivative with respect to ΔV_3 is simply

$$\frac{\partial f}{\partial \Delta V_3} = \frac{2\mu}{V_1^{\,2} r_0} \tag{F.31}$$

Substituting these relations into equation (F.28) and noting the results in equations (F.19) and (F.20) gives

$$\frac{df}{d\Delta V_1} = \left(\frac{4\mu}{V_1^{\,3} r_0}\Delta V_3 - \frac{2\mu}{V_1^{\,2} r_0}\right)(1) + \left(\frac{2\mu}{V_1^{\,2} r_0}\right)(-1) \tag{F.32}$$

Reducing gives

$$\frac{df}{d\Delta V_1} = \frac{4\mu}{V_1^3 r_0}\Delta V_3 - \frac{4\mu}{V_1^2 r_0}. \tag{F.33}$$

Substituting back for V_1 and reducing yields

$$\frac{df}{d\Delta V_1} = \frac{d^2\xi}{d\Delta V_1^2} = \frac{4}{V_1^2}\frac{\mu}{r_0}\left(\frac{\Delta V_1 + \Delta V_3 - \sqrt{\frac{\mu}{r_0}}}{\sqrt{\frac{\mu}{r_0}} - \Delta V_1}\right). \tag{F.34}$$

Recalling that the radical is the initial orbital velocity, some inferences can be drawn. First, the term outside the parentheses is always positive, so it can be ignored. The numerator is positive only when the total ΔV budget exceeds the orbital velocity. Since it's already been proven that the new maneuver is only effective when the budget exceeds the velocity for this analysis, it is assumed that the numerator is always positive. Then, the only sign change can occur in the denominator. And since the sign can still change, this is a saddle point and cannot be evaluated as a minimum or maximum.

Instead a graphical analysis is indicated. Consider Figure F.2. Maximum specific orbital energy can be achieved when the first maneuver, ΔV_1, approaches the orbital velocity. In fact the specific orbital energy approaches infinity as ΔV_1 approaches the orbital velocity. Why? When ΔV_1 approaches the orbital velocity, then the spacecraft's periapse point approaches zero. An inspection of the specific orbital energy equation illustrates that it will approach infinity as periapse distance approaches zero. The analysis of derivatives for specific mechanical energy failed because there is no maximum here, only an asymptotic discontinuity, albeit one that can be exploited for gain.

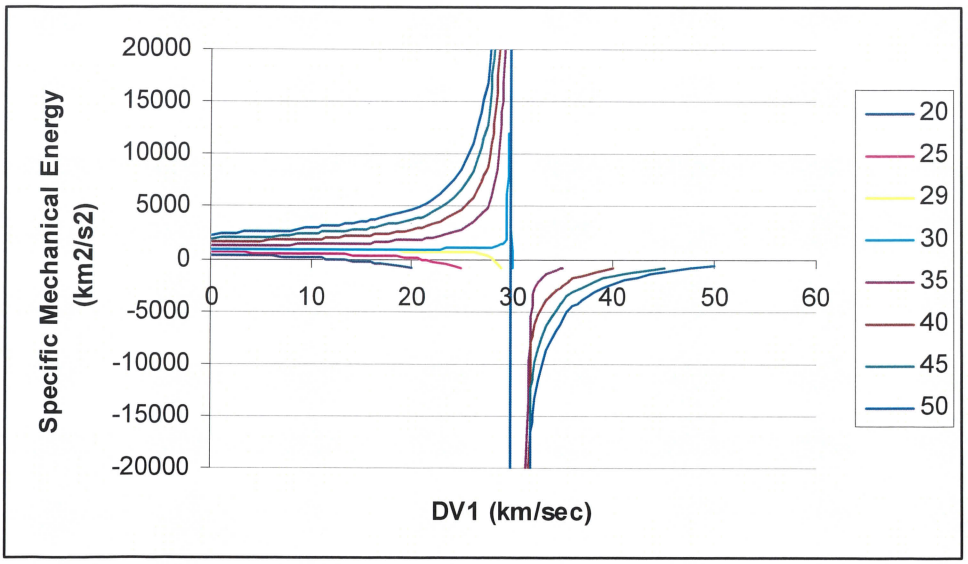

Figure F.2 New maneuver specific mechanical energy ξ_3 vs. ΔV_1 for varying ΔV_{total}. Vertical asymptote at initial orbital velocity, 29.784 km/s. Values represent solar orbit starting at 1 AU (Earth-like orbit)

This seems counterintuitive. How can a spacecraft realize infinite gains in specific energy merely by reducing periapse radius? The author initially had great difficulty with this concept. The answer lies with the perception of potential energy. Potential energy requires definition relative to a reference point. In the derivation of the specific orbital energy equation, that reference point is taken at infinity. Doing so eliminates an extra term in the equation, with the only consequence being spacecraft always having negative potential energy. Imagine the spacecraft orbiting a black hole of miniscule diameter and that the spacecraft itself approaches a point mass. Then, no matter how close the spacecraft is to the black hole, it can convert potential to kinetic energy by dropping a little closer to the black hole. For a point mass spacecraft and a

point mass central body there is always room to move fractionally closer. And the $1/r^2$ nature of the gravitational force means that the rate of change of potential energy goes asymptotic as the spacecraft radius approaches zero.

However, this only describes the conversion of potential to kinetic energy. Understanding the infinite gain in specific mechanical energy requires discussion of another concept. One is tempted to expect only a finite amount of energy to be delivered to a spacecraft due to its latent chemical or nuclear energy. However the propellant has potential energy as well. Imagine the spacecraft is propelled not by accelerating propellant, but by releasing a solid mass (of the same mass as the propellant it replaces) at high velocity, perhaps through use of a spring. The coiled spring in this case represents the latent energy of the propellant or propulsion system energy source. In the direct acceleration option, both masses representing both burns would be released, propelling the vehicle into a higher orbit with periapse equal to the initial orbit. The spring loaded masses would be ejected into a lower orbit with apoapse equal to the initial orbit. The conservation of energy is not violated when one considers the change in kinetic energy of the spacecraft and the ejected masses. For the new maneuver, the first mass is ejected to slow the spacecraft and allow it to drop to a lower orbit. The ejected mass gains velocity and flies to a higher orbit about the central body. At periapse the spacecraft releases the second mass. This mass accelerates the vehicle and itself drops into a lower orbit. The derivations above show that the energy gained by the second mass ejection can greatly overcome the energy lost from the first mass ejection. The second mass can be left in a significantly lower orbit depending on the magnitude of the periapse radius. At the limit, the second mass is ejected from an infinitely small orbital radius, recovering an infinitely

large change in kinetic energy for the spacecraft. For the bi-elliptic case energy is still conserved between the spacecraft and the ejected masses. A mathematical analysis of the conservation of energy for this scenario can be found in Appendix B.

Of course realistically the spacecraft cannot be treated as a point mass and our spacecraft will not be orbiting a miniature black hole in the foreseeable future. However a more realistic example can illustrate the effectiveness of the new maneuver. Assuming that the spacecraft can survive a close approach to the sun of 3 solar radii (a very difficult maneuver to be sure) and a total ΔV budget of 40 km/sec, the new maneuver can produce a change in specific orbital energy approximately three times that of the direct maneuver.

The non-intuitive nature of the gain in specific orbital energy for this maneuver makes the author wonder if it has been seriously considered before. A review of the technical literature found no discussion of this maneuver. Every mission designer and trajectory analyst the author discussed this maneuver with originally felt it would not work. It was not until the author worked out the details proving that energy was conserved that the other analysts started to appreciate the potential of this maneuver. It is possible that the prevalence of similar maneuvers in both the technical and science fiction literature make it seem that this maneuver has been considered before. The new maneuver could easily be confused with a gravity assist maneuver. However, the gravity assist maneuver is based on a massive body such as a planet dragging along the spacecraft for part of the spacecraft's trajectory. Momentum (and specific orbital energy) will be exchanged between the planet and spacecraft. The effect on the spacecraft is substantial, imparting in most cases a ΔV that could not be easily duplicated with current propulsion systems. The effect on the planet is minimal, due to its massive nature relative to the

spacecraft. This momentum exchange is between an external body and the spacecraft and the exchange will occur even if no burn is made by the spacecraft. Conversely the slingshot maneuver will not work unless there is a substantial burn at periapse. The additional energy gained by the spacecraft is represented by the additional loss in specific energy by the propellant expended at the periapse burn. It does not represent a transfer of momentum from the central body to the spacecraft.

It should be noted that this principle is already in use in the context of a gravitational assist. It is well known that performing a burn maneuver at the periapse during a gravitational assist maneuver will enhance the overall ΔV gained from the maneuver. In fact the principle of the Oberth Effect [55] describes how a burn is most effective in accelerating a vehicle when it is conducted at the periapse of the spacecraft's orbit.

Finally science fiction authors, TV shows and movies routinely illustrate slingshot maneuvers. However in almost every case in the author's knowledge of those maneuvers was used to forward a plot specific point like use of a novel new propulsion system based on light pressure or enabling the spacecraft in question to travel back in time. The author did find a description of this maneuver in a 1950's juvenile science fiction novel by Robert A. Heinlein [56]. In it the protagonists are a family living on the moon and purchase a rocket ship to explore the solar system. On a trip to Mars they first swing deeply into the gravity well of earth to make use of the slingshot maneuver. Calculations show that escape from Earth orbit with a vehicle starting from the moon also benefits from this maneuver.

The analysis above stops at the new maneuver. The analyst can take the specific mechanical energy equation and set it equal to zero or to some positive C_3 to represent escape with a non-zero escape velocity. After doing so, the analyst can back out the required ΔV maneuvers using equation (F.42) for the first maneuver and solving equation (F.12) for the second maneuver. For the inverse bi-elliptic, the required calculations are somewhat more extensive. The maneuver at periapse must both provide the required specific mechanical energy to transfer to the final orbit. The periapse point is lower for the inverse bi-elliptic option than for the direct option, so the inverse bi-elliptic will have a larger required insertion burn than will the direct option. It may be that the savings in required ΔV for the inverse bi-elliptic will be offset in full by the requirements of the final burn.

Since the effectiveness of the new maneuver is based in part on the allowable distance from the central body the spacecraft must maintain for survival, it makes sense to calculate the magnitude of the first maneuver as a function of minimum allowable radius. This minimum allowable radius may be defined by the closest the spacecraft can expect to survive the thermal and radiation effects of the sun, or avoiding the atmosphere and topology of a planet or moon should that be the central body. In any case, the derivation of ΔV_1 as a function of r_0 is simple. Noting again that

$$r_2 = 2a_2 - r_1 \tag{F.35}$$

and that

$$a_2 = a_1 = -\frac{\mu}{2\xi_2}, \tag{F.36}$$

the specific orbital energy equation, is

$$\varsigma_2 = \varsigma_1 = \frac{V_1^2}{2} - \frac{\mu}{r_1}, \tag{F.37}$$

may be used to obtain the equation for periapse radius

$$r_2 = 2\left(\frac{-\mu}{2\left(\frac{V_1^2}{2} - \frac{\mu}{r_1}\right)}\right) - r_1 . \tag{F.38}$$

Now recall that $r_0 = r_1$ and that the velocity before and after the first burn is given by

$$V_0 = \sqrt{\frac{\mu}{r_1}} \tag{F.39}$$

$$V_1 = V_0 + \Delta V_1 . \tag{F.40}$$

Results after plugging into equation (F.38) are

$$r_2 = 2\left(\frac{-\mu}{2\left(\frac{\left(\sqrt{\frac{\mu}{r_0}} - \Delta V_1\right)^2}{2} - \frac{\mu}{r_0}\right)}\right) - r_0 . \tag{F.41}$$

Some algebra allows for a solution for ΔV_1 as

$$\Delta V_1 = \sqrt{\frac{\mu}{r_0}}\left(1 - \sqrt{2}\sqrt{\frac{\frac{r_2}{r_0}}{\frac{r_2}{r_0} + 1}}\right). \tag{F.42}$$

This equation is worth examination. If the periapse radius is driven to zero, then ΔV_1 is equal to the initial orbital velocity. This is consistent with the earlier discussion on periapse radius. If the periapse radius is equal to the radius of the initial circular orbit, then ΔV_1 is driven to zero. This also makes sense as no maneuver would result in no change in orbital radius. It should be noted that ΔV_1 remains lower than the initial orbital velocity in all cases. This is consistent with the results depicted in Figure F.2, where ΔV_1 greater than the initial orbital velocity placed the overall specific mechanical energy below the horizontal asymptote.

The next figure emphasizes the amount by which the new maneuver can exceed the direct maneuver. Again it is clear that the new maneuver does not gain relative to a direct burn unless the total ΔV exceeds that of the initial velocity. The figure also shows that the maneuver can gain substantially relative to the direct burn under the right circumstances. The plot also shows the first ΔV required to drop perihelion to that of Mercury and Venus' average orbital distances and that to drop perihelion to within 3 solar radii. It is evident that the spacecraft must come very close to Sol in this scenario to realize significant gains in V_{inf}. Additionally the larger the entire ΔV budget is, the further perihelion can be to realize the same gain in V_{inf}.

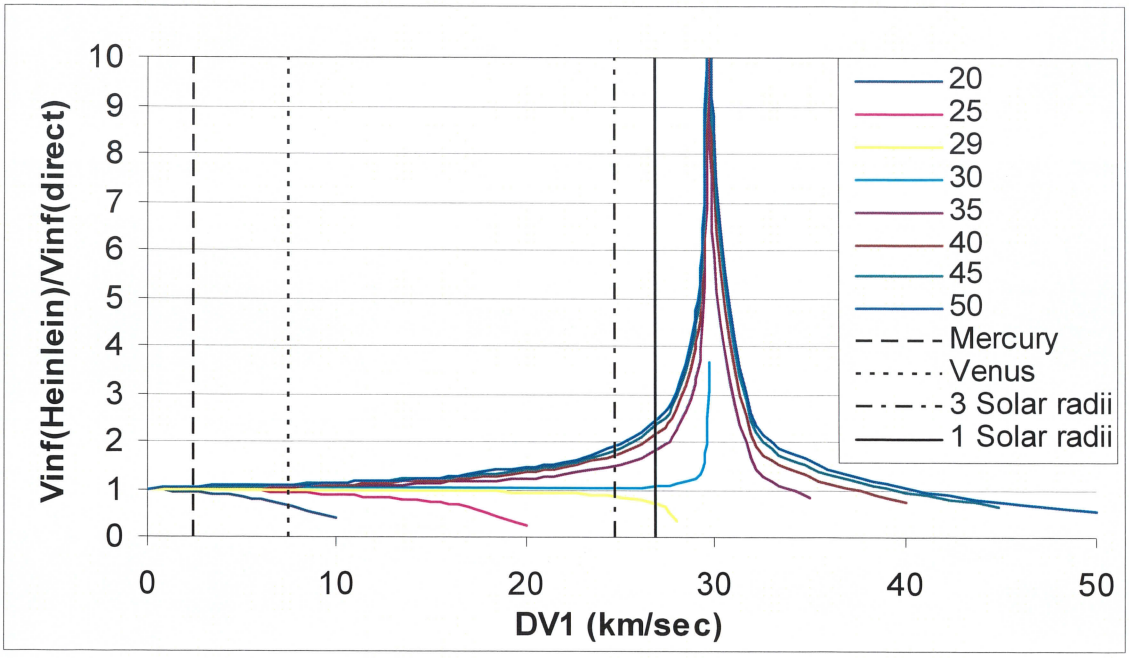

Figure F.3 Ratio of V_{inf} for the new maneuver to the V_{inf} attained through a direct burn. Vertical asymptote is at initial orbital velocity, 29.784 km/s. Values represent solar orbit starting at 1 AU (Earth-like orbit)

Figure F.3 also indicates the possibility of an inverse bi-elliptic maneuver. The idea is to use the new maneuver to replace the first burn of a Hohmann transfer. The third burn of the inverse bi-elliptic burn circularizes into the final orbit. However the maneuver as shown is not more effective than a Hohmann maneuver. This is evident by considering the concept of escape velocity. Given a spacecraft at a certain orbital radius, the minimum velocity that will attain escape from the central body is

$$V_{esc} = \sqrt{\frac{2\mu}{r_0}} \quad \text{(F.43)}$$

Compare escape velocity to initial circular velocity plus the budget allowed for a maneuver.

$$\sqrt{\frac{\mu}{r_0}} + \Delta V_{tot} = \sqrt{\frac{2\mu}{r_0}} \quad \text{(F.44)}$$

So since the new maneuver requires that the ΔV budget exceeds the circular velocity, the left hand side of the equation will always exceed escape velocity. Thus orbit raising maneuvers cannot make use of the new maneuver.

This section started by examining the concept that acceleration along the velocity vector would result in an optimal acceleration of the spacecraft. While acceleration along the velocity vector is locally optimal, it turns out that there is a special maneuver that in certain cases will outperform the "optimal" cross product acceleration by actually decelerating the vehicle and accelerating it when it reaches periapse. The author cannot find mention of this maneuver in the scientific literature. It is presented here as an important maneuver to be considered for high ΔV missions such as interstellar precursor or similar deep space missions and potentially crewed round trip missions to Mars and beyond. Finally, as described by Heinlein, the maneuver is very effective for spacecraft attempting escape when it already is near the top of the central body's gravity well. This has profound implications for future space exploration. Being able to use in-situ resources to create propellants or even construct vehicles on the moon has even greater importance now that the new maneuver can be used to substantially reduce the propulsive requirements for deep space missions.

The ΔV required to complete a mission to Mars and return is 12-13 km/sec for Hohmann transfers. However, radiation exposure, crew supplies and crew mental health

issues have forced vehicle designers to look at much higher ΔV missions that can reduce trip times and mission risk. Mission studies for crewed missions to Mars with a limiting total trip time of 2 years of less have had ΔV requirements above 20 km/sec. Therefore it is possible that the new option could have application in orbit raising maneuvers where limiting mission time is critical.

Since trip time is the critical factor to be reduced in use of the new option, it makes sense to question whether the time required to fly around the sun is longer or shorter than a more direct transfer. Noting that the period of an orbit was given in Chapter 3 to be

$$P = \frac{2\pi}{\sqrt{\mu}} a^{\frac{3}{2}} \quad . \tag{3.125}$$

F.2 New Maneuver Applied to a Semi-Tangential Transfer Scenario

The period for a direct transfer from circular orbit r_0 to new orbit r_5 is

$$P_{direct} = \frac{\pi}{\sqrt{\mu}} \left(\frac{r_0 + r_5}{2} \right)^{\frac{3}{2}} \quad . \tag{F.45}$$

The period to transfer from the initial to the final orbit through the periapse point, r_3 is

$$P_{Inv.Bi} = \frac{\pi}{\sqrt{\mu}} \left(\frac{r_0 + r_3}{2} \right)^{\frac{3}{2}} + \frac{\pi}{\sqrt{\mu}} \left(\frac{r_3 + r_5}{2} \right)^{\frac{3}{2}} \quad . \tag{F.46}$$

The periods can be set equal to one another to determine the break even point. Simple algebra yields

$$\sqrt{(1+R)^3} = \sqrt{(1+\rho)^3} + \sqrt{(\rho+R)^3} \quad , \tag{F.47}$$

where

$$R = \frac{r_5}{r_0}; \rho = \frac{r_3}{r_0} \quad \text{(F.48)}$$

Figure F.4 plots the relationship between R and ρ. If ρ is lower than the line, then the new maneuver will get to the final orbit faster than a Hohmann transfer. Also shown are example ratios for the planets of the solar system relative to Earth. Of course Figure F.4 does not contain any variables that pertain to a specific starting orbit or central body. Thus Figure F.4 pertains to any orbit transfer regardless of starting or ending point and central body. Thus swinging around the sun does not necessarily require more mission time than a direct transfer and can actually save time. Since the closer the spacecraft comes to the central body the greater the boost in orbital energy gained, it is possible to transfer to a higher orbit by swinging around the sun.

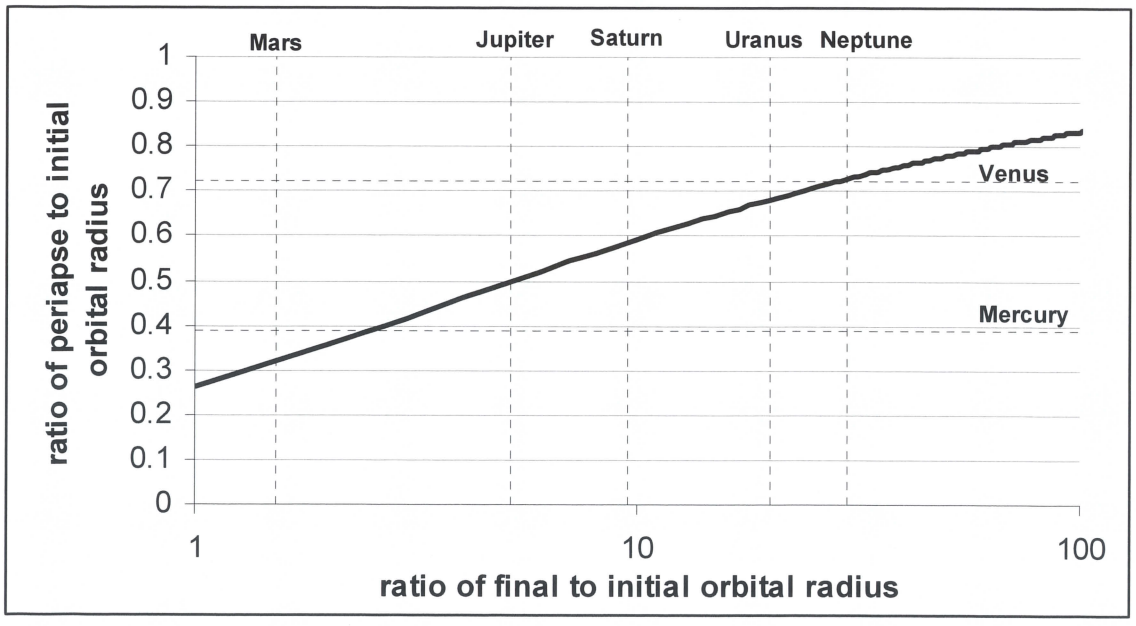

Figure F.4 Break even point in trip time between the inverse bi-elliptic and Hohmann orbit transfers

The next question is whether swinging around the sun has a lower energy requirement than a semi-tangential transfer and determining under which circumstances that is true. Clearly, for an Earth to Mars transfer the direct option is superior.

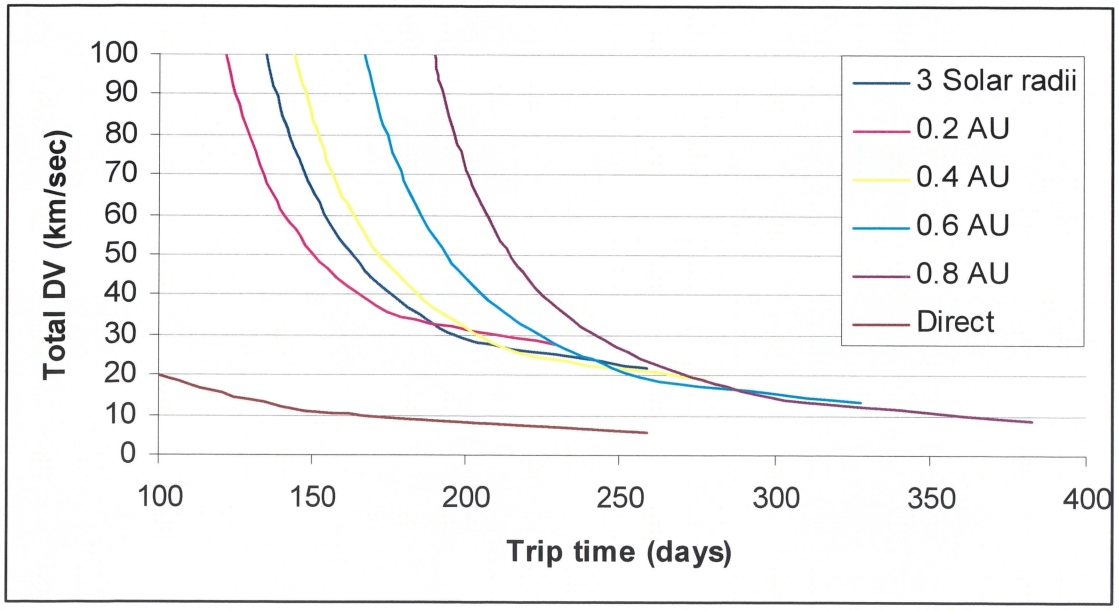

Figure F.5 Comparison of semi-tangential transfer vs. transfer using the new option from Earth to Mars at various periapse radii.

The figure above suggests that the new option will not help in outbound trips to Mars. It is possible that Mars is too close for the potential of the new option to be realized. The following figure illustrates the ΔV requirements vs. trip time for raising an orbit from Earth to 100 AU, well within the Kuiper Belt. Here it is clear that first, for sufficiently short trip times, swinging around the sun at a sufficiently low periapse can reduce trip times for a given total ΔV or reduce total ΔV for a given mission time.

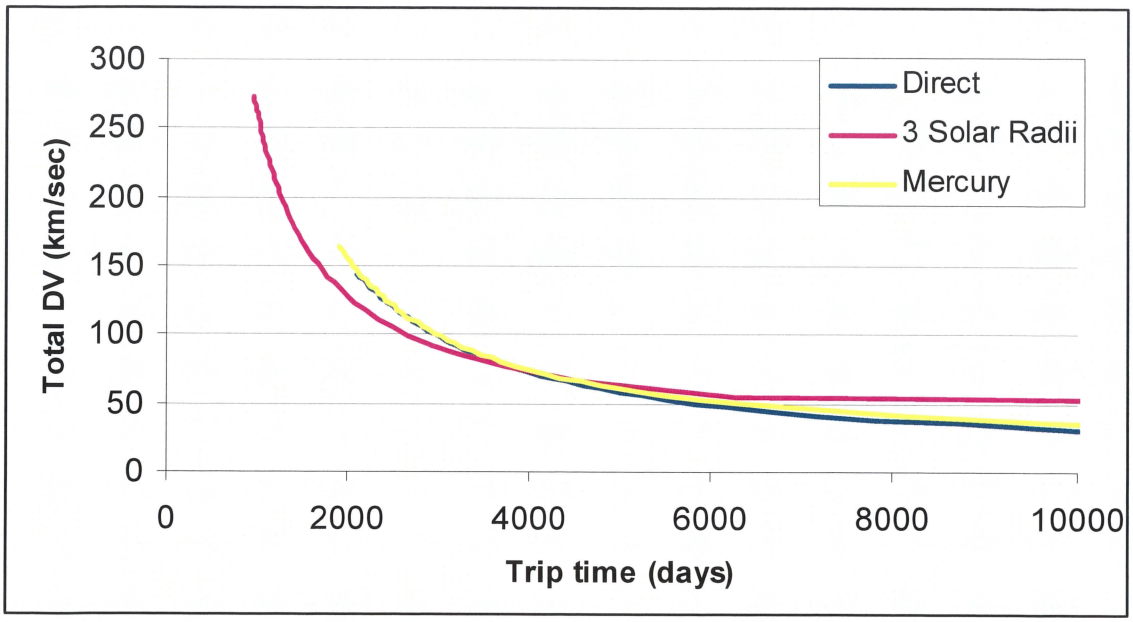

Figure F.6 Total ΔV vs. trip time for orbit raising maneuvers from Earth orbit to 100 AU

Clearly, there are circumstances when the new maneuver can help in orbit raising. It must be a time limited mission as it will never reduce the energy requirements for a Hohmann or bi-elliptic transfer. And it is clear that the greater the ratio between final and initial radius, the more likely it is that the new maneuver will improve performance. The number of calculations required in a semi-tangential transfer (as defined in Chapter 3) defies easy reduction to a form that can be maximized or minimized or compared against itself. The trajectory analyst should consider this maneuver whenever a time critical mission is being evaluated.

One final concept was evaluated in exploring the potential of the new option. The new option requires a first burn that operates against the velocity vector so that the

periapse can be lowered and the second burn is made more efficient by extracting more potential energy from the second burn propellant. However there is a way to lower the periapse of an orbit without destroying specific mechanical energy. The method is contained in the research by Tsien and Levin as described in Chapter 3. Acceleration conducted normal to the velocity vector will not increase specific mechanical energy (unless it surpasses the local gravitational force on the spacecraft), but it will change the orbit's eccentricity. For a given specific mechanical energy, there is a specific semi-major axis, and an increasing eccentricity will result in a lower periapse.

However visualization of the vector diagram of the first maneuver suggests that the magnitude of the first maneuver will be very large to rotate the initial velocity vector sufficiently to reach a sufficiently low periapse. The question remains, will the cost in rotating the initial velocity vector balance the potential savings in not destroying as much specific orbital energy on the first burn? Figure F.7 contains the answer. The figure shows the Vinf attained by conducting the first burn at the designated thrust angle (0 deg is in line with the velocity vector, 180 deg is parallel and opposite the velocity vector). In this figure it is clear that for a budget above the threshold where the new maneuver is sufficient (29.784 km/sec for Earth like orbit around the Sun), then the maximum Vinf is attained at 180 deg. Thrusting at an angle close to 180 deg will still outperform the direct maneuver but not the new maneuver. For budgets lower than the threshold, as indicated by the red lines in the figure, the direct option outperforms at every angle. Again thrusting at angles close to the direct option (very low angles) can outperform the new option, but cannot outperform the direct option. Thus it seems apparent that the optimal

thrust angle on the first burn for escape maneuvers is 180 deg if the total DV budget exceeds the initial orbital velocity and 0 deg otherwise.

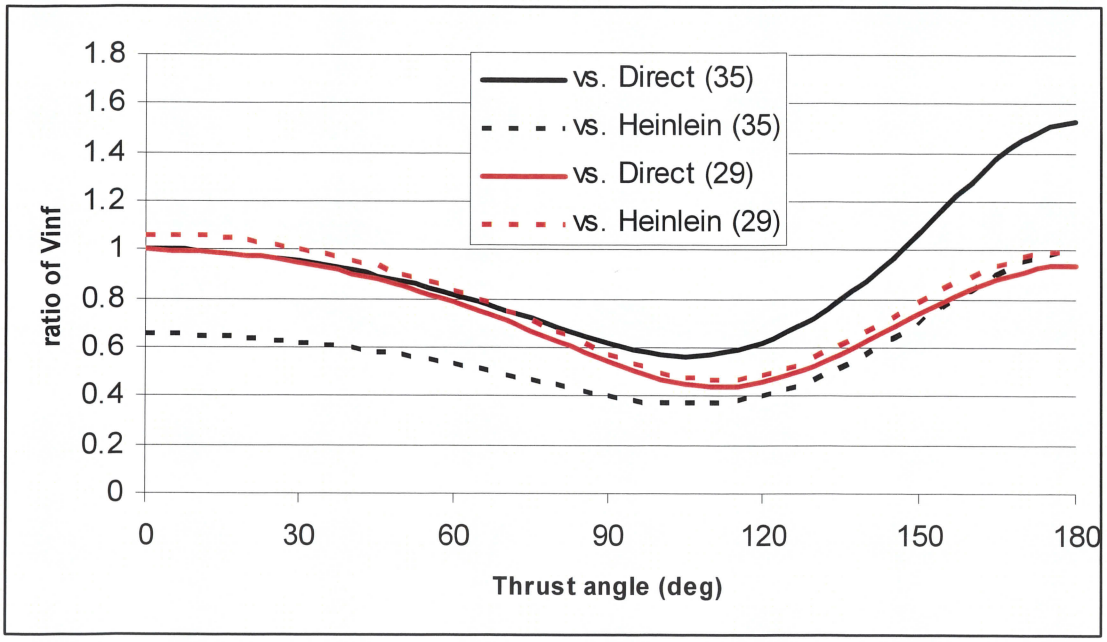

Figure F.7 Ratio of V_{inf} achieved with the first burn at the designated thrust angle vs. the direct and new maneuvers. Black lines indicate a 35 km/sec budget with 25 km/sec used on first burn. Red lines are 29 km/sec budget with 20 km/sec first burn

Appendix G

PAPER SUBMITTAL TO *SCIENCE MAGAZINE*

This appendix contains, in its entirety, the paper submitted to Science Magazine describing a portion of the work completed for this dissertation. Formatting guidelines levied by Science Magazine are followed throughout the appendix.

A New Maneuver for Efficiently Achieving Escape Trajectories in Space Exploration

Robert B. Adams[1] and Georgia A. Richardson[2]

Abstract

A newly developed maneuver to escape the gravitational pull of a central body is described. The maneuver improves efficiency considerably for a wide range of missions of interest in space exploration and scientific investigation. A clear delineation of when the maneuver is more effective is given, as are methods to extract the most advantage

---

[1] Advanced Propulsion Technologist

National Aeronautics and Space Administration

George C. Marshall Space Flight Center

MSFC, AL 35812

robert.b.adams@nasa.gov

[2] Assistant Professor

University of Alabama in Huntsville

Mechanical and Aerospace Engineering Department

Huntsville, AL 35899

richaga@eng.uah.edu

when using the maneuver. (Some examples are given of how this maneuver can enable exploration of the outer solar system, near interstellar space, and crewed missions to Mars and beyond.) The maneuver has the potential to halve the required infrastructure associated with a crewed mission to Mars and achieve solar escape velocities of the order of 0.05 c with existing spacecraft technologies.

1. Introduction

A space vehicle whose motion is only defined by one other body is defined as two-body motion (1). This motion is of primary interest in most in-space applications as the vehicle is strongly affected by the planet (or star) it is orbiting compared with other distant astronomical bodies. Similarly neglected are perturbations due to solar light pressure, atmospheric effects, spacecraft processes or gravitational harmonics due to the deviation from a uniform sphere of the central body. Neglecting the perturbing forces, the summation of forces on the vehicle is simply

$$\ddot{\vec{r}} = -\frac{\mu}{r^2}\left(\frac{\vec{r}}{r}\right) \text{ with } \mu = GM \,, \qquad \textbf{Eq. 1}$$

where $\ddot{\vec{r}}$ is the vehicle acceleration and $\vec{r}$ is the vector from the center of mass of the massive body to the vehicle. From the above equation, the gravitational force is a function of the inverse square of this radius vector. In the Newtonian equation G defines the gravitational constant and M the mass of the large body. The mass of the vehicle, m, is much smaller and generally can be ignored.

From equation Eq. 1 several other equations of primary interest can be derived. Taking the cross product of the above equation with respect to $\dot{\vec{r}}$ yields

$$\vec{h} = \vec{r} \times \vec{V} = rV\cos\gamma = const., \qquad \textbf{Eq. 2}$$

where $\vec{h}$ is the vehicle's angular momentum. This value is constant along the vehicle's orbit assuming no other forces act on the vehicle.

Similarly taking a dot product of equation Eq. 1 with respect to $\vec{r}$ yields

$$\xi = \frac{V^2}{2} - \frac{\mu}{r} = -\frac{\mu}{2a}, \qquad \textbf{Eq. 3}$$

where ξ is referred to as the specific orbital energy of the vehicle. The orbital energy is the sum of the specific kinetic energy (the first term) and the specific potential energy (the second term). In deriving this equation it is convenient to assume that the reference line for potential energy is at infinity. Thus all potential energies are negative. The right hand side of the equation expresses specific orbital energy as a function of the semi-major axis, a.

The equations above define the major parameters of a spacecraft in a coasting trajectory around a central body. In the operation of a spacecraft, changes in the orbit must be made to allow the spacecraft to travel to points of interest such as other planetary bodies. Turning on the spacecraft propulsion system, or performing a 'burn' in industry parlance, will place the vehicle in a new coasting trajectory once the burn is completed.

Conventional chemical propulsion systems are characterized as high thrust. The time to execute a burn is orders of magnitude lower than the overall mission time. High thrust burns are treated as instantaneous, and so the equations above are applied to the new spacecraft velocity after the burn, which is sufficient to describe the new spacecraft orbit. The burn is quantified by another industry term, ΔV, or "delta-vee", which is

determined by the properties of the propulsion system, the types of propellants involved, and the amount of propellant used. Minimizing ΔV is the overriding performance objective in almost all spacecraft design endeavors. A smaller ΔV translates to a smaller spacecraft that is generally less expensive and more reliable to operate, simpler to design, and generally better able to meet mission objectives. It should be noted that for any spacecraft, the size of the spacecraft is linked exponentially to the value of ΔV (2). Examples of high thrust propulsion systems are the conventional chemically powered liquid engines and solid motors seen on launch vehicles and spacecraft since the start of the space age.

Low thrust trajectories are characterized by propulsion systems that are on for large portions of the overall mission. These propulsion systems tend to be proportionally larger than those for high thrust systems, but also tend to require less propellant. Thus vehicles with low thrust propulsion systems are smaller and less massive than their high thrust counterparts in a wide variety of mission scenarios. Examples of low thrust propulsion systems are the nuclear and solar electric systems that have been strongly considered for a number of missions in recent years (3). Additionally solar electric propulsion can be found in previous NASA missions such as Deep Space 1 and can be found under use as station-keeping thrusters for a number of Earth orbiting satellites.

Because low thrust propulsion thrust duration is substantial compared to the mission time the optimal direction of the propulsive thrust at each moment along the trajectory becomes very important. Optimizing the "guidance schedule" of thrust direction and magnitude to limit the ΔV required and therefore the spacecraft size becomes an issue. Generally this is done by complex numerical integration of the

equations of motion coupled with a variety of optimization routines. The optimization problem is very difficult and there are a number of trajectory analysts that are dedicated on a daily basis to optimize these trajectories for missions of interest in space exploration.

Due to the computationally intensive nature of trajectory design, there has been strong interest since the 1950's to determine analytical approximations to low thrust trajectories that would give generally accurate results. A prevalent argument in the derivation of these approximations is that the thrust vector should always be aligned with the spacecraft's velocity vector. The reason can be seen by taking the time derivative of the kinetic energy equation, which is

$$\frac{d}{dt}KE = \frac{d}{dt}\frac{V^2}{2} = \vec{V} \cdot \vec{a} \qquad \textbf{Eq. 4}$$

Thus the instantaneous rate of change of kinetic energy is proportional to both acceleration and velocity. The local maximum is found when the spacecraft velocity and acceleration are parallel. However, as argued by Levin (4), the spacecraft could accelerate in a different direction, forcing the spacecraft into a different orbit with a point of closest approach to the central body, called the periapse, which is closer to the central body than the original orbit. Examination of Eq. 3 notes for a coasting orbit the specific mechanical energy remains constant but that kinetic energy is traded for potential energy. At periapse kinetic energy is at a maximum and potential energy is at minimum, just like for any gravitational force dominated problem like a swinging pendulum or a ball in free flight. By Eq. 4, driving to a lower orbit and then accelerating at periapse would maximize the change in energy of the spacecraft for a given acceleration (and thrust).

2. Theory for new maneuver

As a thought experiment the authors considered a maneuver where the spacecraft would decelerate from an initial circular orbit with a single high thrust burn, dropping into an orbit with a lower specific mechanical energy. When the vehicle reaches the periapse of the new orbit, it accelerates with another high thrust burn. The primary objective of this study is to determine if such a maneuver can produce a higher specific orbital energy than a direct burn from the initial circular orbit. A sketch of the maneuver is illustrated below.

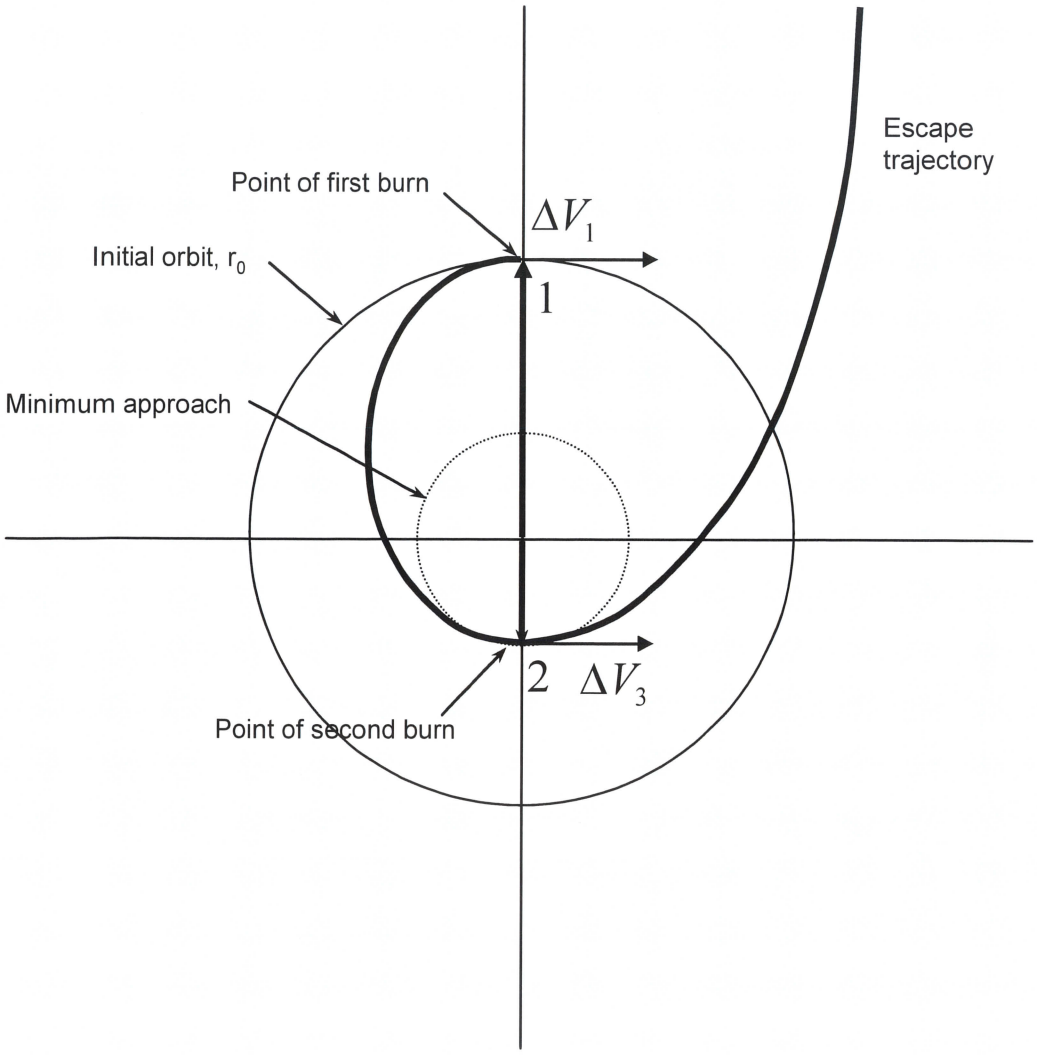

Figure 1– Diagram of the new maneuver

Using the equations derived above, an equation can be derived for the specific mechanical energy of the maneuver. For purposes of this analysis, the comparison is the specific mechanical energy achieved after the second burn at periapse against that of a direct burn to escape. Starting with Equation 3 and designating the second burn at periapse as ΔV_3 the specific mechanical energy equation becomes

$$\xi_3 = \frac{(V_2 + \Delta V_3)^2}{2} - \frac{\mu}{r_3}. \qquad \textbf{Eq. 5}$$

The burn is made at periapse and is assumed here to be an impulse burn so $r_3 = r_2$. The periapse point is given by the definition of semi-major axis as

$$r_2 = 2a_1 - r_1. \qquad \textbf{Eq. 6}$$

The semi-major axis can be calculated by the specific mechanical energy of the orbit before the ΔV_3 burn.

$$a_1 = -\frac{\mu}{2\xi_1}. \qquad \textbf{Eq. 7}$$

Finally the velocity at point 2 can be calculated from

$$V_2 = \sqrt{\frac{2\mu}{r_2} - \frac{\mu}{a_2}}. \qquad \textbf{Eq. 8}$$

Note that since no maneuver happens between points 1 and 2, then $a_1 = a_2$. Substituting all the above into the specific mechanical energy equation and reducing the algebra yields

$$\xi_3 = \frac{\left(\sqrt{\frac{-2\mu}{\frac{\mu}{\xi_1} + r_1} + 2\xi_1} + \Delta V_3\right)^2}{2} + \frac{\mu}{\frac{\mu}{\xi_1} + r_1}. \qquad \textbf{Eq. 9}$$

The specific energy of the orbit at position 1 can be defined from the conditions at position 1.

$$\xi_1 = \frac{V_1^2}{2} - \frac{\mu}{r_1}. \qquad \textbf{Eq. 10}$$

Substituting the above into the specific mechanical energy equation above yields

$$\xi_3 = \frac{\left(\sqrt{\dfrac{-2\mu}{\dfrac{\mu}{\dfrac{V_1^2}{2}-\dfrac{\mu}{r_1}}+r_1}+2\left(\dfrac{V_1^2}{2}-\dfrac{\mu}{r_1}\right)}+\Delta V_3\right)^2}{2}+\frac{\mu}{\dfrac{\mu}{\dfrac{V_1^2}{2}-\dfrac{\mu}{r_1}}+r_1}. \qquad \textbf{Eq. 11}$$

Some simple algebra reduces the equation to

$$\xi_3 = \frac{\left(\sqrt{\dfrac{4\mu^2+r_1^2V_1^4-4\mu r_1V_1^2}{r_1^2V_1^2}}+\Delta V_3\right)^2}{2}+\frac{\mu r_1V_1-2\mu^2}{r_1^2V_1^2}. \qquad \textbf{Eq. 12}$$

The radius before the first burn and after are the same, or $r_0 = r_1$. Finally the initial velocity can be found as

$$V_0 = \sqrt{\frac{\mu}{r_0}}. \qquad \textbf{Eq. 13}$$

Again note that the burn the vehicle makes to depart the initial circular orbit (ΔV_1) is assumed to be instantaneous. Note that the ΔV_1 maneuver opposes the initial velocity of the spacecraft. Define the convenience variable

$$V_1 = \sqrt{\frac{\mu}{r_0}} - \Delta V_1. \qquad \textbf{Eq. 14}$$

After considerable algebraic reduction, the equation for specific mechanical energy becomes

$$\xi_3 = \left(V_1^{\,2} - 2\frac{\mu}{r_0} \right) \cdot \left(\frac{1}{2} - \frac{\Delta V_3}{V_1} \right) + \frac{\Delta V_3^{\,2}}{2} \quad \textbf{Eq. 15}$$

Here the final specific mechanical energy is a function of the radius of the initial orbit and the magnitude of the ΔV maneuvers only.

The specific mechanical energy for the direct burn option is simpler to derive. Noting that the starting velocity has been defined previously, the specific mechanical energy yields

$$\xi_3 = \frac{\left(\sqrt{\frac{\mu}{r_0}} + \Delta V_1 + \Delta V_3 \right)^2}{2} - \frac{\mu}{r_0} \quad \textbf{Eq. 16}$$

Setting the two equal to one another will yield the breakeven point between the direct option and the new option

$$\frac{\left(\sqrt{\frac{\mu}{r_0}} + \Delta V_1 + \Delta V_3 \right)^2}{2} - \frac{\mu}{r_0} = \left(V_1^{\,2} - 2\frac{\mu}{r_0} \right) \cdot \left(\frac{1}{2} - \frac{\Delta V_3}{V_1} \right) + \frac{\Delta V_3^{\,2}}{2} \quad \textbf{Eq. 17}$$

Squaring out the terms yields

$$V_1^{\,2} - 2V_1 \Delta V_3 + \frac{4\mu \Delta V_3}{V_1 r_0} = \frac{\mu}{r_0} + 2\Delta V_1 \sqrt{\frac{\mu}{r_0}} + \Delta V_1^{\,2} + 2\Delta V_1 \Delta V_3 \quad \textbf{Eq. 18}$$

Substituting for V_1 and after considerable algebra the equation reduces to

$$\Delta V_1 + \Delta V_3 = \sqrt{\frac{\mu}{r_0}} \quad \textbf{Eq. 19}$$

Thus the new option can produce a greater specific mechanical energy for a given ΔV budget than a direct burn but only when the total budget exceeds the initial velocity in the initial orbit. So the ΔV budget must be considerable before the slingshot maneuver is

worthwhile. For instance starting from a circular orbit around the sun at a distance equal to earth's orbit, the ΔV budget equal to the initial circular velocity is sufficient to completely escape the solar system with a V_∞ of about 17.5 km/sec. However the ΔV budget is well within the range of many missions of interest to NASA. For instance the interstellar precursor mission presents the challenge of traveling 1000 astronomical units (AU) within 50 years, the career lifetime of the average engineer or scientist. The escape velocity above will deliver a spacecraft to the required distance in over 110 years, so clearly a slingshot maneuver would be useful for this mission. Other deep space missions to the outer planets, Kuiper Belt, Oort Cloud, and heliopause would similarly be enhanced by use of this maneuver.

Finally a class of mission that has received attention by NASA in recent years is the deflection or fragmentation of asteroids and comets that are on a collision course with Earth. The ΔV imparted to an oncoming asteroid is very low, on the order of 1-100 cm/sec (5). This ΔV is sufficient to deflect most asteroids provided that the impulse is applied to the asteroid early enough. Current deflection methods require 2-50 years between application of the impulse and the projected collision date. Therefore the device that will impart the impulse to the asteroid must intercept or rendezvous with the asteroid with all haste. Given the above, the ΔV requirement to intercept an incoming asteroid is generally on the order of 10-30 km/s (6The ΔV requirement to rendezvous can be as high as 70 km/sec. Both values are well within the range necessary to make the new maneuver economical.

If the new maneuver is more economical, it makes sense to figure out the optimal split in ΔV's between the first and second burn to maximize the final specific

mechanical energy. The specific mechanical energy is a function of two variables ΔV_1 and ΔV_3. But we can relate the two variables by noting

$$\Delta V_1 + \Delta V_3 = \Delta V_t, \qquad \textbf{Eq. 20}$$

where the total change in velocity ΔV_t, should be held constant. We can then apply the chain rule to the desired derivative.

$$\frac{d\xi}{d\Delta V_1} = \frac{\partial \xi}{\partial \Delta V_1}\frac{\partial \Delta V_1}{\partial \Delta V_1} + \frac{\partial \xi}{\partial \Delta V_3}\frac{\partial \Delta V_3}{\partial \Delta V_1} = 0 \qquad \textbf{Eq. 21}$$

Equation 20 yields

$$\frac{\partial \Delta V_3}{\partial \Delta V_1} = -1 \qquad \textbf{Eq. 22}$$

Working from equation 15 the derivative with respect to ΔV_1 (with simplification) yields

$$\frac{\partial \xi_3}{\partial \Delta V_1} = \left(2V_1\left(-r_0\right)\right)\left(\frac{1}{2r_0} - \frac{\Delta V_3}{V_1 r_0}\right) + \left(r_0 V_1^{\,2} - 2\mu\right)\frac{\Delta V_3}{V_1^{\,2} r_0^{\,3/2}}\left(-\sqrt{r_0}\right) \qquad \textbf{Eq. 23}$$

Simplifying yields

$$\frac{\partial \xi_3}{\partial \Delta V_1} = \left(-r_0 V_1^{\,3} + \Delta V_3 r_0 V_1^{\,2} - 2\mu\Delta V_3\right)\frac{1}{r_0 V_1^{\,2}} \qquad \textbf{Eq. 24}$$

The derivative with respect to ΔV_3 is

$$\frac{\partial \xi_3}{\partial \Delta V_3} = \frac{-\left(V^{\,2} - 2\mu\right)}{a'\sqrt{r_0}} + \Delta V_3 \qquad \textbf{Eq. 25}$$

Plugging these derivatives into the chain rule above and setting equal to zero gives

$$\frac{d\xi_3}{d\Delta V_1} = \left(-r_0 V_1^{\,3} + \Delta V_3 r_0 V_1^{\,2} - 2\mu\Delta V_3\right)\frac{1}{r_0 V_1^{\,2}}(1) + \left(\frac{-\left(r_0 V_1^{\,2} - 2\mu\right)}{r_0 V_1} + \Delta V_3\right)(-1) = 0 \qquad \textbf{Eq. 26}$$

After some algebra, the equation becomes

$$\frac{d\xi_3}{d\Delta V_1} = \frac{2\mu}{r_0 V_1^{\,2}}\Delta V_3 - \frac{2\mu}{r_0 V_1} = 0 \quad \textbf{Eq. 27}$$

Substituting and doing more algebraic reduction gives an interesting result

$$\Delta V_1 + \Delta V_3 = \sqrt{\frac{\mu}{r_0}} \quad \textbf{Eq. 28}$$

3. Optimization and trends

Consider Figure 2. Maximum specific orbital energy can be achieved when the first maneuver, ΔV_1, approaches the orbital velocity. In fact the specific orbital energy approaches infinity as ΔV_1 approaches the orbital velocity. Why? When ΔV_1 approaches the orbital velocity, then the spacecraft's periapse point approaches zero. An inspection of the specific orbital energy equation (equation 3) illustrates that it will approach infinity as periapse distance approaches zero. The analysis of derivatives for specific mechanical energy failed because there is no maximum here, only an asymptotic discontinuity, albeit one that can be exploited for gain.

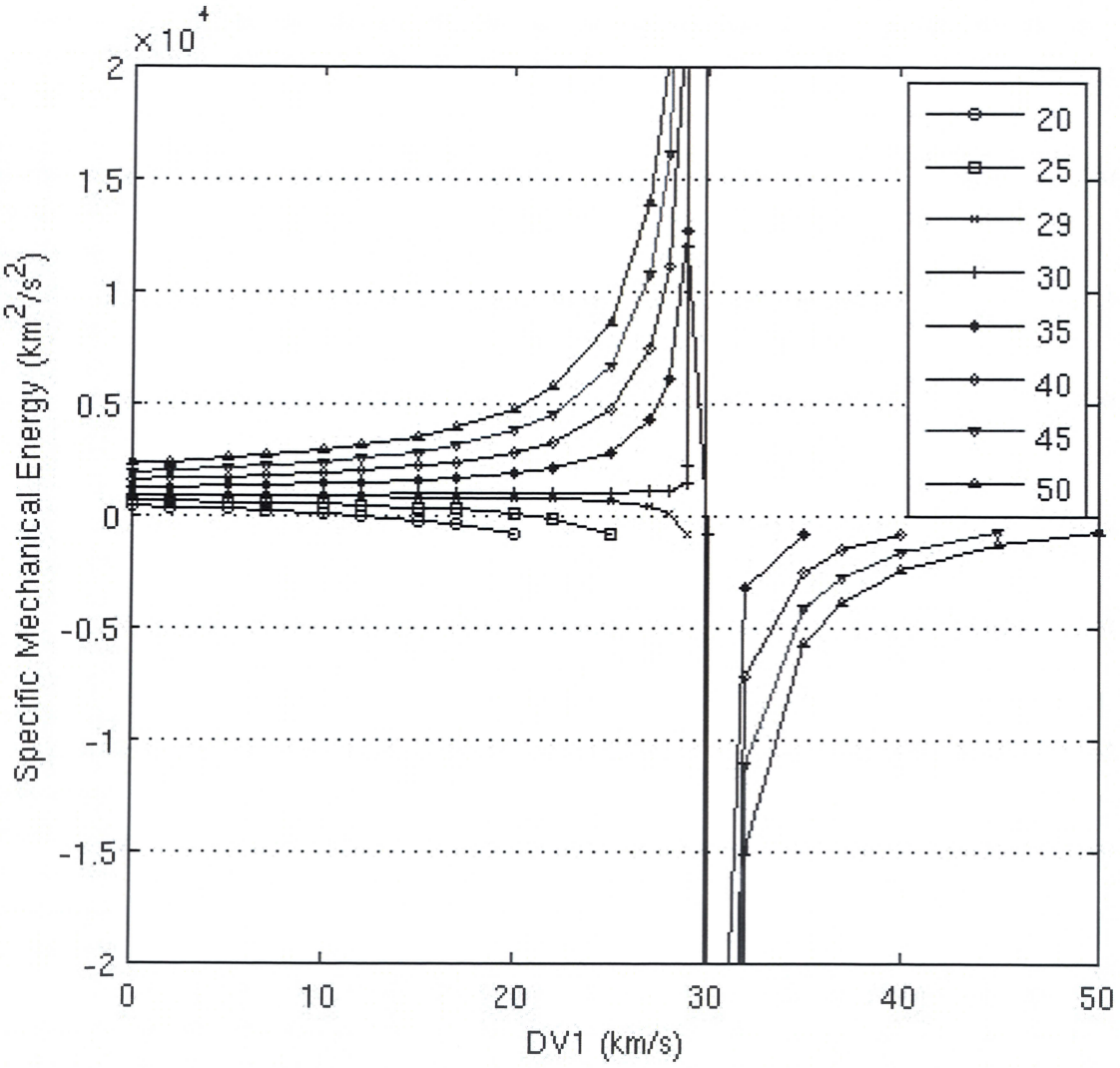

Figure 2 - New maneuver specific mechanical energy ξ_3 vs. ΔV_1 for varying ΔV_{total} . Vertical asymptote at initial orbital velocity, 29.784 km/s. Values represent solar orbit starting at 1 AU (Earth-like orbit)

However this only describes the conversion of potential to kinetic energy. Understanding the infinite gain in specific mechanical energy requires discussion of another concept. One is tempted to expect only a finite amount of energy to be delivered

to a spacecraft due to its latent chemical or nuclear energy. However the propellant has potential energy as well. Imagine the spacecraft is propelled not by accelerating propellant, but by releasing a solid mass (of the same mass as the propellant it replaces) at high velocity, perhaps through use of a spring. The coiled spring in this case represents the latent energy of the propellant or propulsion system energy source. In the direct acceleration option, both masses representing both burns would be released, propelling the vehicle into a higher orbit with periapse equal to the initial orbit. The spring loaded masses would be ejected into a lower orbit with apoapse equal to the initial orbit. The conservation of energy is not violated when one considers the change in kinetic energy of the spacecraft and the ejected masses. For the new option, the first mass is ejected to slow the spacecraft and allow it to drop to a lower orbit. The ejected mass gains velocity and flies to a higher orbit about the central body. At periapse the spacecraft releases the second mass. This mass accelerates the vehicle and itself drops into a lower orbit. The derivations above show that the energy gained by the second mass ejection can greatly overcome the energy lost from the first mass ejection. The second mass can be left in a significantly lower orbit depending on the magnitude of the periapse radius. At the limit, the second mass is ejected from an infinitely small orbital radius, recovering an infinitely large change in kinetic energy for the spacecraft.

4. Discussion

The new option could easily be confused with a gravity assist maneuver. However, the gravity assist maneuver is based on a massive body such as a planet dragging along the spacecraft for part of the spacecraft's trajectory. Momentum (and

specific orbital energy) will be exchanged between the planet and spacecraft. The effect on the spacecraft is substantial, imparting in most cases a ΔV that could not be easily duplicated with current propulsion systems. The effect on the planet is minimal, due to its massive nature relative to the spacecraft. This momentum exchange is between an external body and the spacecraft and the exchange will occur even if no burn is made by the spacecraft. Conversely the slingshot maneuver will not work unless there is a substantial burn at periapse. The additional energy gained by the spacecraft is represented by the additional loss in specific energy by the propellant expended at the periapse burn. It does not represent a transfer of momentum from the central body to the spacecraft.

It should be noted that this principle is already in use in the context of a gravitational assist. It is well known that performing a burn maneuver at the periapse during a gravitational assist maneuver will enhance the overall ΔV gained from the maneuver. In fact the principle known as the Oberth Effect describes how a burn is most effective in accelerating a vehicle when it is conducted at the periapse of the spacecraft's orbit.

In a literature search to determine the originality of the maneuver, the authors did find a description of this maneuver in a 1950's juvenile science fiction novel by Robert A. Heinlein (7). In it the protagonists are a family living on the moon and purchase a rocket ship to explore the solar system. On a trip to Mars they first swing deeply into the gravity well of earth to make use of the slingshot maneuver. Calculations show that escape from Earth orbit with a vehicle starting from the moon also benefits from this maneuver.

The next figure emphasizes the amount by which the new maneuver can exceed the direct maneuver in producing escape velocity. Again it is clear that the new maneuver does not gain relative to a direct burn unless the total ΔV exceeds that of the initial velocity. The figure also shows that the maneuver can gain substantially relative to the direct burn under the right circumstances. The plot also shows the first ΔV required to drop perihelion to that of Mercury and Venus' average orbital distances and that to drop perihelion to within 3 solar radii. It is evident that the spacecraft must come very close to Sol in this scenario to realize significant gains in V_{inf}. Additionally the larger the entire ΔV budget is, the further perihelion can be to realize the same gain in V_{inf}.

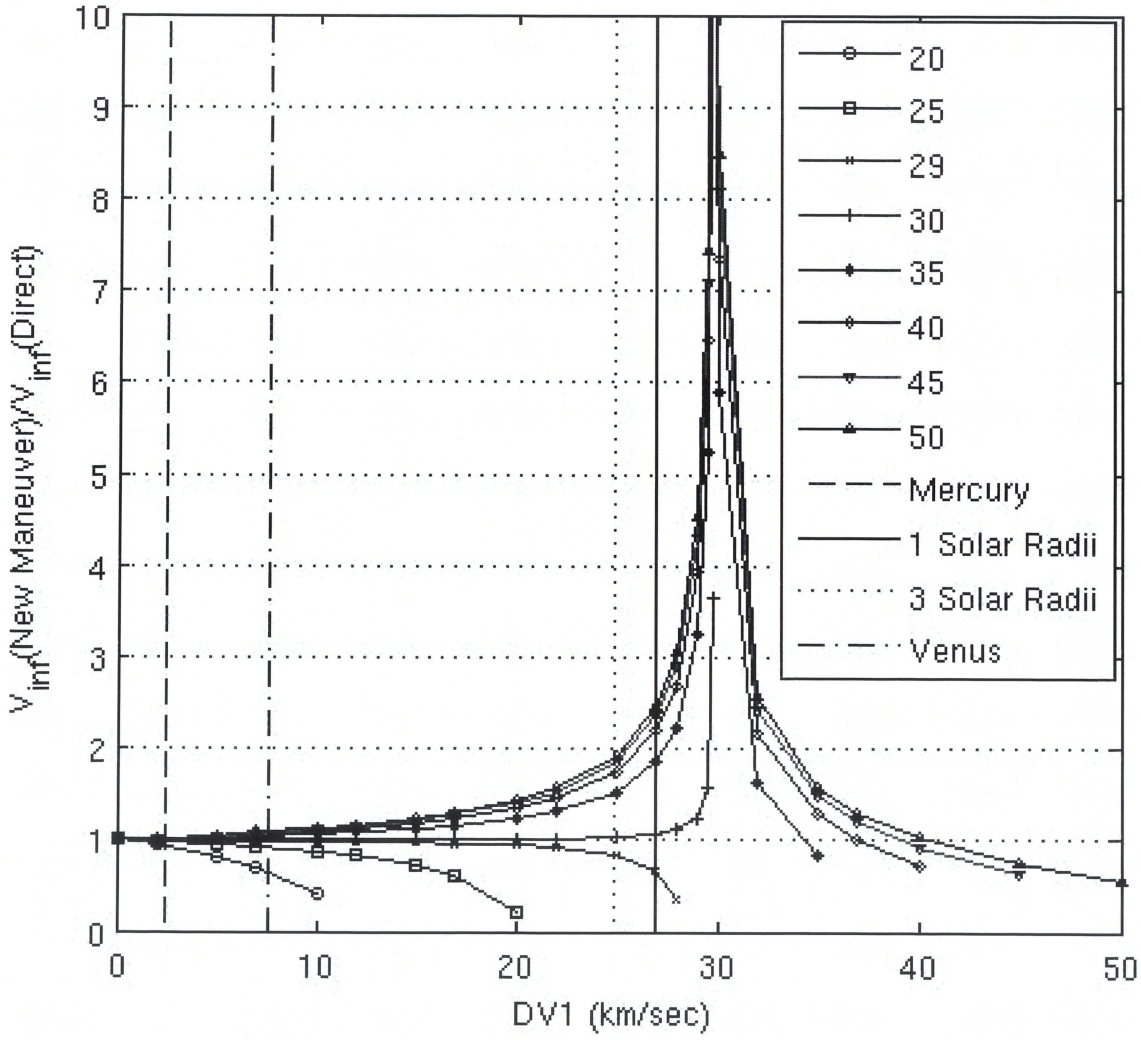

Figure 3 Ratio of V_{inf} for the new maneuver to the V_{inf} attained through a direct burn. Vertical asymptote is at initial orbital velocity, 29.784 km/s. Values represent solar orbit starting at 1 AU (Earth-like orbit)

For instance, assuming that the spacecraft can survive a close approach to the sun of 3 solar radii and a total ΔV budget of 40 km/sec, the slingshot maneuver can produce a change in specific orbital energy approximately three times that of the direct maneuver.

Survival of a three solar radii approach is the goal of Solar Probe+ mission (8), so there is good expectation that this goal is within current technological limits.

There is also the possibility of using the new maneuver not only for escape but also for orbit raising missions. However the maneuver as shown is not more efficient than a Hohmann maneuver. This is evident by considering the concept of escape velocity. Given a spacecraft at a certain orbital radius, the minimum velocity that will attain escape from the central body is

$$V_{esc} = \sqrt{\frac{2\mu}{r_0}} \quad \textbf{Eq. 29}$$

Comparing escape velocity to initial circular velocity plus the budget allowed for a maneuver.

$$\sqrt{\frac{\mu}{r_0}} + \Delta V_{tot} = \sqrt{\frac{2\mu}{r_0}} \quad \textbf{Eq. 30}$$

So since the new maneuver requires that the ΔV budget exceeds the circular velocity, the left hand side of the equation will always exceed escape velocity. Thus the new maneuver is not as efficient as that for a Hohmann transfer. However, frequently a mission requires a fast transfer from one orbit to another, faster than the Hohmann transfer produces. Crewed missions and robotic probes to deep space make waiting for Hohmann transfers prohibitive. Thus the new maneuver could be compared to a semi-tangential trajectory. In this scenario there are some instances where the new maneuver proves more effective. More analysis is indicated in this area.

It should be noted that the analysis in figures 2 and 3 assumes a starting position of an orbit around the sun at earth's distance (1 AU). The premise of this new maneuver

is that burns should be done as low in the gravity well as possible. So in a real situation the first burn, intending to slow the spacecraft so it will drop towards the sun, would be done in Low Earth Orbit. The benefit is that the first burn is done deep in the gravity well of Earth making it less expensive to drop towards the sun. The difference can be significant, and the results above for starting points in orbit around the sun are therefore conservative.

5. Applications

This paper started by examining the concept that acceleration along the velocity vector would result in an optimal acceleration of the spacecraft. While acceleration along the velocity vector is locally optimal, it turns out that there is a special maneuver that in certain cases will outperform the "optimal" cross product acceleration by actually decelerating the vehicle and accelerating it when it reaches periapse. It is presented here as an important maneuver to be considered for high ΔV missions such as interstellar precursor or similar deep space missions and potentially crewed round trip missions to Mars and beyond. Finally, as described by Heinlein, the maneuver is very effective for spacecraft attempting escape when it already is near the top of the central body's gravity well. This has profound implications for future space exploration. Being able to use in-situ resources to create propellants or even construct vehicles on the moon has even greater importance now that the new maneuver can be used to substantially reduce the propulsive requirements for deep space missions.

The ΔV required to complete a mission to Mars and return is 12-13 km/sec for Hohmann transfers. However, radiation exposure, crew supplies and crew mental health

issues have forced vehicle designers to look at much higher ΔV missions that can reduce trip times and mission risk. Mission studies for crewed missions to Mars with a limiting total trip time of 2 years of less have ΔV requirements above 20 km/sec. Therefore it is possible that the new option could have application in orbit raising maneuvers where limiting mission time is critical. A proof of principle calculation shows significant gains in performance for crewed missions to Mars using this maneuver. This gain is predicated on the hope that water ice will be found on the moon and can successfully be turned into useable propellant. Given this assumption, the new maneuver can reduce vehicle size by up to half, or decrease mission time by half. The former dramatically reduces the cost of a Mars trip, while the latter reduces the risk to crew.

Scientific probes escaping the solar system benefit dramatically using this maneuver. Calculations show that the velocity at Pluto of the Pluto-Kuiper Express mission would have been substantially improved using this maneuver with corresponding benefit in shorter periods before observation of Pluto and faster penetration of the outer solar system, Kuiper Belt, heliopause and Oort Cloud. This presumes that the greater speed would be more desirable than longer observation time during the Pluto fly-by. The Thousand Astronomical Unit (TAU) mission could be achieved within the 50 year timeframe using conventional technologies.

Currently, long distance space travel to nearby stars such as Alpha Centauri is not realistic due primarily to limitations in achievable spacecraft velocities. This new maneuver, along with advanced spacecraft technologies, has the potential to advance space travel to the point of making these long distance trips possible with durations on the order of a hundred years.

6. Conclusion

The new maneuver shows considerable promise to enable a variety of scientific and exploration missions in deep space. The authors believe that this new maneuver could have a similar effect on space exploration as the gravity assist. Developed at the very beginning of the space program, the gravity assist enabled missions from Voyager to Cassini to visit the planets of the solar system using the technologies that were then available. Clearly without the gravity assist those technologies would have been inadequate to explore much of the solar system outside of the moon and Mars. Similarly the new maneuver enables exploration of the boundary of the solar system and interstellar space using today's technologies and technologies of the near future. Such missions are difficult to conceive without the advantages of this new maneuver.

7. Acknowledgments

The authors would like to acknowledge Dr. Clark Hawk as an outstanding mentor, colleague and friend. Without his support and guidance, this work would not have been possible.

REFERENCES

1 Vallado, David A., *Fundamentals of Astrodynamics and Applications*, Microcosm Press, El Segundo, CA, 2001

2 Sutton, George P., Bilbarz, Oscar, *Rocket Propulsion Elements*, John Wiley and Sons, Inc., 2001.

3 Lawrence, Timothy J., Witter, Jonathan K., Humble, Ronald W., "Nuclear Rocket Propulsion Systems", Chapter 8 in *Space Propulsion Analysis and Design*, The McGraw-Hill Companies, New York, 1995.

4 Levin, E., "Low Acceleration Transfer Orbits", Section 9.1 in *Handbook of Astronautical Engineering*, edited by Heinz Hermann Koelle, McGraw-Hill Book Company, New York, 1961.

5 *Near-Earth Object Survey and Deflection Analysis of Alternatives*, Report to Congress, NASA, March, 2007.

6 Adams R. B., Alexander, R., Bonometti, J., Chapman, J., Fincher, S., Hopkins, R., Kalkstein, M., Polsgrove, T., Statham, G., White, S., *Survey of Technologies Relevant to Defense from Near-Earth Objects*, NASA, TP-2004-213089.

7 Heinlein, Robert A., *The Rolling Stones*, 1952.

8 Danzler, Andrew A., "Solar Probe+, "Mission Engineering Study Report", NASA's Heliophysics Division, March 10, 2008.

REFERENCES

[1] ANSI/AIAA G-057-1994, *Guide to Terminology for Space Launch Systems*, American Institute of Aeronautics and Astronautics, 1994.

[2] Sutton, G. P., Bilbarz, O., *Rocket Propulsion Elements*, John Wiley and Sons, Inc., 2001.

[3] Adams, R. B., "Launch Vehicle Analysis", Chapter 3 in *Space Launch and Transportation Systems* edited by W. J. Larson, D. Kilpatrick, R. Ryan and V. Weyers, Department of Defense, 2005.

[4] Brauer, G. L., Cornick, D. E., Olson, D. W., Petersen, F. M., Stevenson, R. *Program to Optimize Simulated Trajectories: Volume I Formulation Manual*, Martin Marietta Corporation, September 1990.

[5] Boden, D. G., Erickson, J. W., "Mission Analysis", Chapter 2 in *Space Propulsion Analysis and Design*, edited by Humble, Henry and Larson, The McGraw-Hill Companies, New York, 1995.

[6] Vallado, D. A., *Fundamentals of Astrodynamics and Applications*, Microcosm Press, El Segundo, CA, 2001.

[7] Chobotov, V. A., *Orbital Mechanics*, American Institute of Aeronautics and Astronautics, Reston, VA, 1996.

[8] ANSI/AIAA R-064-1994, "Recommended Practice for Astrodynamics Concepts, Terms, and Symbols – Part 1".

[9] Lawrence, T. J., Witter, J. K., Humble, R. W., "Nuclear Rocket Propulsion Systems", Chapter 8 in *Space Propulsion Analysis and Design*, The McGraw-Hill Companies, New York, 1995.

[10] Borowski, S. K., "A Comparison of Fusion/Antiproton Propulsion Systems for Interplanetary Travel", AIAA 87-1814, 1987.

[11] Bate, R. R., Mueller, D. D., White, J. E., *Fundamentals of Astrodynamics*, Dover Publications, New York, 1971.

[12] McInnes, C. R., *Solar Sailing*, Praxis Publishing, Chichester UK, 1999.

[13] Winglee, R. M., *Mini-Magnetospheric Plasma Propulsion*, NIAC Final Report, May 1999.

[14] Polsgrove, T., Adams, R. B., "Trajectories for High Specific Impulse High Specific Power Deep Space Exploration", AIAA 2002-4433, 2002.

[15] Hill, P., and Peterson, C., *Mechanics and Thermodynamics of Propulsion*, Addison-Wesley Publishing Company, Reading, MA, 1992.

[16] Tsien, H. S., "Take-Off from Satellite Orbit", *ARS Journal*, July-August 1953.

[17] Levin, E., "Low Acceleration Transfer Orbits", Section 9.1 in *Handbook of Astronautical Engineering*, edited by Heinz Hermann Koelle, McGraw-Hill Book Company, New York, 1961.

[18] Edelbaum, T. N., "Propulsion Requirements for Controllable Satellites", *ARS Journal*, August 1961.

[19] Lawden, D. F., "Optimal Escape from a Circular Orbit", *Astronautica Acta*, vol. 4, no 3, pp. 218-233, 1958.
[20] Irving, J. H., Blum, E. K., "Comparative Performance of Ballistic and Low-Thrust Vehicles for Flight to Mars". *Vistas in Aeronautics II*, New York, Pergamon Press, 1959.
[21] Irving, J. H., "Low Thrust Flight: Variable Exhaust Velocity in Gravitational Fields", Chapter 10 in *Space Technology*, edited by Howard Siefert, John Wiley and Sons, Inc., New York, 1959.
[22] Battin, R. H., *An Introduction to the Mathematics and Methods of Astrodynamics*, American Institute of Aeronautics and Astronautics, New York, 1987.
[23] Lawden, D. F., "Optimal Programming of Thrust Direction", Journal of the British Interplanetary Society, 1954.
[24] McInnes, C. R., *Solar Sailing*, Praxis Publishing, Chichester UK, 1999.
[25] Spiegel, M. R., *Mathematical Handbook*, McGraw-Hill, New York, 1996.
[26] Johnson, Forrester T., "Approximate Finite-Thrust Trajectory Optimization", AAS 68-080, AAS/AIAA Astrodynamics Specialist Conference, Jackson, WY, September 3-5, 1968.
[27] Hahn, D. W., Johnson, F. T., Itzen, B. F., *Chebychev Trajectory Optimization Program (ChebyTOP)*, The Boeing Company, Seattle, WA, 1969.
[28] Johnson, F. T., *Improvement of the Digital Computer Program ChebyTOP III*, The Boeing Company, Seattle, WA, 1973.
[29] Kechichian, J. A., "Trajectory Optimization with a Modified Set of Equinoctial Orbit Elements", AAS/AIAA Paper 91-524, Astrodynamics Specialist Conference, Durango, CO, August 19-22,1991.
[30] Kechichian, J. A., "Optimal LEO-GEO Intermediate Acceleration Orbit Transfer", AAS Paper 94-125, AAS/AIAA Spaceflight Mechanics Meeting, Cocoa Beach, FL, 1994.
[31] Bonometti, Joseph, personal communication.
[32] Bussard, R. W., Jameson, L. W., "From SSTO to Saturn's Moons: Superperformance Fusion Propulsion for Practical Spaceflight", in *Fusion Energy in Space Propulsion*, edited by Terry Kammash, AIAA, Washington DC, 1995.
[33] Kammash, T., "Principles of Fusion Energy Utilization in Space Propulsion", in *Fusion Energy in Space Propulsion*, edited by Terry Kammash, AIAA, Washington DC, 1995.
[34] Moeckel, W. E., "Comparison of Advanced Propulsion Concepts for Deep Space Exploration", *AIAA Journal of Spacecraft*, Vol. 9, No. 12, December 1972.
[35] Shepherd, D. G., *Aerospace Propulsion*, American Elsevier Publications., New York, 1972.
[36] Williams, C. H., "An Analytic Approximation to Very High Specific Impulse and Specific Power Interplanetary Space Mission Analysis", AAS 96-151, 1996.
[37] Thio, F., unpublished.
[38] Cole, J., unpublished.
[39] Thompson, W. T., *Introduction to Space Dynamics*, Dover Publications, New York, 1961.

[40] Ehricke, K. A., Solar Propulsion, Section 21.3 in *Handbook of Astronautical Engineering*, edited by H. H. Koelle, McGraw-Hill Book Company, Inc., New York, 1961.
[41] Gilland, J. H., *Mission and System Optimization of Nuclear Electric Propulsion Vehicles for Lunar and Mars Missions*, NASA CR-189058, December 1991.
[42] Chakrabarti, S., Schmidt, G., "Impact of Energy Gain and Subsystem Characteristics on Fusion Propulsion Performance", AIAA, 2002.
[43] Adams, R., Alexander, R., Chapman, J., Fincher, S., Philips, A., Polsgrove, T., Patton, B., Statham, G., White, S., Thio, F., *Conceptual Design of In-Space Vehicles for Human Exploration of the Outer Planets*, NASA TM-2003-212691, November 2003.
[44] Spiegel, M. R., *Probability and Statistics*, Schaum's Outline Series, New York, 1995.
[45] Yates, F., "Contingency Table Involving Small Numbers and the χ^2 Test". *Journal of the Royal Statistical Society* (Supplement) **1**: 217-235, 1934.
[46] Sokal, R. R., Rohlf, F. J., *Biometry: the Principles and Practice of Statistics in Biological Research., 3rd edition.* Freeman, New York, 1994.
[47] Coleman, H. W., Steele, W. G., *Experimentation and Uncertainty Analysis for Engineers*, John Wiley and Sons, Inc., New York, 1999.
[48] Barter, N. J., *Space Data*, Northrop-Grumman, March 2003.
[49] Gelfand, I. M., Fomin, S. V., *Calculus of Variations*, Dover Publications, Inc., Mineola, NY, 1963.
[50] White, F. M., *Fluid Mechanics, Second Edition*, McGraw-Hill, Inc., New York, 1986.
[51] Moeckel, 1961.
[52] Land, N. S., *A Compilation of Non-Dimensional Numbers*, NASA SP-274, Washington DC, 1972.
[53] *Near-Earth Object Survey and Deflection Analysis of Alternatives*, Report to Congress, NASA, March 2007.
[54] Adams, R. B., Alexander, R., Bonometti, J., Chapman, J., Fincher, S., Hopkins, R., Kalkstein, M., Polsgrove, T., Statham, G., White, S., *Survey of Technologies Relevant to Defense from Near-Earth Objects*, NASA, TP-2004-213089.
[55] http://en.wikipedia.org/wiki/Oberth_effect, accessed January 2008.
[56] Heinlein, R. A., *The Rolling Stones*, Charles Scribner's Sons, New York, 1952.